Niobia-supported Cobalt Catalysts for Fischer-Tropsch Synthesis

Arjan den Otter

ISBN: 978-90-393-6561-8

Niobia-supported Cobalt Catalysts for Fischer-Tropsch Synthesis

Niobiumoxide-gedragen Kobaltkatalysatoren voor de Fischer-Tropschsynthese

(met een samenvatting in het Nederlands)

Proefschrift

ter verkrijging van de graad van doctor aan de Universiteit Utrecht op gezag van de rector magnificus, prof.dr. G.J. van der Zwaan, ingevolge het besluit van het college voor promoties in het openbaar te verdedigen op maandag 30 mei 2016 des ochtends te 10.30 uur

door

Jan Huibert den Otter

geboren op 30 januari 1986 te ‘s-Hertogenbosch

Promotor: Prof.dr.ir. K.P. de Jong

Dit proefschrift werd mede mogelijk gemaakt met financiële steun van Companhia Brasileira de Metalurgia e Mineração.

Table of contents

Chapter 1

General Introduction

Fischer-Tropsch synthesis

Over the last decades the world energy consumption has increased drastically due to a growing world population and an increasing level of welfare. Currently ~ 87 % of the energy used originates from oil (33 %), gas (24 %) and coal (30 %) as shown in Figure 1.1.[1] Especially for the production of transportation fuels, dependence on crude oil is large. Reserves of crude oil are reported to be large and new reserves are still being discovered nowadays (Figure 1.2A); however, these will eventually deplete or be not exploitable due to high investment costs, political situation or environmental concerns.

Natural gas is an alternative to crude oil; however, due to the often remote location and the high transportation costs of gasses, difficult to exploit and associated gas from oil wells might even be flared. Other energy sources include coal and biomass, of which the latter could result in a renewable cycle. However, natural gas, coal or biomass cannot be directly implemented in the current fuel production facilities or in an internal combustion engine.

To be able to transport and exploit these carbon feedstocks, conversion into liquid hydrocarbons is required and the typical route is via synthesis gas (syngas) generation and conversion. Syngas is a mixture of H_2 and CO, usually produced by steam reforming of natural gas or by high-temperature gasification of coal or biomass.[2] Syngas can be catalytically converted into long-chain hydrocarbons according to the following equation: $n\ CO + (2n+1)\ H_2 \rightarrow C_nH_{2n+2} + n\ H_2O$. Depending on the carbon feedstock, the overall process of syngas generation and conversion is often referred to as gas-to-liquid (GTL), coal-to-liquid (CTL) or biomass-to-liquid (BTL).

The hydrogenation of carbon monoxide to hydrocarbons was first reported in the early 1900s and patented by the BASF researchers Mittasch and Schneider.[3] The process however was named after the German researchers Fischer and Tropsch who realized the potential for production of synthetic liquid fuels using supported cobalt catalysts.[4,5]

Investments in commercialization of the Fischer-Tropsch process have been largely dependent on the price of crude oil (Figure 1.2B) and international politics. Large scale application of the Fischer-Tropsch process in CTL was first applied by the German industry during the Nazi regime in the period 1927-1945 in order to be independent of oil imports.[6] In the 1950s, large new

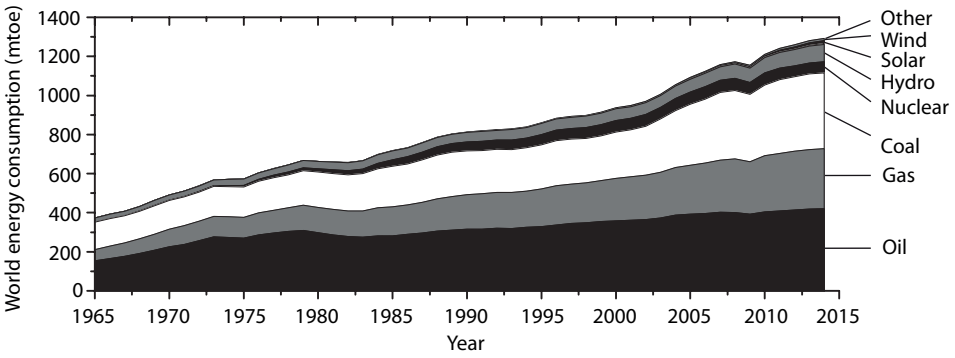

Figure 1.1. World energy consumption over time in million tonnes of oil equivalent (mtoe).[1]

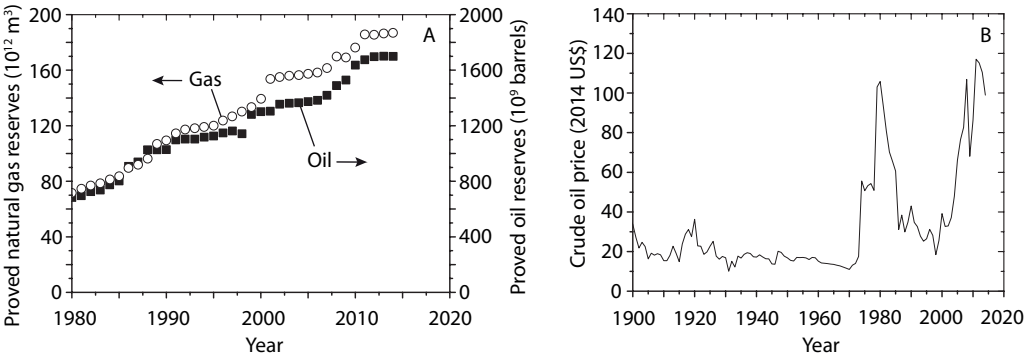

Figure 1.2. Development of worldwide proved reserves of natural gas and oil (A) and inflation-corrected annual-average crude oil price (B).[1]

reserves of crude oil were discovered, making the FT process in CTL economically less viable and only applied in South Africa to meet the energy demands during the apartheid regime. Renewed attention to the FT process was obtained after the oil crisis in 1973, also stimulated by the more and more stringent legislation regarding vehicle emissions. Due to the very low concentrations of sulfur, nitrogen and aromatics in Fischer-Tropsch derived fuels, important improvements can be made in the development of combustion engines and automotive catalytic converters and reduced emissions of SO_2, NO_x and particulate matter are reported for engines operated on Fischer-Tropsch diesel compared to conventional crude oil-based diesel.[7,8]

Currently several large-scale GTL and CTL plants are operated with an approximate summed capacity of 400,000 barrels per day (bpd). Plants are located in South Africa (Secunda, Sasol, 160,000 bpd, CTL), Qatar (Pearl, Shell, 140,000 bpd, GTL and Oryx, Sasol, 34,000 bpd GTL), Nigeria (Escravos, Chevron, 34,000 bpd, GTL), Malaysia (Bintulu, Shell, 15,000 bpd, GTL) and China (Yitai and Lu'an, 4,000 bpd, CTL). The fluctuating price of crude oil however also largely determines the feasibility of construction of new industrial Fischer-Tropsch plants. Due to the low current oil price, construction of large (> 100,000 bpd) Fischer-Tropsch GTL plants, exploiting shale gas in Louisiana, USA was postponed by Shell and Sasol.

Fischer-Tropsch catalysts

Group 8 - 10 metals Fe, Co, Ni and Ru have been shown to be active Fischer-Tropsch catalysts since these metals can dissociatively adsorb CO.[9,10] Ruthenium is the most active of these metals and is widely applied in academic studies. However, due to its limited availability and high costs, large-scale industrial application of ruthenium is less feasible. Nickel catalysts exhibit high selectivity towards methane and are therefore mainly applied for removal of undesired CO traces in feed gasses or for the production of synthetic natural gas.[11]

Iron and cobalt are widely used Fischer-Tropsch catalysts and the choice of metal mainly depends on the feed gas and the desired products. Iron is cheaper than cobalt and can be applied

for the conversion of CO-rich synthesis gas (H_2/CO = 1), typically obtained from biomass or coal. When operated at high temperatures (HTFT, ~ 340 °C), the main products are (lower) olefins.[12,13] Due to the high activity in the water-gas shift reaction (WGS: $CO + H_2O \rightarrow CO_2 + H_2$), the main side-product is carbon dioxide. Due to coke deposition iron catalysts are prone to rapid deactivation.[13,14] Cobalt catalysts exhibit higher activity at lower temperatures (200 - 240 °C) and higher stability against deactivation by water; however, are more prone to poisoning by contaminants like sulfur than iron catalysts. The high selectivity towards heavy hydrocarbons in combination with high stability and the absence of WGS makes cobalt the preferred catalyst for the low temperature Fischer-Tropsch reaction (LTFT).[15–18]

Industrial catalysts for LTFT synthesis typically consist of 10-30 wt% cobalt, 0.05-1 wt% noble metal promoter, 1-10 wt% transition-metal oxide promoter and a high-surface-area oxide support.[19] The active phase is metallic cobalt and the activity per cobalt surface atom (turnover frequency, TOF) was reported to be independent of particle size for cobalt particle sizes above 6-8 nm.[20,21] Typically, the metallic cobalt is obtained by reduction of Co_3O_4. Reduction of Co_3O_4 is found to be difficult especially for small particles and in the case of strong interaction with the support[22] and can be promoted by the addition of a noble metal like Pt, Pd, Ru or Re. The role of the noble metal is believed to be dissociation of H_2 and spill-over of hydrogen atoms to cobalt oxide, leading to a higher degree of reduction at lower temperature and ultimately a higher number of metallic cobalt surface sites.[23–26]

To offer thermal, mechanical and chemical stability, metal nanoparticles are often supported by mesoporous metal oxides. Industrially applied supports include γ-Al_2O_3 or TiO_2, while many fundamental studies have been performed on silica[27,28], carbon[21,29] and zeolite[30,31] supported catalysts. It has been found that the nature of the support can affect the catalyst performance.[32] High support pore volume and surface area allow for facile catalyst preparation and high cobalt loadings[33] while the support pore diameter is reported to affect the catalyst selectivity, either by influencing the cobalt particle size[18,34,35] or affecting diffusion of reactants and products[36–38]. The nature of the support determines the interaction with cobalt species; strongly interacting supports like γ-Al_2O_3 usually lead to high cobalt dispersions but also hard to reduce cobalt oxide species and vice versa.[39,40] The presence of acid support groups can introduce isomerization or hydrocracking activity to the catalyst.[30,31,41]

Partially reducible transition-metal oxide (TMO) promoters like manganese oxide, zirconia, titania or niobia, are typically added to promote the selectivity to higher hydrocarbons (often referred to as C_{5+} selectivity) and activity of the catalyst by electronic interaction between cobalt and the TMO.[42,43] The selectivity promoting mechanism is thought to be related to partial reduction of the TMO followed by migration onto metallic cobalt which is often referred to as strong metal-support interaction (SMSI) and reported by Tauster et al. and Haller et al. for TiO_2-supported catalysts.[44–46] TMO promoters can thus be present as small species in close vicinity to or on the cobalt particles[17,47–53], by modification of a silica or alumina-support with a TMO[54–56] or as support material like in the case of Co/TiO_2[57–59], Co/CeO_2[60,61] Co/ZrO_2[62–64] or Co/Nb_2O_5[65–69] catalysts.

Niobia in Fischer-Tropsch synthesis

The application of Co/Nb_2O_5 catalysts in Fischer-Tropsch synthesis was first reported in 1993 by Frydman et al.[68] and is subject of several research papers and patents.[41,69,70] In comparison to alumina-supported catalysts higher C_{5+} selectivities were reported in Fischer-Tropsch synthesis at 1 bar.[66] Upon increasing reduction temperature (300 - 500 °C), the catalyst activity was found to decrease whereas the C_{5+} selectivity increased and was explained in terms of SMSI (vide supra).[66] Influence of reactor pressure was investigated by Mendes et al. for Co, RuCo and $ReCo/Nb_2O_5$ catalysts.[71] Enhanced C_{5+} selectivities were observed upon increasing pressure up to 20 bar.

Niobia-modified alumina was prepared by Mendes et al. and investigated as support material for cobalt Fischer-Tropsch catalysts.[54,72] Enhanced C_{5+} selectivities were observed upon niobia-modification of alumina. Using a temperature-programmed surface reaction technique (TPSR) and in situ diffuse reflectance spectroscopy (DRS) Co^0, Co^{2+}-Co and Co^0-NbO_x were suggested to be the active surface sites. Co^{2+}-Co was proposed to be responsible for methanation and Co^0-NbO_x responsible for hydrocarbon chain growth, making the relative abundance of Co^{2+} affect the catalyst performance.[54,73] The presence of Co^0-NbO_x species was confirmed in Co/Nb_2O_5 catalysts[54] and model catalysts.[74]

Bimetallic $PtCo/Nb_2O_5$ and $RhCo/Nb_2O_5$ catalysts were applied in Fischer-Tropsch synthesis by Noronha et al. and Frydman et al.[75,76] For $PtCo/Nb_2O_5$ catalysts, a factor 2-3 increase of the cobalt-weight normalized activity was reported at 1 bar, which could not be explained only by an increased number of active sites. This observation was previously reported for Ru-promoted Co/TiO_2 and recently also upon promotion of Co/TiO_2 with Ag, Pt, Re or Ru.[58] This indicates that the intrinsic activity (TOF) of the active sites increased, which is rare in cobalt Fischer-Tropsch catalysts. Iglesia et al. proposed that the activity promoting role of Ru in Co/TiO_2 was related to inhibited deactivation by carbon[77], whereas Eschemann et al. suggested that increased hydrogenation activity accelerated water formation in promoted catalysts and/or gives rise to hydrogen-assisted CO dissociation.[58]

Scope and outline of this thesis

The goal of this thesis is to more deeply investigate the application of niobia as support and promoter in cobalt Fischer-Tropsch Catalysts and to study the role of reaction conditions and noble metal promoters on the performance of niobia-containing catalysts.

In Co/niobia Fischer-Tropsch catalysts typically crystalline, low specific surface area supports are used with low cobalt loadings (~ 5 wt%) and dispersions. In **Chapter 2**, the influence of process conditions and carbon-templating on porosity and surface area of crystalline niobia is studied. Besides that, the influence of niobia phase and cobalt loading and deposition method on the catalyst structure and performance in Fischer-Tropsch synthesis is investigated.

In **Chapter 3,** the activity and selectivity of a 5 wt% Co/Nb_2O_5 catalyst was investigated in Fischer-Tropsch synthesis at industrially relevant conditions in comparison to a 28 wt% Co/γ-alumina catalyst. The influence of a wide range of reaction temperatures was

investigated and was utilized to compensate for the low cobalt loading on the niobia support.

The extent and origin of Pt-promotion on the activity and selectivity of Co/Nb_2O_5 Fischer-Tropsch catalysts is investigated in comparison to γ-Al_2O_3- and α-Al_2O_3-supported catalysts in **Chapter 4**. A wide range of techniques, including environmental X-ray diffraction (XRD), environmental Transmission Electron Microscopy (TEM), a kinetic study and Steady-State Isotopic Transient Kinetic Analysis (SSTIKA), was applied to study the effect of Pt addition on the number and the nature of the active sites.

The low porosity of niobia limits the cobalt loading in niobia-supported catalysts to ~ 5 wt%, which is much lower than industrial catalysts. To combine the selectivity-promoting properties of niobia with a highly porous support, niobia-modified silica was applied as support for Co and PtCo catalysts in **Chapter 5**. The extent and origin of activity and selectivity promotion by niobia and platinum is investigated at 1 bar and low CO conversion and at industrially relevant conditions and correlated to the catalyst structure.

Finally, **Chapter 6** provides a summary of the main results in this thesis and some concluding remarks.

References

[1] *BP Statistical Review of World Energy, June 2015*.

[2] Steynberg, A. P. *Stud. Surf. Sci. Catal.* **2004**, *152*, 1–63.

[3] Mittasch, A.; Schneider, C. DRP 293787 **1913**.

[4] Fischer, F.; Tropsch, H. *Brennst. Chemie* **1923**, *4*, 276–285.

[5] Fischer, F.; Tropsch, H. *Brennst. Chemie* **1924**, *5*, 201–208.

[6] Stranges, A. N. *Stud. Surf. Sci. Catal.* **2007**, *163*, 1–27.

[7] Verbeek, R. *TNO report 2014 R10588*; **2014**.

[8] http://www.shell.com/global/future-energy/natural-gas/gtl/products.html (Accessed Dec 17, 2015).

[9] Vannice, M. A. *J. Catal.* **1977**, *50*, 228–236.

[10] Dry, M. E. *Catal. Today* **2002**, *71*, 227–241.

[11] Kopyscinski, J.; Schildhauer, T. J.; Biollaz, S. M. A. *Fuel* **2010**, *89*, 1763–1783.

[12] Torres Galvis, H. M.; Bitter, J. H.; Khare, C. B.; Ruitenbeek, M.; Dugulan, A. I.; de Jong, K. P. *Science.* **2012**, *335*, 835–838.

[13] Torres Galvis, H. M.; de Jong, K. P. *ACS Catal.* **2013**, *3*, 2130–2149.

[14] Dry, M. E. *Catal. Letters* **1991**, *7*, 241–251.

[15] Iglesia, E. *Appl. Catal., A* **1997**, *161*, 59–78.

[16] Davis, B. H.; Occelli, M. L. *Stud. Surf. Sci. Catal.* **2007**, *163*, 1–420.

[17] Khodakov, A. Y.; Chu, W.; Fongarland, P. *Chem. Rev.* **2007**, *107*, 1692–1744.

[18] Borg, Ø.; Eri, S.; Blekkan, E. A.; Storsater, S.; Wigum, H.; Rytter, E.; Holmen, A. *J. Catal.* **2007**, *248*, 89–100.

[19] Oukaci, R.; Singleton, A. H.; Goodwin, J. G. *Appl. Catal., A* **1999**, *186*, 129–144.

[20] Soled, S. L.; Iglesia, E.; Fiato, R. A.; Baumgartner, J. E.; Vroman, H.; Miseo, S. *Top. Catal.* **2003**, *26*, 101–109.

[21] Bezemer, G. L.; Bitter, J. H.; Kuipers, H. P. C. E.; Oosterbeek, H.; Holewijn, J. E.; Xu, X.; Kapteijn, F.; van Dillen, A. J.; de Jong, K. P. *J. Am. Chem. Soc.* **2006**, *128*, 3956–3964.

[22] Khodakov, A. Y.; Lynch, J.; Bazin, D.; Rebours, B.; Zanier, N.; Moisson, B.; Chaumette, P. *J. Catal.* **1997**, *168*, 16–25.

[23] Diehl, F.; Khodakov, A. Y. *Oil Gas Sci. Technol. - Rev. l'IFP* **2009**, *64*, 11–24.

[24] Conner, W. C.; Falconer, J. L. *Chem. Rev.* **1995**, *95*, 759–788.

[25] Jacobs, G.; Das, T. K.; Zhang, Y.; Li, J.; Racoillet, G.; Davis, B. H. *Appl. Catal., A* **2002**, *233*, 263–281.

[26] Das, T. K.; Jacobs, G.; Patterson, P. M.; Conner, W. A.; Li, J.; Davis, B. H. *Fuel* **2003**, *82*, 805–815.

[27] Munnik, P.; Krans, N. A.; de Jongh, P. E.; de Jong, K. P. *ACS Catal.* **2014**, *4*, 3219–3226.

[28] Eggenhuisen, T. M.; Munnik, P.; Talsma, H.; de Jongh, P. E.; de Jong, K. P. *J. Catal.* **2013**, *297*, 306–313.

[29] Bezemer, G. L.; Falke, U.; van Dillen, A. J.; de Jong, K. P. *Chem. Commun.* **2005**, 731–733.

[30] Sartipi, S.; Makkee, M.; Kapteijn, F.; Gascon, J. *Catal. Sci. Technol.* **2014**, *4*, 893–907.

[31] Sartipi, S.; Parashar, K.; Makkee, M.; Gascon, J.; Kapteijn, F. *Catal. Sci. Technol.* **2013**, *3*, 572–575.

[32] Prieto, G.; De Mello, M. I. S.; Concepción, P.; Murciano, R.; Pergher, S. B. C.; Martínez, A. *ACS Catal.* **2015**, *5*, 3323–3335.

[33] Munnik, P.; de Jongh, P. E.; de Jong, K. P. *Chem. Rev.* **2015**, *115*, 6687–6718.

[34] Rane, S.; Borg, Ø.; Yang, J.; Rytter, E.; Holmen, A. *Appl. Catal., A* **2010**, *388*, 160–167.

[35] Storsater, S.; Borg, Ø.; Blekkan, E. A.; Holmen, A. *J. Catal.* **2005**, *231*, 405–419.

[36] Iglesia, E.; Soled, S. L.; Fiato, R. A. *J. Catal.* **1992**, *137*, 212–224.

[37] Lualdi, M.; Lögdberg, S.; Di Carlo, G.; Järås, S.; Boutonnet, M.; Venezia, A. M.; Blekkan, E. A.; Holmen, A. *Top. Catal.* **2011**, *54*, 1175–1184.

[38] Vervloet, D.; Kapteijn, F.; Nijenhuis, J.; van Ommen, J. R. *Catal. Sci. Technol.* **2012**, *2*, 1221–1233.

[39] Jacobs, G.; Ji, Y.; Davis, B. H.; Cronauer, D.; Kropf, A. J.; Marshall, C. L. *Appl. Catal., A* **2007**, *333*, 177–191.

[40] Khodakov, A. Y. *Catal. Today* **2009**, *144*, 251–257.

[41] Jothimurugesan, K.; Das, T.; Kibby, C. L.; Saxton, R. J. US patent US 20120129959 A1 **2012**.

[42] Morales, F.; Weckhuysen, B. M. In: *Catalysis*; Spivey, J. J. and Dooley, K. M., Ed.; RSC Publishing: Cambridge, **2006**; pp. 1–40.

[43] Prieto, G.; Concepción, P.; Martínez, A.; Mendoza, E. *J. Catal.* **2011**, *280*, 274–288.

[44] Tauster, S. J.; Fung, S. C. *J. Catal.* **1978**, *55*, 29–35.

[45] Tauster, S. J.; Fung, S. C.; Garten, R. L. *J. Am. Chem. Soc.* **1978**, *100*, 170–175.

[46] Haller, G. L.; Resasco, D. E. *Adv. Catal.* **1989**, *36*, 173–235.

[47] Morales, F.; de Groot, F. M. F.; Gijzeman, O.; Mens, A. J. M.; Stephan, O.; Weckhuysen, B. M. *J. Catal.* **2005**, *230*, 301–308.

[48] Morales, F.; de Smit, E.; de Groot, F. M. F.; Visser, T.; Weckhuysen, B. M. *J. Catal.* **2007**, *246*, 91–99.

[49] Moradi, G. R.; Basir, M. M.; Taeb, A.; Kiennemann, A. *Catal. Commun.* **2003**, *4*, 27–32.

[50] Dinse, A.; Aigner, M.; Ulbrich, M.; Johnson, G. R.; Bell, A. T. *J. Catal.* **2012**, *288*, 104–114.

[51] Johnson, G. R.; Werner, S.; Bell, A. T. *ACS Catal.* **2015**, *5*, 5888–5903.

[52] Ali, S.; Chen, B.; Goodwin, J. G. *J. Catal.* **1995**, *157*, 35 – 41.

[53] den Breejen, J. P.; Frey, A. M.; Yang, J.; Holmen, A.; Schooneveld, M. M.; Groot, F. M. F.; Stephan, O.; Bitter, J. H.; de Jong, K. P. *Top. Catal.* **2011**, *54*, 768–777.

[54] Mendes, F. M. T.; Perez, C. A. C.; Noronha, F. B.; Souza, D. D.; Cesar, D. V.; Freund, H.-J.; Schmal, M. *J. Phys. Chem. B* **2006**, *110*, 9155–9163.

[55] Rohr, F.; Lindvåg, O. .; Holmen, A.; Blekkan, E. . *Catal. Today* **2000**, *58*, 247–254.

[56] Shi, H.; Li, Q.; Dai, X.; Yu, C.; Shen, S. *Pet. Sci.* **2005**, *2*, 107–111.

[57] Eschemann, T. O.; Bitter, J. H.; de Jong, K. P. *Catal. Today* **2014**, *228*, 89–95.

[58] Eschemann, T. O.; Oenema, J.; de Jong, K. P. *Catal. Today* **2016**, *261*, 60–66.

[59] Eschemann, T. O.; de Jong, K. P. *ACS Catal.* **2015**, *5*, 3181–3188.

[60] Spadaro, L.; Arena, F.; Granados, M. L.; Ojeda, M.; Fierro, J. L. G.; Frusteri, F. *J. Catal.* **2005**, *234*, 451–462.

[61] Gnanamani, M. K.; Ribeiro, M. C.; Ma, W.; Shafer, W. D.; Jacobs, G.; Graham, U. M.; Davis, B. H. *Appl. Catal., A* **2011**, *393*, 17–23.

[62] Zhao, H.; Lu, H. *React. Kinet. Catal. Lett.* **2009**, *97*, 289–293.

[63] Zhao, H. X.; Lü, H. L. *Adv. Mater. Res.* **2014**, *850-851*, 120–123.

[64] Zhao, H. X.; Lü, H. L. *Adv. Mater. Res.* **2014**, *850-851*, 124–127.

[65] Soares, R. R.; Frydman, A.; Schmal, M. *Catal. Today* **1993**, *16*, 361–370.

[66] Silva, R. R. C. M.; Schmal, M.; Frety, R.; Dalmon, J. A. *J. Chem. Soc. - Faraday Trans.* **1993**, *89*, 3975–3980.
[67] de Souza, C. D.; Cesar, D. V.; Marchetti, S. G.; Schmal, M. *Stud. Surf. Sci. Catal.* **2007**, *167*, 147–152.
[68] Frydman, A.; Soares, R. R.; Schmal, M. *Stud. Surf. Sci. Catal.* **1993**, *75*, 2797–2800.
[69] de Oliveira, A. K.; dos Santos, B. C. A.; Monteiro, R. de S.; Moraes, L. J.; Pereira, T. A.; Schmal, M.; Sousa-Aguiar, F. E.; Sugaya, M. de F.; Vicentini, V. P. World patent WO 2005/085390 A1 **2005**.
[70] Zennaro, R.; Gusso, A.; Chaumette, P.; Roy, M. US patent US 6075062 A **2000**.
[71] Mendes, F. M. T.; Noronha, F. B.; de Souza, C. D.; Silva, M. A. P.; Gaspar, A. B.; Schmal, M. *Stud. Surf. Sci. Catal.* **2004**, *147*, 361–366.
[72] Mendes, F. T.; Noronha, F. B.; Schmal, M. *Stud. Surf. Sci. Catal.* **2000**, *130*, 3717–3722.
[73] Mendes, F. M. T.; Perez, C. A. C.; Noronha, F. B.; Schmal, M. *Catal. Today* **2005**, *101*, 45–50.
[74] Mendes, F. M. T.; Uhl, A.; Starr, D. E.; Guimond, S.; Schmal, M.; Kuhlenbeck, H.; Shaikhutdinov, S. K.; Freund, H.-J. *Catal. Letters* **2006**, *111*, 35–41.
[75] Noronha, F. B.; Frydman, A.; Aranda, D. A. G.; Perez, C.; Soares, R. R.; Morawek, B.; Castner, D.; Campbell, C. T.; Frety, R.; Schmal, M. *Catal. Today* **1996**, *28*, 147–157.
[76] Frydman, A.; Castner, D. G.; Campbell, C. T.; Schmal, M. *J. Catal.* **1999**, *188*, 1–13.
[77] Iglesia, E.; Soled, S. L.; Fiato, R. A.; Via, G. H. *J. Catal.* **1993**, *143*, 345–368.

Chapter 2

Exploratory Studies for Synthesis of Niobia-supported Cobalt Fischer-Tropsch Catalysts

Abstract

In Co/niobia Fischer-Tropsch catalysts typically crystalline, low specific surface area supports are used with low cobalt loadings (~ 5 wt%) and dispersions. In this chapter the influence of temperature and atmosphere on the morphology, crystallinity and porosity of niobia was studied. Higher porosity crystalline niobia was prepared by carbon-templated crystallization of amorphous niobia and by niobia synthesis in a porous carbon template. 4 - 21 wt% cobalt was deposited on the prepared crystalline supports and on amorphous niobia by impregnation and deposition precipitation. Deposition precipitation of cobalt precursor led to precipitation in the solution separate from the crystalline niobia support due to insufficient interaction. For 5 wt% Co/Nb_2O_5 prepared by impregnation of crystalline niobia both high cobalt-weight normalized activity and high C_{5+} selectivity was obtained, previously only observed for promoted Co catalysts. Lower cobalt-weight normalized activities and C_{5+} selectivities were observed for catalysts prepared by multiple cobalt impregnation cycles, by deposition precipitation or using amorphous niobia as support.

Introduction

Co/Nb_2O_5 Fischer-Tropsch catalysts are typically prepared by impregnation of crystalline Nb_2O_5.[1–3] This support is usually obtained by thermal treatment at 500 - 600 °C of a niobium precursor or amorphous niobium oxide, yielding low specific surface area and low porosity. Consequently cobalt loadings from incipient wetness impregnation are limited to ~ 5 wt% much lower than industrial Fischer-Tropsch catalysts with 20 - 25 wt%. Higher porosity niobia would allow application of higher cobalt loadings and dispersions. Amorphous niobia has been reported to exhibit superior porosity compared to crystalline niobia[4]; however, has not been reported as support for Fischer-Tropsch catalysts.

Carbon-templating was reported to yield largely preserved porosity upon crystallization of mesoporous Nb-Ta mixed oxide.[5] BET surface area and pore volume decreased only from 184 to 94 $m^2\ g^{-1}$ and 0.34 to 0.23 mL g^{-1}, respectively. In this chapter carbon-templated crystallization of high-surface-area niobium oxide hydrate is investigated as a method to obtain high-surface-area crystalline niobia.

Synthesis methods to obtain high-surface-area niobia were reviewed by Nowak and Ziolek[6] and included the synthesis of microporous niobium oxide and niobium silicate molecular sieves[7,8], the synthesis of mesoporous amorphous niobium oxides using amphiphilic block copolymers[9–11] and the synthesis of Nb_2O_5 by roll-up of layered $K_4Nb_6O_{17}$ crystals.[12] A wet chemical route to synthesize porous metal oxides using a carbon template was reported by Schwickardi et al.[13] and involves the impregnation of activated carbon with a concentrated metal nitrate solution and subsequent calcination to decompose the nitrate precursor and burn off the carbon material. MgO, Fe_2O_3, Cr_2O_3, TiO_2 and several mixed oxides were synthesized with significantly higher porosity than without the use of a carbon template. In this chapter impregnation of a carbon template with a niobium-precursor and subsequent crystallization and carbon burn-off is investigated as another route to synthesize high-surface-area crystalline niobia.

Deposition precipitation (DP) is a method to prepare supported catalysts with high metal loadings without being limited by the support porosity.[14] Two main routes for deposition precipitation of cobalt have been reported: precipitation from an acidic solution upon increasing pH by slow hydrolysis of urea[15] or from an alkaline solution upon decreasing pH by evaporation of ammonia.[16–18] The probability that cobalt will precipitate on a suspended support depends on the extent of interaction between the precipitating agent and the support surface. Since the niobia surface charge was reported to be highly dependent on the pretreatment[19], both methods of deposition precipitation are explored in this chapter as a potential route for Co/Nb_2O_5 preparation.

In this chapter, the influence of process conditions and carbon-templating on porosity and surface area of crystalline niobia is investigated. Amorphous niobia is treated at 120 - 900 °C or crystallized after pore-filling with carbon. Carbon templated synthesis of crystalline niobia is performed by decomposition of ammonium niobium oxalate using a porous carbon template. The influence of niobia phase and cobalt loading and deposition method on the catalyst structure and performance in Fischer-Tropsch synthesis is investigated. 4 - 21 wt% Co/niobia catalysts are

prepared by impregnation and deposition precipitation using amorphous and crystalline niobia as support. Catalyst performance is evaluated in Fischer-Tropsch synthesis at 1 bar and 220 °C.

Experimental methods

Preparation

Niobium oxide hydrate (HY-340, AD/4465, 72.6 wt% Nb_2O_5, LOI 26.7 wt%, purity data see Appendix A) was obtained from Companhia Brasileira de Metalurgia e Mineração - CBMM. Thermal treatment of ~ 5 g niobium oxide hydrate at 120 - 900 °C (5 °C min^{-1}, 2 h) was performed in a muffle oven (NbxM, x indicates temperature) or in a quartz U-shaped fixed bed reactor (i.d. = 10 mm) at 600 °C (5 °C min^{-1}, 2 h) in stagnant air (Nb600SA) or in a 0.5 L min^{-1} g^{-1} air flow (Nb600AF) or N_2 flow (Nb600NF). An overview of the samples is shown in Table 2.1.

For carbon-templated crystallization of niobia[5], 0.8 g niobium oxide hydrate was dried for 16 h at 120 °C in a muffle oven, sieved to 75 - 150 µm and impregnated[20] with 0.5 g of a solution containing 1.4 g sucrose, 0.14 g 95 wt% H_2SO_4 and 5.1 g H_2O. After drying at 120 °C for 72 h in stagnant air and decomposition of the carbon precursor at 200 °C (3 °C min^{-1}, 2 h) in a 1 L min^{-1} g^{-1} N_2 flow, 0.38 g of the resulting sample was impregnated with another 0.12 g of the acidic sucrose solution. The sample was dried at 60 °C for 19 h in stagnant air, followed by carbon precursor decomposition at 200 °C (3 °C min^{-1}, 2 h) in a 1 L min^{-1} g^{-1} air flow, crystallization at 600 °C (5 °C min^{-1}, 2 h) in a 1 L min^{-1} g^{-1} N_2 flow and carbon burn-off at 400 °C (3 °C min^{-1}, 4 h) in a 1 L min^{-1} g^{-1} air flow (Nb-CTC-S). Alternatively, 2 g niobium oxide hydrate was dried for 16 h at 120 °C in a muffle oven, sieved to 75 - 150 µm and impregnated[20] with 0.6 g of a mixture of 6 g furfuryl alcohol and 0.024 g anhydrous oxalic acid. After drying at 120 °C for 16 h in stagnant air, the carbon precursor was decomposed at 200 °C (3 °C min^{-1}, 2 h) in a 1 L min^{-1} g^{-1} air flow, the sample was crystallized at 600 °C (5 °C min^{-1}, 2 h) in a 1 L min^{-1} g^{-1} N_2 flow and carbon was burned off at 400 °C (3 °C min^{-1}, 4 h) in a 1 L min^{-1} g^{-1} air flow (Nb-CTC-F).

To synthesize crystalline niobia using a porous carbon template[13], 1 g activated carbon (AC, Norit, SX Ultra, A-5049, SA_{BET}: 839 m^{-2} g^{-1}, PV: 0.79 mL g^{-1}) was impregnated[20] with 3 g of a 200 g L^{-1} aqueous solution of ammonium niobium oxalate (ANO, CBMM, AD/4823), dried for 10 days at room temperature in stagnant air and at 120 °C (3 °C min^{-1}, 2 h) in a 1 L min^{-1} g^{-1} N_2 flow. The sample was crystallized at 600 °C (3 °C min^{-1}, 2 h) in a 1 L min^{-1} g^{-1} N_2 flow and the carbon template was burned off at 500 °C (3 °C min^{-1}, 2 h) in a 1 L min^{-1} g^{-1} air flow (Nb-ACTS). Alternatively, 2 g carbon black (CB, Cabot Black Pearls 2000, GP-3848, SA_{BET}: 1422 m^{-2} g^{-1}, PV: 1.8 mL g^{-1}) was impregnated twice with 4.4 g of a 200 g L^{-1} ANO (aq) solution and dried at 60 °C for 16 h in stagnant air after each impregnation step. The sample was crystallized at 600 °C (3 °C min^{-1}, 2 h) in a 1 L min^{-1} g^{-1} N_2 flow and the carbon template was burned off at 550 °C (3 °C min^{-1}, 2 h) in a 1 L min^{-1} g^{-1} air flow (Nb-CBTS).

Cobalt was deposited on amorphous niobia (Nb120M) or crystalline niobia (Nb600M). Prior to cobalt deposition, niobia pellets were pressed (125 MPa), crushed and sieved to 75 - 150 µm and dried under dynamic vacuum at 80 °C for 1 h. Impregnation[20] (IWI) was

performed with an aqueous 4.0 M $Co(NO_3)_2 \cdot 6\,H_2O$ (Acros, p.a.) solution, multiple impregnations were performed to achieve Co loadings > 5 wt%. After each impregnation, the catalyst was dried at 60 °C for 16 h in stagnant air and subsequently calcined at 350 °C (2 h, 3 °C min^{-1}) in a fixed bed reactor in a 1 L min^{-1} g^{-1} N_2 flow. Co loading was 4 - 21 wt% based on intake and was defined as the mass of metallic cobalt per gram of reduced catalyst.

For catalyst preparation using deposition precipitation by ammonia evaporation[16–18] (DPA, 7 - 9 wt% Co), 2.0 g Nb120M or Nb600M was suspended in a mixture of 6 mL of an aqueous 0.42 M $CoCO_3$ (Acros, p.a.), 7.5 M NH_3 (Merck, p.a.), 0.52 M $(NH_4)_2CO_3$ (Acros, p.a.) solution and 44 mL of a 9 wt% ammonia solution. In a PTFE flask equipped with a reflux cooler, the mixture was heated to 100 °C for 4.5 h to allow ammonia evaporation. After cooling to room temperature, the solids were filtered off, washed thoroughly with water and dried at 120 °C in stagnant air for at least 16 h and calcined at 400 °C (4 h, 5 °C min^{-1}) in a 1 L min^{-1} g^{-1} N_2 flow.

For catalyst preparation using deposition precipitation by urea hydrolysis[15] (DPU, 5 wt% Co), 3.1 g Nb120M or Nb600M was suspended in 1.5 L water and heated to 90 °C in a stirred, double-walled, thermostatic vessel. 0.83 g $Co(NO_3)_2 \cdot 6\,H_2O$ was added, the pH was adjusted to 3 by adding HNO_3 and 10 mL of a 4.7 M aqueous urea solution was added. After 16 h the pH was 9, the suspension was cooled to room temperature, solids were filtered off, washed thoroughly with water and dried at 120 °C in stagnant air for at least 16 h and calcined at 400 °C (4 h, 5 °C min^{-1}) in a 1 L min^{-1} g^{-1} N_2 flow.

Characterization

Powder X-ray diffraction (XRD) patterns were measured using a Bruker-AXS D2 Phaser X-ray diffractometer using Co-Kα radiation (λ = 1.789 Å). Co_3O_4 crystallite size was calculated by applying the Scherrer equation (k = 0.9) to the (311) diffraction line at 43.0 ° 2θ or in case of overlap with the crystalline support the (220) diffraction line at 36.5 ° 2θ. Environmental XRD was measured using a Bruker-AXS D8 Advance X-ray diffractometer using Co-Kα radiation (λ = 1.789 Å). Sample was heated to 350 °C (2 h, 5 °C min^{-1}) in 25 vol% H_2/He.

N_2 physisorption measurements were performed at -196 °C, using a Micromeritics TriStar 3000 apparatus. Prior to analysis, ~ 100 mg sample was dried at 120 °C for 20 h in an N_2 flow. Surface area was calculated using the BET theory for p/p_0 = 0.06 - 0.25. Pore size distribution was determined using the BJH theory applied to the adsorption branch. The pore volume was calculated using single point adsorption at p/p_0 = 0.98.

TEM samples were prepared by dispersing the sample in ethanol and allowing the ethanol to evaporate on the TEM grid at room temperature. For ultramicrotomy, the sample was embedded in a two-component epoxy resin (Epofix, EMS) and cured at 60 °C for at least 16 h. Using a Diatome Ultra 35 ° diamond knife mounted on a Reichert-Jung Ultracut E microtome, the embedded sample was cut in sections with a nominal thickness of 50 nm which were collected on a TEM grid. Bright field TEM imaging was performed on a Tecnai 12 operated at 120 kV and HR-TEM imaging on a Tecnai 20 equipped with a field emission gun and operated at 20 kV.

Temperature programmed reduction (TPR) experiments were performed using a Micromeritics Autochem 2920 instrument. Typically 100 mg sample was dried at 120 °C for 1 h in an Ar flow

and reduced up to 1000 °C (10 °C min^{-1}) in a 5 vol% H_2/Ar flow.

Hydrogen chemisorption measurements were performed using a Micromeritics ASAP 2020 instrument. Prior to the measurements, ~ 200 mg sample was dried for 1 h in dynamic vacuum at 100 °C and reduced in an H_2 flow at 350 °C (1 °C min^{-1}, 2 h). H_2 adsorption isotherms were measured at 150 °C, as recommended by Reuel for supported cobalt particles.[21] Metallic cobalt-specific surface area and average particle size were calculated assuming a surface stoichiometry H/Co = 1 and an atomic cross-sectional area of 0.0662 nm^2.

Fischer-Tropsch synthesis

Catalyst testing was performed in a quartz glass plug-flow reactor (i.d. = 3 mm), typically loaded with 15 - 20 mg catalyst grains (38 - 150 μm), diluted with 200 mg SiC (200 - 400 μm). The catalysts were reduced in situ at 350 °C (5 °C min^{-1}, 2 h) in a 20/40 mL min^1 H_2/Ar flow. Fischer-Tropsch catalysis was performed at 220 °C, 1 bar, H_2/CO = 2.0, GHSV = 24 - 48 * 10^3 h^{-1}, CO conversion < 5 %. C_1-C_{18} products were analyzed by online gas chromatography (Varian 430 GC, CP sil-5 column). Activity and selectivities were reported after at least 40 h on stream. GHSV was defined as total gas flow divided by the catalyst volume.

Table 2.1. Niobia phase, BET surface area (SA_{BET}), pore volume (PV) and pore diameter (PD) for niobia prepared by niobium oxide hydrate crystallization in a muffle oven, in a quartz reactor, by carbon-templated crystallization of niobium oxide hydrate and subsequent carbon burn-off and by decomposition of ammonium niobium oxalate without template and in an activated carbon (AC) or carbon black (CB) template and subsequent carbon burn-off. For physisorption isotherms and pore size distributions see Appendix A, Figure A3 - A6.

Sample designation	Crystallization conditions	Niobia phase	SA_{BET} (m^2 g^{-1})	PV (mL g^{-1})	PD (nm)
Nb120M	120 °C, muffle oven	Amorphous	173	0.19	2 - 5
Nb400M	400 °C, muffle oven	Amorphous	86	0.12	2 - 7
Nb600M	600 °C, muffle oven	T	16	0.06	> 50
Nb600SA	600 °C, stagnant air, quartz reactor	TT	25	0.11	5 - 60
Nb600AF	600 °C, air flow, quartz reactor	TT	22	0.06	5 - 25
Nb600NF	600 °C, N_2 flow, quartz reactor	TT	22	0.06	5 - 25
Nb-CTC-S	Carbon-templated crystallization - sucrose-based	TT	75	0.10	2 - 12
Nb-CTC-F	Carbon-templated crystallization - furfuryl alcohol-based	TT	55	0.11	2 - 18
Nb-S-NT	Niobia synthesis, no template	TT	9	0.03	< 5
Nb-ACTS	AC-templated niobia synthesis	T, NbO_2	32	0.12	5 - 60
Nb-CBTS	CB-templated niobia synthesis	T, NbO_2	27	0.16	10 - 100

Results and discussion

Niobia crystallization

An overview of the niobia samples prepared in this chapter including sample designations is shown in Table 2.1.

Thermal treatment niobium oxide hydrate

Niobium oxide hydrate was found to be X-ray amorphous after calcination in a muffle oven up to 400 °C (Figure 2.1) After calcination at 500 °C, low-crystalline pseudo-hexagonal Nb_2O_5 (TT-phase) was observed. Splitting of the peaks at 33 ° 2θ and 42 ° 2θ after calcination above 600 °C indicated transformation to orthorhombic Nb_2O_5 (T-phase). After calcination at 900 °C, monoclinic Nb_2O_5 was observed in line with previous results.[4,22,23]

Using Transmission Electron Microscopy (TEM) 50 - 200 nm particles with 2 - 5 nm mesopores were observed after drying at 120 °C (Figure 2.2A). After calcination at 600 °C in a muffle oven, the 2 - 5 nm mesopores had disappeared and the size of the primary particles decreased to 20 - 100 nm as shown in Figure 2.2B. Using high resolution TEM (Figure 2.2C), lattice planes with a spacing of 0.39 nm were observed, corresponding to the (001) diffraction observed using XRD at 26.4 ° 2θ for orthorhombic (T-phase) Nb_2O_5

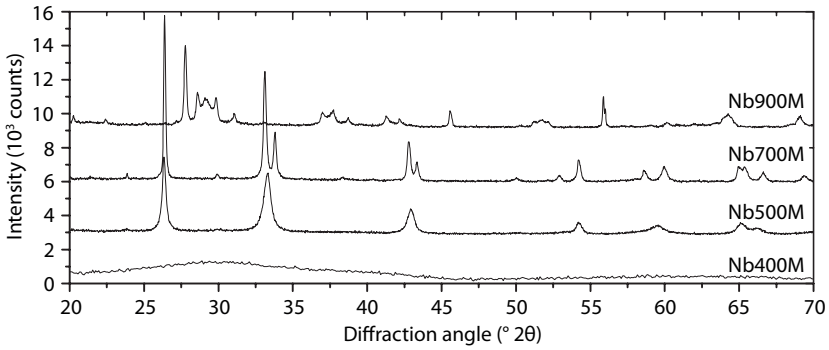

Figure 2.1. X-ray diffractograms (Co-Kα radiation) for Nb400M, Nb500M, Nb700M and Nb900M.

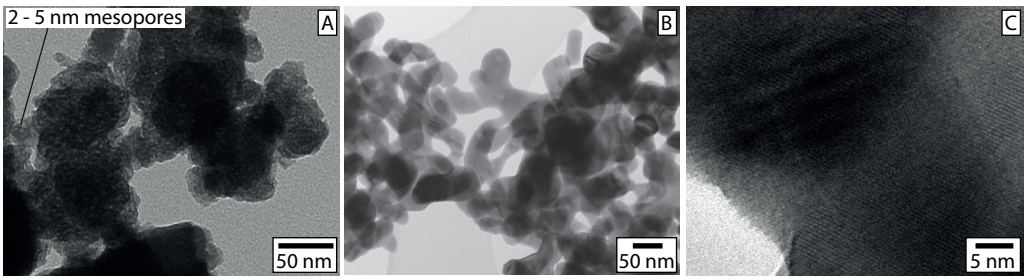

Figure 2.2. Bright field TEM images for Nb120M (A) and Nb600M (B, C).

The mesoporosity of niobia after thermal treatment at 120 - 900 °C was determined using nitrogen physisorption. The hysteresis observed at p/p_0 = 0.4 - 0.7 indicated the presence of 2 - 5 nm mesopores after thermal treatment up to 400 °C which disappeared upon calcination at higher temperatures (Figure 2.3A, additional isotherms in Appendix A), as also observed using TEM. After calcination at 600 °C only hysteresis at p/p_0 = 0.9 was apparent (pores > 50 nm), brought about by the porosity between the Nb_2O_5 particles (Figure 2.3B). After drying at 120 °C, the BET surface area and mesopore volume were found to be 173 $m^2 g^{-1}$ and 0.19 mL g^{-1} respectively and decreased upon thermal treatment (Figure 2.3C), which is in agreement with data reported by Chai et al.[4]

Modified niobia crystallization

The influence of the gas atmosphere (stagnant air, air flow or N_2 flow) during niobia crystallization at 600 °C in a plug flow reactor was investigated. Independent of the gas flow, pseudohexagonal niobia (TT-phase) with a BET surface of 22 - 25 $m^2 g^{-1}$ was obtained (Table 2.1). Upon calcination in stagnant air, a higher pore volume (0.11 mL g^{-1}) was obtained than after calcination in an N_2 or air flow (0.06 mL g^{-1}).

To further inhibit porosity loss, niobia pores were filled with a carbon precursor prior to crystallization. Niobium oxide hydrate was impregnated with a sucrose or furfuryl alcohol solution and subsequently crystallized in an N_2 flow. After impregnation and pyrolysis, the niobia pores were found to be not accessible for nitrogen adsorption (Appendix A, Figure A4 - A5).

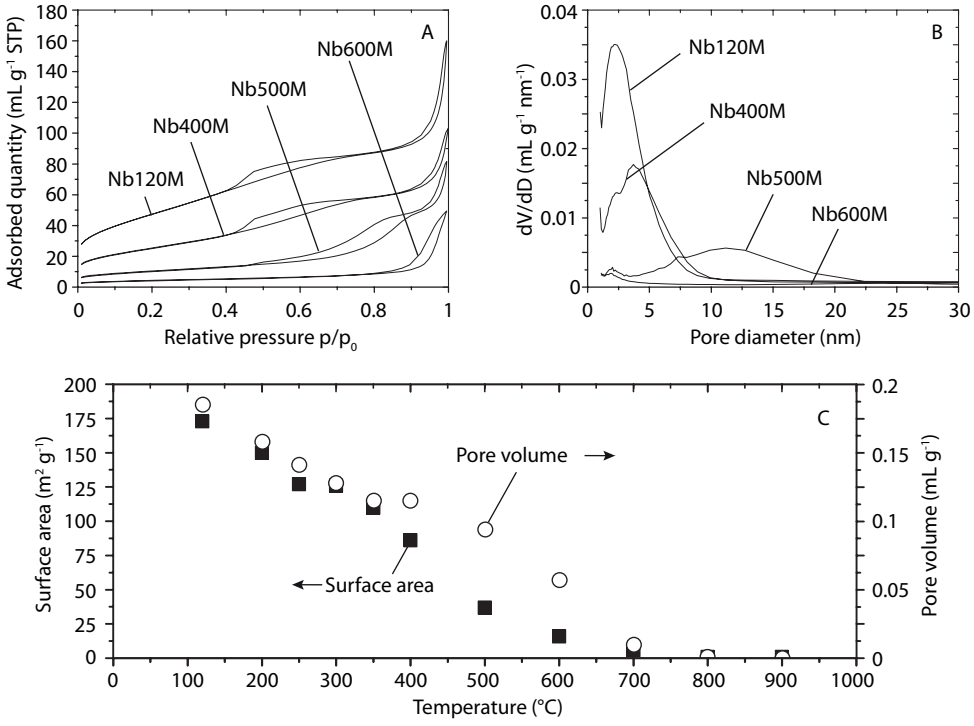

Figure 2.3. N_2 physisorption isotherms (A) and pore size distributions (B) for Nb120M, Nb400M, Nb500M and Nb600M and BET surface area and pore volume for NbxM (C).

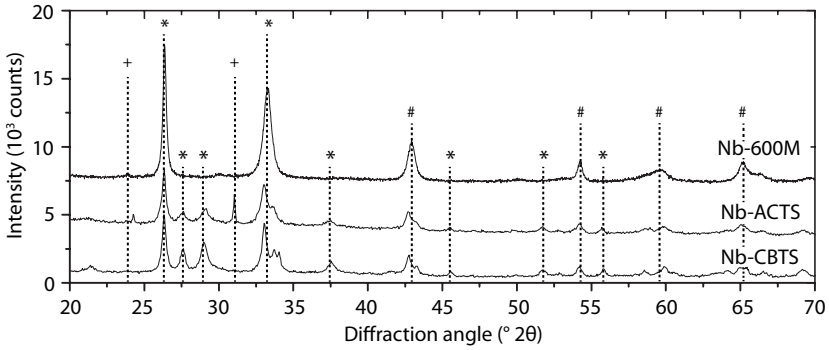

Figure 2.4. X-ray diffractograms (Co-Kα radiation) for Nb600M, Nb-ACTS and Nb-CBTS. * indicate Nb_2O_5 (TT- or T-phase) lines, # indicate NbO_2 lines, + indicate activated carbon lines

Table 2.2. Support, cobalt deposition method, cobalt loading based on intake, cobalt particle size based on H_2 chemisorption (d_{app}) and cobalt-weight normalized activity and C_{5+} selectivity in Fischer-Tropsch synthesis at 1 bar, 220 °C, H_2/CO = 2.0 v/v for Co/niobia catalysts.

Catalyst designation	Support	Co deposition method	Co loading (wt%)	d_{app} (nm)	Activity ($mol_{CO}\ g_{Co}^{-1}\ s^{-1}$)	C_{5+} selectivity (wt%)
4IWI-Nb120M	Nb120M	IWI, 1x	4			
10IWI-Nb120M	Nb120M	IWI, 2x	10		$< 0.3 * 10^{-5}$	45
14IWI-Nb120M	Nb120M	IWI, 3x	14			
5IWI-Nb400M	Nb400M	IWI, 1x	5		$0.5 * 10^{-5}$	49
5IWI-Nb600M	Nb600M	IWI, 1x	5	18	$3.0 * 10^{-5}$	70
10IWI-Nb600M	Nb600M	IWI, 2x	10	29	$2.5 * 10^{-5}$	64
15IWI-Nb600M	Nb600M	IWI, 3x	15	19	$2.2 * 10^{-5}$	60
17IWI-Nb600M	Nb600M	IWI, 4x	17	23	$1.5 * 10^{-5}$	55
21IWI-Nb600M	Nb600M	IWI, 4x	21	35	$2.1 * 10^{-5}$	42
6IWI-Nb-CTC-F	Nb-CTC-F	IWI	6		$0.5 * 10^{-5}$	48
9DPA-Nb120M	Nb120M	DPA	9			
7DPA-Nb600M	Nb600M	DPA	7		$0.6 * 10^{-5}$	51
5DPU-Nb120M	Nb120M	DPU	5		$< 0.1 * 10^{-5}$	-
5DPU-Nb600M	Nb600M	DPU	5		$0.6 * 10^{-5}$	42

After crystallization and carbon burn-off, pseudohexagonal niobia (TT-phase) with mainly 5 - 10 nm pores was obtained. Surface area and pore volume were found to be higher due to carbon-templated crystallization (Table 2.1). However, the enhanced porosity mainly involved pores < 10 nm. The off-white color of the sample after carbon burn-off indicated that carbon was not completely removed or niobia was partially reduced.

Carbon-templated niobia synthesis

Crystalline niobia was synthesized using porous carbon as template by impregnation with an ammonium niobium oxalate solution, decomposition and crystallization in a nitrogen flow and subsequent carbon burn-off in an air flow. The predominant phase after carbon burn-off was the orthogonal (T) niobia phase, whereas after crystallization of niobium oxide hydrate pseudohexagonal (TT) niobia was observed (Figure 2.4). Additional diffraction peaks were attributed to NbO_2, the latter probably formed due to partial reduction of Nb_2O_5 during carbon burn-off. The diffraction peaks at 24 and 31 ° 2θ were attributed to remains of the activated carbon template.

Surface area and pore volume were found to be higher for Nb-ACTS and Nb-CBTS than for Nb600M (Table 2.1). Especially the increased pore diameter after synthesis using a carbon black template (Nb-CBTS) was promising; however, surface area and pore volume are still low compared to typical Fischer-Tropsch catalyst supports like TiO_2, SiO_2 or γ-Al_2O_3 and will impede facile catalyst preparation and application of high cobalt loadings.

Cobalt deposition

An overview of the catalysts prepared in this chapter including sample properties is shown in Table 2.2.

Impregnation

Niobia-supported catalysts were prepared by (multiple) impregnation of amorphous (Nb120M) or crystallized niobia (Nb600M) with a cobalt nitrate solution, aiming for 4 - 21 wt% Co loading. Using XRD no crystalline cobalt species were observed after cobalt deposition on amorphous niobia up to 10 wt% Co (Figure 2.5A). For 14IWI-Nb120M, crystalline Co_3O_4 was observed in the calcined sample, the crystallite size was estimated to be 9 nm.

After impregnation and cobalt nitrate decomposition on Nb600M, no crystalline cobalt species were observed up to 10 wt% Co (Figure 2.5B). Also after reduction in 25 vol% H_2/He at 350 °C in the X-ray diffractometer, no crystalline cobalt was observed up to 10 wt% Co loading, indicating that at low loadings, independent of support pretreatment, very small or poorly crystalline cobalt or Co-Nb species were formed. After 3 and 4 impregnation cycles (> 13 wt% Co), crystalline Co_3O_4 was observed. Noronha et al. also observed that up to a certain albeit different loading, no crystalline cobalt species could be detected for Co/Nb_2O_5 catalysts.[2]

Imaging Co/niobia catalysts using transmission electron microscopy, and especially distinguishing between cobalt oxide and niobia, is difficult due to the similar electron density of Nb_2O_5 and Co_3O_4. In the pores between the niobia particles, irregularly shaped 5 - 30 nm cobalt

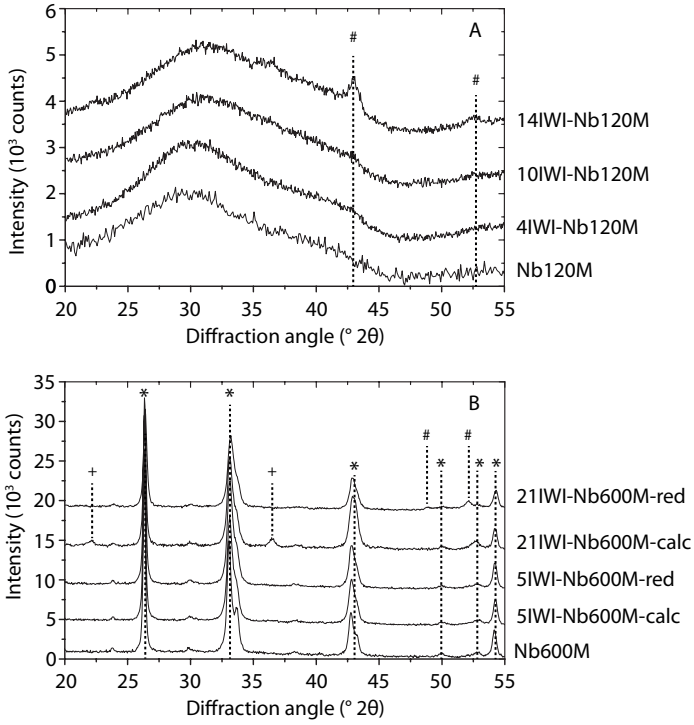

Figure 2.5. X-ray diffractograms (Co-Kα radiation) for Nb120M and calcined 4-14IWI-Nb120M catalysts (A) and for Nb600M and calcined (calc) or in situ reduced (red) 5-21IWI-Nb600M catalysts (B). * indicate Nb_2O_5 lines (T-phase), $^{+}$ indicate Co^0 lines, $^{\#}$ indicate Co_3O_4 lines.

oxide particles were observed (Figure 2.6). Due to the irregular shape of the cobalt oxide particles and the low contrast between niobium oxide and cobalt oxide, determining an accurate particle size distribution was not possible based on the current TEM study. After cobalt deposition on Nb120M, no cobalt oxide particles were observed, indicating the formation of cobalt oxide particles < 2 nm or mixed Co-Nb species.

For 5IWI-Nb600M, cobalt reduction was found to occur in two steps (Figure 2.7), reported before to be the reduction of Co_3O_4 to CoO and CoO to metallic Co.[2,24,25] The reduction temperature was found to be significantly lower than for Co/SiO_2 and $Co/\gamma\text{-}Al_2O_3$ and allows reduction at temperatures < 400 °C without the application of noble metal promoters.[26]

For 10IWI-Nb120M and 6IWI-Nb350M no distinct cobalt oxide reduction peaks were observed up to 400 °C (Figure 2.7). The continuous H_2 consumption was attributed to reduction of the support. The reason for this variant reduction behavior might be that no Co_3O_4 was formed after cobalt nitrate decomposition but cobalt was present as a mixed Co-Nb phase.

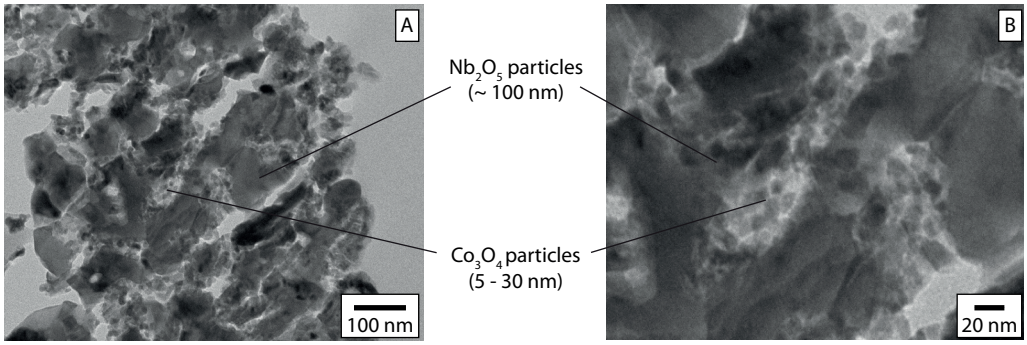

Figure 2.6. Bright field TEM images for calcined 10IWI-Nb600M. TEM sample was prepared using ultramicrotomy.

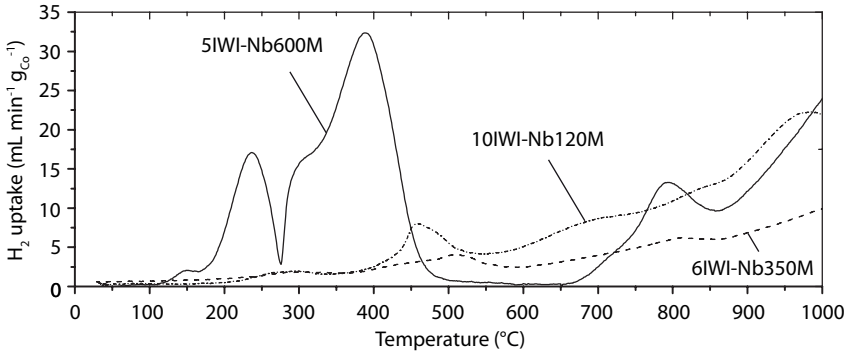

Figure 2.7. Temperature programmed reduction profiles for 10IWI-Nb120M, 6IWI-Nb350M and 5IWI-Nb600M.

Using H_2 chemisorption, the apparent cobalt particle size was determined for 5-21IWI-Nb600M (Table 2.2) and was found to increase with increasing cobalt loading as reported before.[3] For 4-14IWI-Nb120M and 6IWI-Nb350M, no or low H_2 uptake was observed during chemisorption, indicating that no metallic cobalt was accessible after reduction at 350 °C.

Cobalt deposition using deposition precipitation

To prepare catalysts with higher metal loadings in a single step and obtain more homogeneous dispersions and distributions, cobalt was deposited using deposition precipitation (DP). Starting from a basic or acidic aqueous solution containing the support and a cobalt precursor, cobalt was deposited by slowly decreasing the pH from basic to neutral by ammonia evaporation (DPA) or increasing the pH from acidic to neutral by urea hydrolysis (DPU)

Using TEM, large 50 - 100 nm clusters of cobalt particles were observed for 7DPA-Nb600M (Figure 2.8A). Probably precipitation of cobalt in the solution had occurred due to weak interaction between the support surface and the precipitating cobalt species. Using XRD, crystalline Co_3O_4 was observed with a crystallite size of 22 nm.

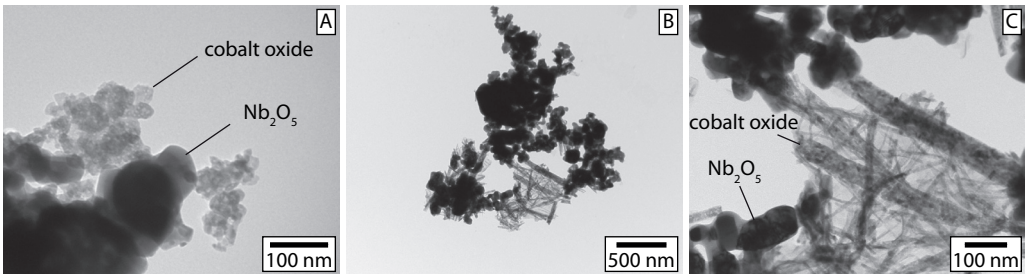

Figure 2.8. Bright field TEM images for calcined 7DPA-Nb600M (A) and calcined 5DPU-Nb600M (B, C).

8 - 20 nm thick needles with a length up to 1 μm were observed using TEM for calcined 5DPU-Nb600M (Figure 2.8B, C). Nucleation and growth of unsupported cobalt needles was probably caused by limited or repulsive interaction between the support surface and the precipitating cobalt species. No crystalline cobalt species were observed using XRD.

For 9DPA-Nb120M and 5DPU-Nb120M, no cobalt species were observed using TEM, probably due to the formation of mixed Co-Nb species or a similar morphology of cobalt oxide and amorphous niobia. Using XRD no crystalline cobalt species were observed.

Fischer-Tropsch synthesis

The performance of Co/niobia was investigated in Fischer-Tropsch catalysis at 1 bar, 220 °C, $H_2/CO = 2.0$. After reduction at 350 °C, a combination of high activity ($3 * 10^{-5}$ mol_{CO} g_{Co}^{-1} s^{-1}) and C_{5+} selectivity (~ 70 wt%) was observed after 40 h on stream for 5IWI-Nb600M (Figure 2.9A), previously only observed for a Pt- and MnO-promoted Co/SiO_2 catalyst.[27] The activity decrease was mainly due to decreasing methane production while the absolute C_{5+} production remained constant, yielding an increasing C_{5+} selectivity.

After reduction at 500 °C, the cobalt-weight normalized activity of 5IWI-Nb600M was a factor of 10 lower than after reduction at 350 °C. This could be explained by coverage of the cobalt particles due to SMSI at high reduction temperatures. A decreased number of active sites and associated activity decrease with increasing reduction temperature was also observed by Silva et al.[1]

For 10IWI-Nb120M and 5IWI-Nb350M low activity was observed (Table 2.2), which was attributed to the formation of non-reducible cobalt or Co-Nb species during catalyst preparation and the absence of metallic cobalt after catalyst reduction, as observed using TPR and H_2 chemisorption respectively. Another explanation is that cobalt was present in the 2 - 5 nm pores and was not accessible for catalysis or was encapsulated by niobia during cobalt nitrate decomposition or catalyst reduction. Apparently, niobia was too reactive without niobia crystallization to allow formation of easily reducible cobalt particles and crystalline Nb_2O_5 was required to act as a support material for Co/niobia catalysts. For 6IWI-Nb-CTC-F the activity ($0.5 * 10^{-5}$ mol_{CO} g_{Co}^{-1} s^{-1}) and C_{5+} selectivity (48 wt%) were significantly lower than after niobia crystallization without carbon template (Table 2.2).

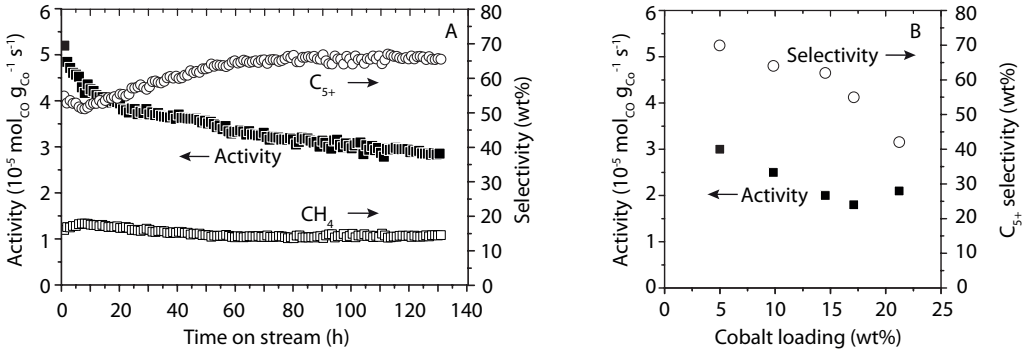

Figure 2.9. Cobalt-weight normalized activity and selectivity in Fischer-Tropsch synthesis at 1 bar, 220 °C, $H_2/CO = 2.0$ for 5IWI-Nb600M (A) and after 40 h on stream for 5-21IWI-Nb600M (B).

Cobalt-weight normalized activity and C_{5+} selectivity were observed to be inferior for 9DPA-Nb600M and 5DPU-Nb600M, compared to 5IWI-Nb600M (Table 2.2). The lower activity could be explained by the low cobalt dispersion due to the formation of large unsupported particles. The lower C_{5+} selectivity could be explained by limited cobalt-support interaction due to the presence of unsupported cobalt and decreased selectivity promotion by the support.

For catalysts prepared by multiple impregnation cycles of Nb600M, the catalyst-weight normalized activity increased (Appendix A, Table A3) but the cobalt-weight normalized activity decreased (Figure 2.9B). This could be partially explained by decreased dispersion of cobalt as observed by H_2 chemisorption (Table 2.2). Higher Co loading might lead to the formation of larger particles, due to particle growth during subsequent impregnations or by sintering due to the decreased interparticle distance at higher Co loading.

The C_{5+} selectivity was found to decrease with increasing cobalt loading (Figure 2.9B). Up to 10 wt% Co, the C_{5+} selectivity was largely maintained but decreased at higher loadings. In larger particles a smaller fraction of the cobalt will be in close vicinity to the niobia support. This indicates that at the cobalt-niobia interface the chain growth probability is higher. A decreasing C_{5+} selectivity with increasing cobalt loading was also observed for Co/Nb_2O_5 catalysts in Fischer-Tropsch synthesis at 20 bar as shown in Chapter 3.[3]

Conclusions

Niobium oxide hydrate was found to be amorphous and exhibited an intricate pore structure with 2 - 5 nm mesopores. Upon thermal treatment these pores disappeared, the surface area and porosity decreased drastically and crystallization occurred at thermal treatment above 400 °C.

Higher surface area and pore volume crystalline niobia was obtained by carbon-templated niobia crystallization or carbon templated niobia synthesis. Due to partial reduction during carbon burn-off, NbO_2 was partially formed.

After cobalt deposition using impregnation, crystalline Co_3O_4 was only observed at cobalt loadings > 10 wt%. Deposition precipitation of cobalt yielded precipitation in the solution due to low or repulsive interaction between the support and the precipitating agent.

Niobia crystallization prior to cobalt deposition was found to be required to allow formation of reducible cobalt species. Consequently no activity in Fischer-Tropsch synthesis was observed for catalysts prepared using amorphous niobia.

After reduction at 350 °C, very high C_{5+} selectivity and high cobalt-weight normalized activity were observed for 5 wt% Co/Nb_2O_5 prepared by impregnation of crystalline Nb_2O_5, previously only observed for promoted Co catalysts. Co/Nb_2O_5 reduction at 500 °C significantly decreased the catalyst activity, probably due to severe SMSI covering the cobalt surface sites.

Application of higher cobalt loadings than 5 wt% led to increased catalyst-weight normalized activity; however, the cobalt-weight normalized activity decreased due to formation of larger cobalt particles and decreased interaction of cobalt with the support. Selectivity promotion by niobia was suppressed due to decreased cobalt-support interaction and consequently lower C_{5+} selectivities were observed.

Acknowledgements

Dr. Robson Monteiro and Mr. Rogério Ribas (CBMM) are acknowledged for useful discussions and for supplying niobia and ANO samples. Mr. Hans Meeldijk (HR-TEM), Dr. Peter Munnik (ultramicrotomy, TEM), Mrs. Marjan Versluijs-Helder (TGA, XRD), Dr. Carlo Angelici (TPR), Dr. Thomas Eschemann (TPR), Dr. Korneel Cats (TPR) and Mr. Gang Wang (TPR) are acknowledged for assistance and execution of indicated analyses.

References

[1] Silva, R. R. C. M.; Schmal, M.; Frety, R.; Dalmon, J. A. *J. Chem. Soc. - Faraday Trans.* **1993**, *89*, 3975–3980.
[2] Noronha, F. B.; Perez, C. A.; Frety, R. *Phys. Chem. Chem. Phys.* **1999**, *1*, 2861–2867.
[3] den Otter, J. H.; de Jong, K. P. *Top. Catal.* **2014**, *57*, 445–450.
[4] Chai, S.; Wang, H.-P.; Liang, Y.; Xu, B.-Q. *J. Catal.* **2007**, *250*, 342–349.
[5] Kondo, J. N.; Domen, K. *Chem. Mater.* **2008**, *20*, 835–847.
[6] Nowak, I.; Ziolek, M. *Chem. Rev.* **1999**, *99*, 3603–3624.
[7] Sun, T.; Ying, J. Y. *Angew. Chemie, Int. Ed.* **1998**, *37*, 664–667.
[8] Prakash, A. M.; Kevan, L. *J. Am. Chem. Soc.* **1998**, *120*, 13148–13155.
[9] Yang, P.; Zhao, D.; Margolese, D. I.; Chmelka, B. F.; Stucky, G. D. *Nature* **1998**, *396*, 152–155.
[10] Yang, P.; Zhao, D.; Margolese, D. I.; Chmelka, B. F.; Stucky, G. D. *Chem. Mater.* **1999**, *11*, 2813–2826.
[11] Lee, J.; Orilall, M. C.; Warren, S. C.; Kamperman, M.; DiSalvo, F. J.; Wiesner, U. *Nat. Mater.* **2008**, *7*, 222–228.
[12] Lee, S.; Teshima, K.; Niina, Y.; Suzuki, S.; Yubuta, K.; Shishido, T.; Endo, M.; Oishi, S. *CrystEngComm* **2009**, *11*, 2326-2331.
[13] Schwickardi, M.; Johann, T.; Schmidt, W.; Schüth, F. *Chem. Mater.* **2002**, *14*, 3913–3919.
[14] de Jong, K. P. In: *Synthesis of Solid Catalysts*; de Jong, K. P., Ed.; Wiley-VCH: Winnheim, **2009**; pp. 111–132.
[15] Morales, F.; Grandjean, D.; Mens, A.; de Groot, F. M. F.; Weckhuysen, B. M. *J. Phys. Chem. B* **2006**, *110*, 8626–8639.
[16] Lok, C. M. European patent EP 1542794 A1 **2010**.
[17] Bezemer, G. L.; Radstake, P. B.; Koot, V.; van Dillen, A. J.; Geus, J.; de Jong, K. P. *J. Catal.* **2006**, *237*, 291–302.

[18] Bonne, R. L. C.; Lok, C. M. World patent WO 1996/004072 A1 **1996**.
[19] Chai, S.-H.; Wang, H.-P.; Liang, Y.; Xu, B.-Q. *Green Chem.* **2007**, *9*, 1130-1136.
[20] Munnik, P.; de Jongh, P. E.; de Jong, K. P. *Chem. Rev.* **2015**, *115*, 6687–6718.
[21] Reuel, R. C. *J. Catal.* **1984**, *85*, 63–77.
[22] Frevel, L. K.; Rinn, H. W. *Anal. Chem.* **1955**, *27*, 1329–1330.
[23] Schäfer, H.; Gruehn, R.; Schulte, F. *Angew. Chemie, Int. Ed.* **1966**, *5*, 40–52.
[24] Sexton, B. *J. Catal.* **1986**, *97*, 390–406.
[25] Jacobs, G.; Ji, Y.; Davis, B. H.; Cronauer, D.; Kropf, A. J.; Marshall, C. L. *Appl. Catal., A* **2007**, *333*, 177–191.
[26] Jacobs, G.; Das, T. K.; Zhang, Y.; Li, J.; Racoillet, G.; Davis, B. H. *Appl. Catal., A* **2002**, *233*, 263–281.
[27] den Breejen, J. P.; Frey, A. M.; Yang, J.; Holmen, A.; Schooneveld, M. M.; Groot, F. M. F.; Stephan, O.; Bitter, J. H.; de Jong, K. P. *Top. Catal.* **2011**, *54*, 768–777.

Chapter 3

Highly Selective and Active Niobia-supported Cobalt Catalysts for Fischer-Tropsch Synthesis

Abstract

The performance of Co/Nb_2O_5 was compared to that of $Co/\gamma\text{-}Al_2O_3$ for the Fischer-Tropsch synthesis at 20 bar and over the temperature range of 220 - 260 °C. The C_{5+} selectivity of Nb_2O_5-supported cobalt catalysts was found to be very high, i.e. up to 90 wt% C_{5+} at 220 °C. The cobalt-weight normalized activity was found to be similar for Nb_2O_5- and $\gamma\text{-}Al_2O_3$-supported catalysts at identical reaction temperature. However, due to the low porosity of crystalline Nb_2O_5, the cobalt loading was limited to 5 wt% and consequently the cobalt-weight normalized activity was lower than of $Co/\gamma\text{-}Al_2O_3$ catalysts with higher cobalt loadings. This low activity was largely compensated by increasing the reaction temperature, although the C_{5+} selectivity decreased upon increasing reaction temperature. Due to the high intrinsic C_{5+} selectivity, Nb_2O_5-supported catalysts could be operated up to ~ 250 °C at a target C_{5+} selectivity of 80 wt%, whereas $\gamma\text{-}Al_2O_3$-supported catalysts called for an operation temperature of ~ 210 °C. At this target C_{5+} selectivity, the catalyst-weight normalized activity was found to be identical for 5 wt% Co/Nb_2O_5 and 28 wt% $Co/\gamma\text{-}Al_2O_3$, while the cobalt-weight normalized activity was a factor of four higher for the Nb_2O_5-supported catalyst.

Introduction

For Co/Nb_2O_5 catalysts, very high selectivities towards heavy hydrocarbons were reported by Schmal and coworkers.[1–5] In these studies, catalyst activity was investigated at atmospheric pressure and in a limited temperature range. The support material was thermally treated at 500 - 600 °C to obtain crystalline Nb_2O_5, prior to cobalt deposition. The porosity of crystalline Nb_2O_5 is low compared to typical supports for Fischer-Tropsch catalysts like γ-Al_2O_3 and SiO_2. This complicates catalyst preparation and limits the cobalt loading to ~ 5 wt% for Nb_2O_5-supported catalysts, with consequent low catalyst-weight normalized activities compared to γ-Al_2O_3- and SiO_2-supported catalysts with cobalt loadings up to 20 wt%.

In this chapter, the influence of a wide range of reaction temperatures on the activity and selectivity of Nb_2O_5-supported cobalt Fischer-Tropsch catalysts is investigated. 5 - 17 wt% Co/Nb_2O_5 catalysts are prepared and applied in Fischer-Tropsch synthesis at 20 bar in the temperature range 220 - 260 °C. The performance of these catalysts is investigated in comparison to 28 wt% Co/γ-Al_2O_3.

Experimental methods

Preparation

Niobium oxide hydrate (HY-340, AD/4465, 72.6 wt% Nb_2O_5, LOI 26.7 wt%, purity data see Appendix A) was obtained from Companhia Brasileira de Metalurgia e Mineração - CBMM and calcined at 600 °C (5 °C min^{-1}, 2 h) in stagnant air to obtain crystalline Nb_2O_5 (T-phase, SA_{BET}: 16 m^2 g^{-1}, PV: 0.06 mL g^{-1}). Co/Nb_2O_5 catalysts were prepared via a single (5 wt%), double (10 wt%) or fourfold (21 wt%) impregnation of the crystalline Nb_2O_5 with an aqueous 4.0 M $Co(NO_3)_2 \cdot 6\,H_2O$ solution (Acros, > 99 %). Co/γ-Al_2O_3 catalysts were prepared via a double impregnation of γ-Al_2O_3 (Puralox SSCa-5/200, SA_{BET}: 185 m^2 g^{-1}, PV: 0.5 mL g^{-1}) with an aqueous 4.0 M $Co(NO_3)_2 \cdot 6\,H_2O$ solution, aiming for a cobalt loading of 28 wt%. After each impregnation step, the catalysts were dried for 16 h at 60 °C in stagnant air and subsequently calcined at 350 °C (3 °C min^{-1}, 2 h) in a fixed bed reactor in a 1 L min^{-1} g_{cat}^{-1} N_2 flow. Cobalt loading is expressed as the mass of metallic cobalt per gram of reduced catalyst.

Characterization

Temperature programmed reduction (TPR) experiments were performed using a Micromeritics Autochem 2920 instrument. Typically 100 mg sample was dried at 120 °C for 1 h in an Ar flow and reduced up to 1000 °C (10 °C min^{-1}) in a 5 vol% H_2/Ar flow. The degree of reduction was determined from the H_2 uptake during isothermal reduction at 350 °C (Co/Nb_2O_5) or 500 °C (Co/γ-Al_2O_3) for 3 h (Appendix B, Figure B1). $H_2/Co = 1.33$ was assumed for full reduction from Co_3O_4 to Co.

H_2 chemisorption measurements were performed using a Micromeritics ASAP 2020 instrument. Prior to the measurements, ~ 200 mg sample was dried for 1 h in dynamic vacuum

at 100 °C and reduced in an H_2 flow at 350 °C (Co/Nb_2O_5) or 500 °C ($Co/\gamma\text{-}Al_2O_3$), 5 °C min^{-1}, 2 h. H_2 adsorption isotherms were measured at 150 °C, as recommended by Reuel for supported cobalt particles.[6] Metallic cobalt-specific surface area and average particle size were calculated assuming a surface stoichiometry H/Co = 1 and an atomic cross-sectional area of 0.0662 nm^2.

Fischer-Tropsch synthesis

Catalytic testing was performed using an Avantium Flowrence 16 parallel, continuous flow, fixed bed reactor system. 20 - 200 mg catalyst (38 - 75 μm) was diluted with 100 - 200 mg SiC (200 μm) and loaded in a stainless steel reactor, i.d. = 2 mm, to achieve a bed height of 4 - 6 cm. The catalysts were reduced in situ at atmospheric pressure in a 25 vol% H_2/He flow, GHSV 1 - 20 * 10^3 h^{-1}, for 8 h at 350 °C (Co/Nb_2O_5) or 500 °C ($Co/\gamma\text{-}Al_2O_3$) with a heating rate of 1 °C min^{-1}. After cooling to 180 °C the gas stream was switched to synthesis gas, H_2/CO = 2.0 v/v, GHSV 1 - 20 * 10^3 h^{-1}, and the reactors were pressurized to 20 bar and subsequently heated to the reaction temperature (1 °C min^{-1}). Fischer-Tropsch synthesis was performed at 220 - 260 °C. The GHSV was adjusted to obtain 40 - 60 % CO conversion. Products up to C_9 were analyzed using an online Agilent Technologies 7890A gas chromatograph. The reported catalyst performance was determined after at least 80 h on stream. The GHSV was defined as the total gas flow divided by the catalyst volume.

Results and discussion

Cobalt oxide deposited on Nb_2O_5 was found to be reduced in two steps (Figure 3.1). These steps were previously reported to be the reduction of Co_3O_4 to CoO and CoO to metallic Co.[7–9] The peak maxima were found at 235 and 395 °C respectively for 5 wt% Co/Nb_2O_5. H_2 consumption above 500 °C was attributed to reduction of the support. The reduction of Co_3O_4 deposited on $\gamma\text{-}Al_2O_3$ was found to occur at significantly higher temperatures, 300 and 660 °C respectively, for 28 wt% $Co/\gamma\text{-}Al_2O_3$ (Figure 3.1). The onset of the second peak was found at significantly lower temperatures than the peak maxima, 300 °C and 450 °C respectively, so for the catalytic tests isothermal reduction for 8 h at 350 °C for Co/Nb_2O_5 and 500 °C for $Co/\gamma\text{-}Al_2O_3$ was performed.

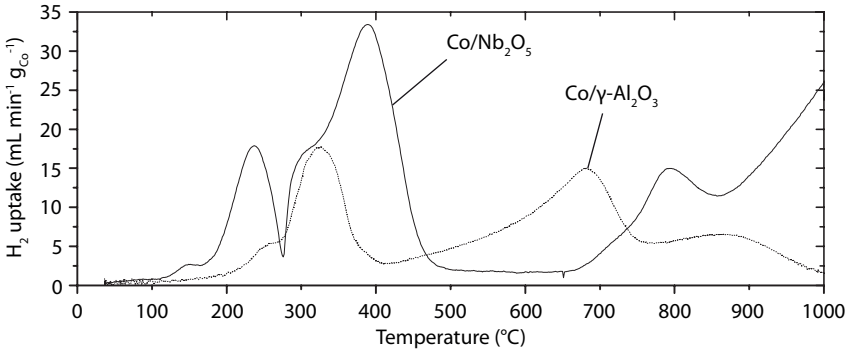

Figure 3.1. Temperature programmed reduction profiles for 5 wt% Co/Nb_2O_5 and 28 wt% $Co/\gamma\text{-}Al_2O_3$.

Table 3.1. Surface-specific cobalt loading based on intake and metallic cobalt-specific surface area (MSA) and cobalt particle size (d_{app}) for 5 - 21 wt% Co/Nb_2O_5 and 28 wt% $Co/\gamma\text{-}Al_2O_3$, determined using H_2 chemisorption.

Catalyst	Cobalt loading ($mg_{Co}\ m_{support}^{-2}$)	MSA ($m^2\ g_{Co}^{-1}$)	d_{app} (nm)
5 wt% Co/Nb_2O_5	3.3	37	18
10 wt% Co/Nb_2O_5	7.2	22	30
21 wt% Co/Nb_2O_5	17	17	39
28 wt% $Co/\gamma\text{-}Al_2O_3$	2.1	37	18

The degree of reduction was calculated from the total H_2 uptake during isothermal reduction at 350 °C for Co/Nb_2O_5 and 500 °C for $Co/\gamma\text{-}Al_2O_3$ (Appendix B, Figure B1). The degree of reduction was estimated to be ~ 90 % for 5 wt% Co/Nb_2O_5 and ~ 60 % for 28 wt% $Co/\gamma\text{-}Al_2O_3$. Reduction of $Co/\gamma\text{-}Al_2O_3$ at 500 °C is known to occur non-quantitative[10] and could theoretically be enhanced by a higher reduction temperature or the addition of a noble metal promoter. However, a higher reduction temperature will also lead to more extensive sintering of cobalt particles while the addition of a reduction promoter was undesirable since it might influence the catalyst performance in different ways whereas the aim of this study was to study the effect the support material only.

The cobalt particle size as determined using H_2 chemisorption for Co/Nb_2O_5 and $Co/\gamma\text{-}Al_2O_3$ is shown in Table 3.1. The surface-average cobalt particle size of Co/Nb_2O_5 catalysts was found to increase significantly with increasing cobalt loading, leading to a decreased metallic cobalt-specific surface area and a decreased metal-support contact area. The calculated cobalt particle size of 5 wt% Co/Nb_2O_5 and 28 wt% $Co/\gamma\text{-}Al_2O_3$, catalysts with a similar surface-specific cobalt loading, was found to be identical (Table 3.1). The small metallic cobalt-specific surface area found for 28 wt% $Co/\gamma\text{-}Al_2O_3$ might be caused by the formation of large cobalt particles due to the high cobalt loading applied, due to sintering during the high-temperature reduction or due to incomplete reduction as shown using TPR. Due to the lower cobalt loading applied on the Nb_2O_5-supported catalyst the specific metal surface area was significantly lower, 2 and 10 $m^2\ g_{cat}^{-1}$ respectively.

5 wt% Co/Nb_2O_5 was investigated in Fischer-Tropsch catalysis at 220 °C, 20 bar, H_2/CO = 2.0 v/v. The CO conversion was found to be constant after 60 h on stream with concomitant selectivity data shown in Figure 3.2. This catalyst was found to have a very high selectivity towards liquid hydrocarbons (90 wt% C_{5+}) compared to $\gamma\text{-}Al_2O_3$- and SiO_2-supported cobalt catalysts (80 - 83 wt%) at similar reaction conditions.[11,12] As shown in Figure 3.2, the selectivity towards methane was very low (6 wt%). The high C_{5+} selectivity of Nb_2O_5-supported Co catalysts has been reported previously in Fischer-Tropsch synthesis at 1 bar[13–16] and was thought to be related to partial reduction of the support and the formation Co-NbO_x species due to strong metal support interaction (Chapter 1). The origin of the superior C_{5+} selectivity at 20 bar was studied in more detail in Chapter 4.

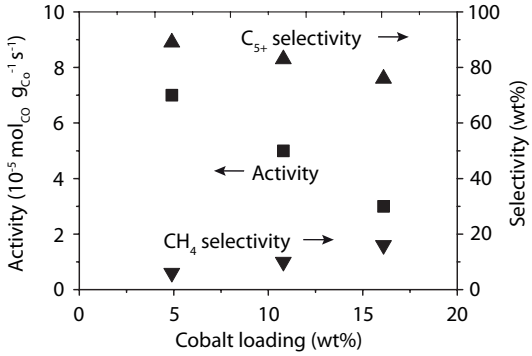

Figure 3.2. CH_4 and C_{5+} selectivity and cobalt-weight normalized activity (CTY) in Fischer-Tropsch synthesis at 220 °C, 20 bar, H_2/CO = 2.0 v/v, after 80 h on stream for 5 - 17 wt% Co/Nb_2O_5.

Application of higher cobalt loadings was found to yield an increased catalyst-weight normalized activity (WTY); however, the cobalt-weight normalized activity (CTY) was found to decrease (Figure 3.2). This is attributed to the formation of larger cobalt particles as indicated by H_2 chemisorption data (Table 3.1). Also the C_{5+} selectivity was found to decrease with increasing cobalt loading (Figure 3.2). The selectivity loss coincides with the reduced metal-support contact area due to the formation of larger particles. This might confirm that the chain growth promoting effect is related to the intimate contact between cobalt and niobia at the metal-support interface.

The influence of reaction temperature on the performance of 5 wt% Co/Nb_2O_5 was investigated in Fischer-Tropsch synthesis at 220 - 260 °C. The activity was found to increase significantly upon increasing reaction temperature (Figure 3.3A). Stable CO conversion after 60 h on stream was obtained at 220 - 260 °C, indicating that increasing the reaction temperature up to 260 °C has no apparent effect on the stability up to 90 h on stream (Figure 3.4). The activity of 5 wt% Co/Nb_2O_5 was compared to 28 wt% $Co/\gamma\text{-}Al_2O_3$, a catalyst with a similar surface-specific cobalt loading and cobalt particle size (Table 3.1). The CTY was found to be similar, but due to the higher cobalt loading applied on the $\gamma\text{-}Al_2O_3$-supported catalyst, the WTY was a factor of 4 - 5 higher on the

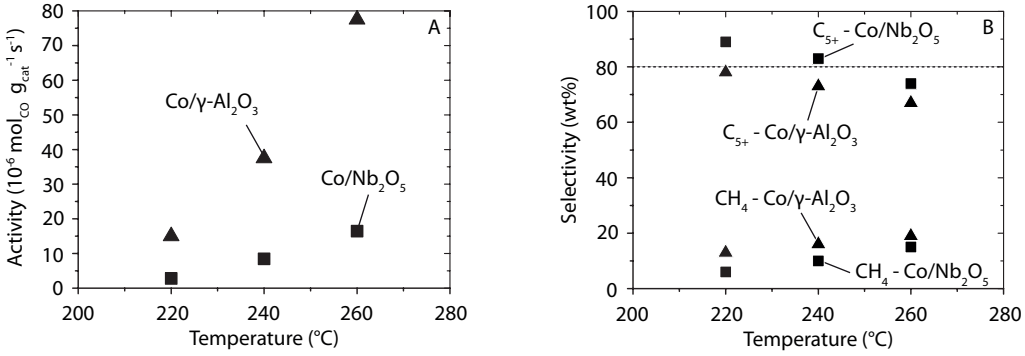

Figure 3.3. Catalyst-weight normalized activity (WTY, A) and CH_4 and C_{5+} selectivity (B) in Fischer-Tropsch synthesis at 220 - 260 °C, 20 bar, H_2/CO = 2.0 v/v, after 80 h on stream for 5 wt% Co/Nb_2O_5 and 28 wt% $Co/\gamma\text{-}Al_2O_3$.

Table 3.2. CO conversion (X_{CO}), catalyst-weight normalized activity (WTY), cobalt-weight normalized activity (CTY) and turnover frequency (TOF) in Fischer-Tropsch synthesis at 220 - 260 °C, 20 bar, H_2/CO = 2.0 v/v, after 80 h on stream for 5 wt% Co/Nb_2O_5 and 28 wt% $Co/\gamma\text{-}Al_2O_3$.

Catalyst	Temperature (°C)	GHSV (h^{-1})	X_{CO} (%)	WTY ($mol_{CO}\ g_{cat}^{-1}\ s^{-1}$)	CTY ($mol_{CO}\ g_{Co}^{-1}\ s^{-1}$)	TOF (s^{-1})
5 wt% Co/Nb_2O_5	220	$1.7 * 10^3$	37	$3 * 10^{-6}$	$6 * 10^{-5}$	0.06
	240	$3.7 * 10^3$	47	$8 * 10^{-6}$	$18 * 10^{-5}$	0.19
	260	$5.6 * 10^3$	62	$16 * 10^{-6}$	$35 * 10^{-5}$	0.38
28 wt% $Co/\gamma\text{-}Al_2O_3$	220	$9.5 * 10^3$	37	$15 * 10^{-6}$	$6 * 10^{-5}$	0.06
	240	$21 * 10^3$	44	$38 * 10^{-6}$	$15 * 10^{-5}$	0.16
	260	$32 * 10^3$	59	$78 * 10^{-6}$	$31 * 10^{-5}$	0.33

$\gamma\text{-}Al_2O_3$-supported catalyst (Figure 3.3A). The TOF was calculated to be 0.06 s^{-1} at 220 °C for both catalysts (Table 3.2). These values are well in agreement with the TOF reported for SiO_2-, $\gamma\text{-}Al_2O_3$- and TiO_2-supported catalysts.[11] The apparent activation energy was calculated to be slightly higher for the Nb_2O_5-supported catalyst than for the $\gamma\text{-}Al_2O_3$-supported catalyst, 101 and 93 kJ mol^{-1} respectively and indicates that diffusion limitation did not play a role.

The C_{5+} selectivity of the Nb_2O_5-supported catalyst was found to be superior relative to the $\gamma\text{-}Al_2O_3$-supported catalyst in the full temperature range investigated (Figure 3.3B). Decreasing selectivity towards liquid hydrocarbons with increasing reaction temperature was observed for both catalysts and is well-known in cobalt-based Fischer-Tropsch catalysis. Due to the high intrinsic selectivity of the Nb_2O_5-supported catalyst, the C_{5+} selectivity is ≥ 80 wt% up to ~ 250 °C, whereas the $\gamma\text{-}Al_2O_3$-supported catalyst calls for operation at 210 °C to obtain 80 wt% C_{5+} selectivity.

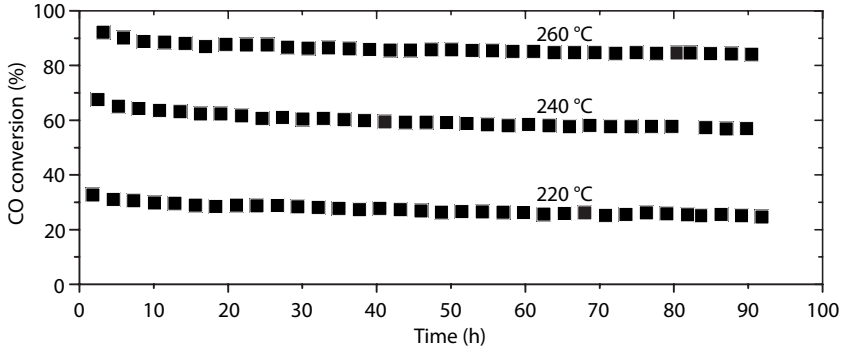

Figure 3.4. CO conversion with time on stream in Fischer-Tropsch synthesis at 220 - 260 °C, 20 bar, H_2/CO = 2.0 v/v, GHSV 3.4 * 10^3 h^{-1} for 5 wt% Co/Nb_2O_5.

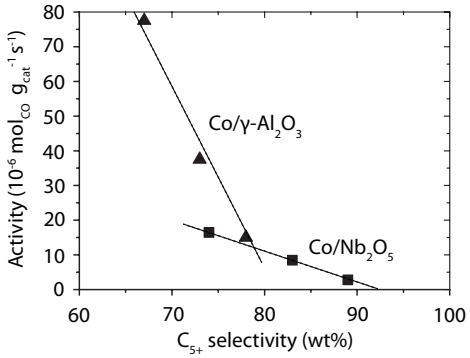

Figure 3.5. Catalyst-weight normalized activity related to the C_{5+} selectivity in Fischer-Tropsch synthesis at 220 - 260 °C, 20 bar, H_2/CO = 2.0 v/v, after 80 h on stream for 5 wt% Co/Nb_2O_5 and 28 wt% Co/γ-Al_2O_3. Lines were added to guide the eye.

In Figure 3.5, for the two catalysts the catalyst weight-normalized activity is shown in relation to the target C_{5+} selectivity. At low target C_{5+} selectivities, the catalysts can be operated at high temperature and correspondingly high activities. Higher target C_{5+} selectivities call for a lower reaction temperature and consequently lower activity. At a target C_{5+} selectivity of ~ 80 wt% the curves for 5 wt% Co/Nb_2O_5 and 28 wt% Co/γ-Al_2O_3 coincide, which means that at this target C_{5+} selectivity, the catalyst-weight normalized activities of these catalysts are identical, albeit at different reaction temperatures. This reaction temperature difference largely compensates for the lower cobalt loading applied on the Nb_2O_5-supported catalyst. In other words, the utilization of cobalt on a weight basis is ~ four times higher on Nb_2O_5 than on γ-Al_2O_3 at a target C_{5+} selectivity of ~ 80 wt%.

Conclusions

In this chapter, the performance of Co/Nb_2O_5 catalysts was investigated in Fischer-Tropsch synthesis in the temperature range 220 - 260 °C and compared to a Co/γ-Al_2O_3 catalyst. For 5 wt% Co/Nb_2O_5, a very high selectivity towards liquid hydrocarbons of 90 wt% at 220 °C was found. Since crystallization of niobia is required to obtain a stable support material, the support porosity was very low compared to γ-Al_2O_3. Due to this limited support porosity, application of higher cobalt loadings led to the formation of larger cobalt particles as shown using H_2 chemisorption. In Fischer-Tropsch catalysis, the presence of these larger particles was found to yield inferior cobalt-weight normalized activity and decreased selectivity towards liquid hydrocarbons due to decreased metallic cobalt-specific surface area and decreased metal-support interaction.

The cobalt-weight normalized activity and turnover frequency was found to be almost identical for 5 wt% Co/Nb_2O_5 and 28 wt% Co/γ-Al_2O_3. However, for industrial application the catalyst-weight or catalyst-volume normalized activity is more relevant. Due to the low cobalt loading

that could be applied with Nb_2O_5-supported catalysts, the catalyst-weight normalized activity, was significantly lower. Increasing the reaction temperature from 220 - 260 °C led to increased activity and decreased C_{5+} selectivity for both catalysts. The C_{5+} selectivity of 5 wt% Co/Nb_2O_5 was found to be ≥ 80 wt% up to ~ 250 °C, whereas 28 wt% $Co/\gamma\text{-}Al_2O_3$ called for an operation temperature at or below ~ 210 °C to obtain 80 wt% C_{5+} selectivity. This means that 5 wt% Co/Nb_2O_5 could be operated at higher temperatures and correspondingly higher activities at this target C_{5+} selectivity. At a target C_{5+} selectivity of 80 wt%, the cobalt-weight normalized activity was found to be identical. This means that 5 wt% Co/Nb_2O_5 and 28 wt% $Co/\gamma\text{-}Al_2O_3$ can have identical catalyst-weight normalized activity at a similar C_{5+} selectivity, while a factor of four less cobalt is required.

Acknowledgements

Dr. Robson Monteiro and Mr. Rogério Ribas (CBMM) are acknowledged for useful discussions and for supplying niobia samples. Dr. Jinbao Gao and Dr. Korneel Cats are acknowledged for performing TPR experiments.

References

[1] Soares, R. R.; Frydman, A.; Schmal, M. *Catal. Today* **1993**, *16*, 361–370.
[2] Silva, R. R. C. M.; Schmal, M.; Frety, R.; Dalmon, J. A. *J. Chem. Soc. - Faraday Trans.* **1993**, *89*, 3975–3980.
[3] de Souza, C. D.; Cesar, D. V.; Marchetti, S. G.; Schmal, M. *Stud. Surf. Sci. Catal.* **2007**, *167*, 147–152.
[4] Frydman, A.; Soares, R. R.; Schmal, M. *Stud. Surf. Sci. Catal.* **1993**, *75*, 2797–2800.
[5] de Oliveira, A. K.; dos Santos, B. C. A.; Monteiro, R. de S.; Moraes, L. J.; Pereira, T. A.; Schmal, M.; Sousa-Aguiar, F. E.; Sugaya, M. de F.; Vicentini, V. P. World patent WO 2005/085390 A1 **2005**.
[6] Reuel, R. C. *J. Catal.* **1984**, *85*, 63–77.
[7] Noronha, F. B.; Perez, C. A.; Frety, R. *Phys. Chem. Chem. Phys.* **1999**, *1*, 2861–2867.
[8] Sexton, B. *J. Catal.* **1986**, *97*, 390–406.
[9] Jacobs, G.; Ji, Y.; Davis, B. H.; Cronauer, D.; Kropf, A. J.; Marshall, C. L. *Appl. Catal., A* **2007**, *333*, 177–191.
[10] Jacobs, G.; Das, T. K.; Zhang, Y.; Li, J.; Racoillet, G.; Davis, B. H. *Appl. Catal., A* **2002**, *233*, 263–281.
[11] Storsater, S.; Borg, Ø.; Blekkan, E. A.; Holmen, A. *J. Catal.* **2005**, *231*, 405–419.
[12] Bukur, D. B.; Pan, Z.; Ma, W.; Jacobs, G.; Davis, B. H. *Catal. Letters* **2012**, *142*, 1382–1387.
[13] Ahón, V. R.; Lage, P. L. C.; de Souza, C. D.; Mendes, F. M. T.; Schmal, M. *J. Nat. Gas Chem.* **2006**, *15*, 307–312.
[14] Mendes, F. M. T.; Uhl, A.; Starr, D. E.; Guimond, S.; Schmal, M.; Kuhlenbeck, H.; Shaikhutdinov, S. K.; Freund, H.-J. *Catal. Letters* **2006**, *111*, 35–41.
[15] Mendes, F. M. T.; Perez, C. A. C.; Noronha, F. B.; Schmal, M. *Catal. Today* **2005**, *101*, 45–50.
[16] Mendes, F. M. T.; Perez, C. A. C.; Noronha, F. B.; Souza, D. D.; Cesar, D. V.; Freund, H.-J.; Schmal, M. *J. Phys. Chem. B* **2006**, *110*, 9155–9163.

Chapter 4

On the Superior Activity and Selectivity of $PtCo/Nb_2O_5$ Fischer-Tropsch Catalysts

Abstract

In this chapter Co/Nb_2O_5 catalysts and the effect of Pt-promotion thereon are investigated in comparison to γ-Al_2O_3- and α-Al_2O_3-supported catalysts for the Fischer-Tropsch (FT) synthesis. Upon Pt-promotion of Co/Nb_2O_5 the cobalt-weight normalized FT activity was found to increase by a factor of 2.4, while the high C_{5+} selectivity of 85 wt% was maintained. Based on environmental TEM results no indications were found that Pt affected the cobalt particle size in Co/Nb_2O_5 catalysts. A kinetic study indicates an increased number of active sites upon Pt-promotion whereas Steady-State Isotopic Transient Kinetic Analysis experiments show that a combination of an increased number of active sites and an increased turnover frequency is at the origin of the enhanced activity in Co/Nb_2O_5 catalysts upon Pt-promotion. Pt was tentatively proposed to bring about more efficient promotion of Co by NbO_x being present as smaller clusters.

Introduction

The selectivity of cobalt catalysts towards liquid hydrocarbons (C_{5+}) can be promoted by partially reducible transition-metal oxides like MnO and ZrO_2.[1–6] These promoters can be present as small particles in the close proximity to cobalt or as support material in the case of Co/TiO_2[5,7,8] or Co/Nb_2O_5[9–14] catalysts. For Nb_2O_5-supported cobalt catalysts, high selectivities towards heavy hydrocarbons were reported in Fischer-Tropsch synthesis at 1 bar[10–14] and more recently also at 20 bar (Chapter 3). The promoting effect of niobia as support material at low pressure was extensively studied using XPS, TPR, TPO, CO TPD and IR spectroscopy and was attributed to partial reduction of the support and consequent strong metal support interaction (SMSI).[15–19] The presence of Co^0-NbO_x species was confirmed by Mendes et al. in Co/Nb_2O_5 catalysts[17] and model catalysts.[18]

Noble-metal addition is a well-known method to enhance the activity of Fischer-Tropsch catalysts by facilitating cobalt oxide reduction and consequently increasing the number of active sites.[20–23] Upon noble metal promotion of Co/TiO_2 and Co/Nb_2O_5 catalysts[24–27] and recently also niobia-promoted Co/SiO_2 catalysts (Chapter 5), an increase of the cobalt-weight normalized activity was observed which could not be explained only by an increased number of active sites.

In this chapter the extent and origin of Pt-promotion on the activity and selectivity of Co/Nb_2O_5 Fischer-Tropsch catalysts is investigated in comparison to γ-Al_2O_3- and α-Al_2O_3-supported catalysts using amongst others environmental Transmission Electron Microscopy (TEM)[28], a kinetic study and Steady-State Isotopic Transient Kinetic Analysis (SSTIKA).[29]

Experimental methods

Preparation

Niobium oxide hydrate (HY-340, AD/4465, 72.6 wt% Nb_2O_5, LOI 26.7 wt%, purity data see Appendix A) was obtained from Companhia Brasileira de Metalurgia e Mineração - CBMM and calcined at 600 °C (5 °C min^{-1}, 2 h) in stagnant air to obtain crystalline Nb_2O_5 (T-phase, SA_{BET}: 16 m^2 g^{-1}, PV: 0.06 mL g^{-1}). γ-Al_2O_3 (Sasol, Puralox SSCa-5/200, SA_{BET}: 185 m^2 g^{-1}, PV: 0.5 mL g^{-1}) and α-Al_2O_3 (BASF, SA_{BET}: 7 m^2 g^{-1}, PV: 0.015 mL g^{-1}) were used as received. For physisorption isotherms and pore size distributions, see Appendix C, Figure C1.

Supports were sieved to 75 - 150 μm and dried at ~ 80 °C for 1 h in dynamic vacuum. Cobalt was deposited by single (Nb_2O_5, α-Al_2O_3) or double (γ-Al_2O_3) impregnation[30] in static vacuum at room temperature with an aqueous 4.0 M $Co(NO_3)_2 \cdot 6\ H_2O$ solution or by co-impregnation with an aqueous 4.0 M $Co(NO_3)_2 \cdot 6\ H_2O$, 0.03 M $Pt(NH_3)_4(NO_3)_2$ (Co/Pt = 140) solution, aiming for a cobalt loading of 2 - 8 mg_{Co} m^{-2}. After drying overnight at 60 °C in stagnant air, the cobalt nitrate precursor was calcined at 350 °C (3 °C min^{-1}, 2 h) in a 1 L min^{-1} g_{sample}^{-1} N_2 flow. Cobalt loading is expressed as the mass of metallic cobalt per gram of reduced catalyst. An overview of the prepared catalysts can be found in Table 4.1.

Characterization

Samples were analyzed after cobalt nitrate decomposition as described above (calcined) and after reduction at 350 °C, 3 °C min^{-1}, 2 h in 25 vol% H_2/N_2 (GHSV 60 * 10^3 h^{-1}) and subsequent exposure to air at room temperature (passivated).

Environmental Powder X-ray diffraction (XRD) patterns were measured using a Bruker-AXS D8 Advance X-ray diffractometer using Co-Kα radiation (λ = 1.789 Å). Calcined and passivated samples were analyzed in air at room temperature and heated to 350 °C (5 °C min^{-1}, 2 h) in 25 vol% H_2/He ($Co/\gamma\text{-}Al_2O_3$: 500 °C) in the X-ray diffractometer.

TEM samples were prepared by dry dispersion of the passivated catalyst onto a Mo grid with a holey carbon supporting film. TEM analysis was performed using an FEI Titan ETEM G2 microscope described before.[28] Samples were observed in vacuum at room temperature and in 100 Pa H_2 at 350 °C, microscope was operated at 300 kV, elemental analysis was performed using Scanning Transmission Electron Microscopy-Electron Energy Loss Spectroscopy (STEM-EELS).

Temperature programmed reduction (TPR) experiments were performed using a Micromeritics Autochem 2920 instrument. 25 - 100 mg calcined catalyst (6 - 7 mg Co) was dried at 120 °C for 1 h in an Ar flow and reduced up to 1000 °C (10 °C min^{-1}) in a 5 vol% H_2/Ar flow.

H_2 chemisorption measurements were performed using a Micromeritics ASAP 2020 instrument. 50 - 200 mg calcined catalyst was dried for 1 h in dynamic vacuum at 100 °C and reduced in an H_2 flow at 350 °C, 1 °C min^{-1} for 2 h, ($Co/\gamma\text{-}Al_2O_3$: 500 °C). H_2 adsorption isotherms were measured at 150 °C, as recommended by Reuel for supported cobalt particles.[31] Metallic cobalt-specific surface area and average particle size were calculated assuming a surface stoichiometry H/Co = 1 and an atomic cross-sectional area of 0.0662 nm^2.

CO chemisorption measurements were performed in a setup described before.[32] 30 - 100 mg calcined catalyst (75 - 150 μm) diluted with an equal mass of SiC was reduced at 350 °C, 5 °C min^{-1}, for 2 h ($Co/\gamma\text{-}Al_2O_3$: 500 °C) in 10 mL min^{-1} H_2. The amount of reversibly adsorbed CO was determined from a ^{12}CO/Ar to ^{13}CO/Kr switch (1.5/33.5 mL min^{-1}) at 100 °C, 1.85 bar. Effluent gas was analyzed using a Balzers QMG 422 Quadrupole mass spectrometer. Surface residence time (τ_{CO}) was determined by integration of the normalized transient curve: $\tau_i = \int Fi\,(t)\,dt$ and was corrected for gas phase hold-up using the Ar signal. Amount of reversibly adsorbed CO ($N_{CO,\,total}$) was calculated using the CO inlet flow ($Q_{CO,\,in}$): $N_{CO,total} = \tau_{CO} * Q_{CO,\,in}$.

Fischer-Tropsch synthesis

Catalyst testing at 1 bar was performed using a U-shaped, continuous down-flow, fixed bed reactor system. 10 - 50 mg calcined catalyst (75 - 150 μm) was diluted with 200 mg SiC (200 - 400 μm) and loaded in a glass reactor, i.d. = 3 mm, to achieve a bed height of 2 cm. 500 mg SiC was loaded on top of the catalyst bed to ensure gas preheating. The catalysts were reduced at atmospheric pressure in a 33 vol% H_2/Ar flow, GHSV 1.7 - 3.7 * 10^5 h^{-1}, at 350 °C, 5 °C min^{-1}, for 2 h ($Co/\gamma\text{-}Al_2O_3$: 500 °C). After cooling to 220 °C the gas stream was switched to synthesis gas, H_2/CO = 2.0 v/v, GHSV 25 - 100 * 10^3 h^{-1}, CO conversion 1 - 5 %. Products up to C_{18} were analyzed using an online Varian 430-GC equipped with FID. Activity and selectivity were

calculated based on the hydrocarbons formed. The reported catalyst performance was determined after at least 15 h on stream. A kinetic study was performed in this setup, H_2 flow (4 - 8 mL min^{-1}, p_{H_2} = 0.27 - 0.53 bar) and CO flow (2 - 4 mL min^{-1}, p_{CO} = 0.13 - 0.27 bar) were varied independently, total gas flow was kept constant at 15 mL min^{-1} by addition of Ar (4 - 8 mL min^{-1}). H_2 and CO reaction orders (Y and Z, respectively) and pre-exponential factor k' were determined from the cobalt-weight normalized activity, the latter calculated from the CO conversion level (X_{CO}), incoming CO flow ($F_{CO, in}$) and the mass of reduced catalyst (m_{cat}) using: $X_{CO} * F_{CO,\,in} * m_{cat}^{-1} = k' * p_{H_2}^{\ y} * p_{CO}^{\ z}$.

Catalyst testing at 20 bar was performed using an Avantium Flowrence 16 parallel, continuous flow, fixed bed reactor system. 30 - 175 mg calcined catalyst (75 - 150 μm) was diluted with 100 - 200 mg SiC (200 - 400 μm) and loaded in a stainless steel reactor, i.d. = 2 - 2.6 mm, to achieve a bed height of 4 - 5 cm. Catalysts were reduced at atmospheric pressure in a 25 vol% H_2/He flow, GHSV 1.6 - 10 * 10^3 h^{-1}, at 350 °C, 1 °C min^{-1}, for 8 h (Co/γ-Al_2O_3: 500 °C). After cooling to 180 °C the gas stream was switched to synthesis gas, H_2/CO = 2.0 v/v, GHSV 1.8 - 12 * 10^3 h^{-1}, the reactors were pressurized to 20 bar and subsequently heated to 220 °C. The GHSV was adjusted to obtain 20 - 30 % CO conversion. Products up to C_9 were analyzed using an online Agilent Technologies 7890A gas chromatograph. The reported catalyst performance was determined after at least 100 h on stream. The GHSV was defined as the total gas flow divided by the catalyst volume.

Steady State Isotopic Transient Kinetic Analysis (SSITKA) measurements and data treatment were performed as described before.[32] 30 - 100 mg calcined catalyst (75 - 150 μm) diluted with an equal mass of SiC was reduced at 350 °C, 5 °C min^{-1}, for 2 h (Co/γ-Al_2O_3: 500 °C) in a 10 mL min^{-1} H_2 flow. CO and CH_4 transient curves were determined from a $^{12}CO/H_2/Ar$ to $^{13}CO/H_2/Kr$ switch (1.5/15/33.5 mL min^{-1}) at 210 °C, 1.85 bar after at least 15 h at these conditions. Effluent gas was analyzed using a Balzers QMG 422 Quadrupole mass spectrometer and using a GC-MS (Agilent GC7890B – MSD5977A) equipped with TCD, FID and MSD detectors.

Table 4.1. Cobalt loading based on intake, number of reversible CO adsorption sites determined using CO chemisorption at 100 °C ($N_{CO, total}$), adsorbed amount of H_2 (N_{H_2}) and apparent Co particle size determined using H_2 chemisorption (d_{Co}, H_2) and estimated Co particle size from environmental TEM (d_{Co}, TEM).

Catalyst	Co loading		$N_{CO, total}$	N_{H_2}	d_{Co}, H_2	d_{Co}, TEM
	(wt%)	(mg_{Co} m^{-2})	($mmol_{CO}$ g_{Co}^{-1})	($mmol_{H_2}$ g_{Co}^{-1})	(nm)	(nm)
Co/Nb_2O_5	5.9	3.9	0.28	0.36	24	9.2
$PtCo/Nb_2O_5$	5.9	3.9	0.48	0.45	19	8.7
Co/γ-Al_2O_3	28	2.1	0.20	0.45	19	
PtCo/γ-Al_2O_3	28	2.1	0.43	0.65	13	
Co/α-Al_2O_3	6.3	8.4	0.38	0.53	16	
PtCo/α-Al_2O_3	6.0	8.0	0.55	0.62	14	

Results and discussion

An overview of the catalysts used in this study is shown in Table 4.1. Using XRD at ambient conditions no crystalline cobalt phases were observed for calcined or passivated Co/Nb_2O_5 and $PtCo/Nb_2O_5$ catalysts. Also after reduction at 350 °C in the X-ray diffractometer no crystalline cobalt phases were observed for Co/Nb_2O_5 and $PtCo/Nb_2O_5$, even after application of higher cobalt loadings by double impregnation (~ 10 wt%, Appendix C, Figure C2), whereas for $Co/\gamma\text{-}Al_2O_3$ and $PtCo/\gamma\text{-}Al_2O_3$ the reduction of Co_3O_4 to crystalline Co^0 was observed at these conditions (Figure 4.1). Overlap of diffraction lines with Nb_2O_5 lines impedes detection of weak cobalt and cobalt oxide diffraction lines. Absence of crystalline cobalt oxide diffraction lines in Nb_2O_5-supported catalysts is in line with XRD observations by Noronha et al.[19]

TEM imaging of calcined Co/Nb_2O_5 catalysts showed that cobalt was present in anisotropically shaped particles in the pores between the Nb_2O_5 particles, see Appendix C, Figure C3. After reduction and passivation restructuring of cobalt had occurred into anisotropic cobalt oxide particles on the Nb_2O_5 surface (Figure 4.2A). Upon exposure to H_2 at 350 °C in the electron microscope, spherical metallic cobalt particles of ~ 9 nm were formed as shown in

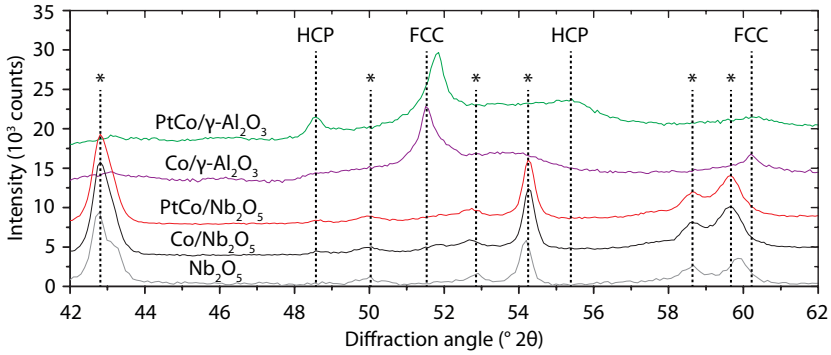

Figure 4.1. Environmental X-ray diffractograms (Co-Kα radiation) at 350 °C in 25 vol% H_2/He ($Co/\gamma\text{-}Al_2O_3$: 500 °C) for (Pt) 28 wt% $Co/\gamma\text{-}Al_2O_3$ and (Pt) 6 wt% Co/Nb_2O_5. Nb_2O_5 lines (*) and hcp and fcc Co lines are indicated.[33]

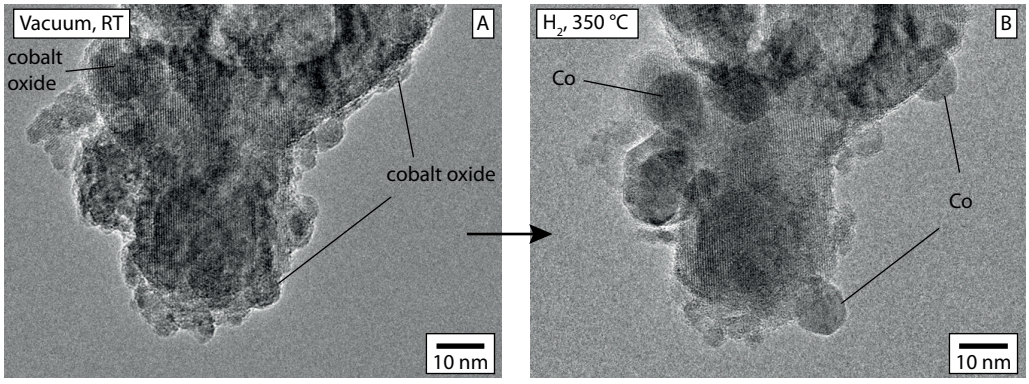

Figure 4.2. Bright field TEM images in vacuum at room temperature (A) and in 100 Pa H_2 at 350 °C (B) for Co/Nb_2O_5 after ex situ reduction and passivation.

Figure 4.2B. Reduction was confirmed using STEM-EELS (Appendix C, Figure C8). For $PtCo/Nb_2O_5$ (Appendix C, Figure C7), similar morphology and restructuring was observed and based on the current study no evidence was found for a large cobalt particle size difference between Co/Nb_2O_5 and $PtCo/Nb_2O_5$. The larger surface tension of metallic cobalt in combination with the higher mobility of metal atoms leads to these rounded off particles and can only be clearly observed using environmental TEM.[34,35]

Using H_2 chemisorption, an increased number of adsorption sites was observed upon Pt-promotion (Table 4.1) due to facilitated cobalt oxide reduction (TPR, Appendix C, Figure C10), in line with previous reports.[20–23] Remarkably also for $PtCo/Nb_2O_5$ a higher number of active sites was observed than for Co/Nb_2O_5 although full reduction at 350 °C would be expected without Pt present, based on TPR results and also inferred from environmental TEM results (vide supra). For Nb_2O_5-supported catalysts a larger cobalt particle size (19 - 24 nm) was calculated than expected based on environmental TEM (~ 9 nm) probably due to coverage of cobalt sites by NbO_x and consequent decrease of the number of metallic cobalt surface sites available for chemisorption.

A more accurate method to estimate the number of sites active in Fischer-Tropsch catalysis has been proposed to be CO chemisorption.[32] A factor of 1.7, 2.2 and 1.4 increase of the number of reversibly adsorbed CO molecules was observed upon Pt-promotion of Co/Nb_2O_5, $Co/\gamma\text{-}Al_2O_3$ and $Co/\alpha\text{-}Al_2O_3$, respectively (Table 4.1).

Catalyst selectivity (Figure 4.3) and activity (Figure 4.4) were evaluated in Fischer-Tropsch synthesis at 1 and 20 bar (more data are available in Appendix C, Table C2-C3). Furthermore, Table 4.2 shows results from the kinetic study investigating the influence of support and Pt-promotion on the H_2 and CO reaction order and the SSITKA study performed to determine surface coverages and turnover frequencies (Full data in Appendix C, Figure C14 - C17).

In Fischer-Tropsch synthesis at 1 bar superior C_{5+} selectivities were observed for $\gamma\text{-}Al_2O_3$- and Nb_2O_5-supported catalysts, compared to $\alpha\text{-}Al_2O_3$-supported catalysts (Figure 4.3A). This is thought to be related either to the presence of Co^{2+} due to incomplete cobalt oxide reduction ($\gamma\text{-}Al_2O_3$) or to SMSI (Nb_2O_5), as also reported by Mendes et al.[15–19] Upon Pt-promotion decreased

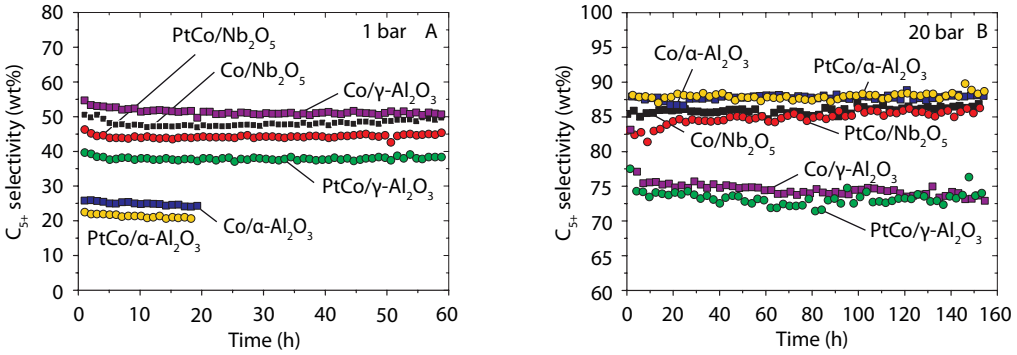

Figure 4.3. C_{5+} selectivity in Fischer-Tropsch synthesis at 1 bar, CO conversion 1 - 5 % (A) and 20 bar, CO conversion 21 - 34 % (B), 220 °C, H_2/CO = 2.0 v/v for (Pt)Co/Nb_2O_5, (Pt)$Co/\gamma\text{-}Al_2O_3$ and (Pt)$Co/\alpha\text{-}Al_2O_3$ catalysts.

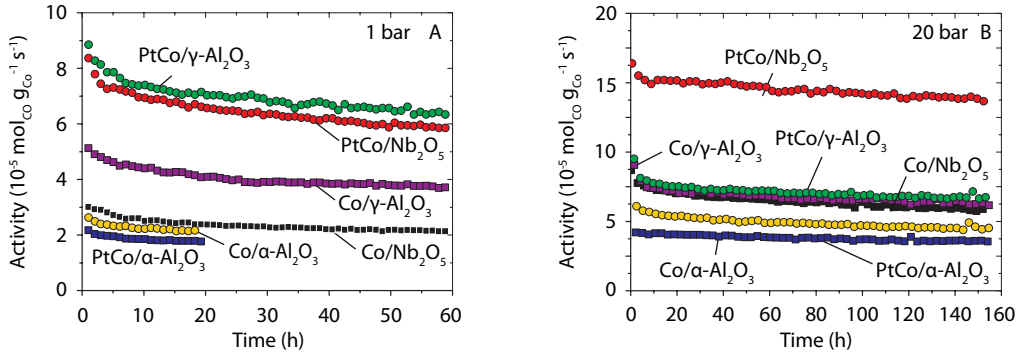

Figure 4.4. Cobalt-weight normalized activity in Fischer-Tropsch synthesis at 1 bar, CO conversion 1 - 5 % (A) and 20 bar, CO conversion 21 - 34 % (B), 220 °C, H_2/CO = 2.0 v/v for (Pt)Co/Nb_2O_5, (Pt)Co/γ-Al_2O_3 and (Pt)Co/α-Al_2O_3 catalysts.

C_{5+} selectivities were observed due to increased hydrogenation activity, as also inferred from the increasing paraffin-to-olefin ratio (Appendix C, Table C2). At 20 bar, superior C_{5+} selectivities were observed for catalysts supported by α-Al_2O_3 and Nb_2O_5 compared to γ-Al_2O_3 (Figure 4.3B). The positive relation between pore diameter and C_{5+} selectivity was previously reported by e.g. Holmen et al. and was attributed to cobalt particle size and diffusion effects.[36–39] At 20 bar, no large influence of Pt on the C_{5+} selectivity was observed (Figure 4.3B).

At 1 bar, the cobalt weight-normalized activity of Co/γ-Al_2O_3 and Co/Nb_2O_5 was found to increase by a factor of 1.7 and 2.8 upon Pt-promotion (Figure 4.4A). For Co/α-Al_2O_3, low activity and only slight influence of Pt-promotion were observed at 1 bar. At 20 bar, no large influence of Pt-promotion on the cobalt-weight normalized activity of Co/γ-Al_2O_3 and Co/α-Al_2O_3 was observed, whereas for Co/Nb_2O_5, a factor of 2.4 increase of the activity per unit weight of cobalt was observed (Figure 4.4B).

To investigate the origin of the unique activity increase upon Pt-promotion of Co/Nb_2O_5, a kinetic study was performed at 1 bar in which H_2 and CO reaction orders and the effect of Pt addition thereon were studied (Table 4.2). For catalysts supported by γ-Al_2O_3 and Nb_2O_5 higher reaction orders in CO and lower orders in H_2 were observed compared to α-Al_2O_3-supported catalysts (Appendix C, Figure C14) which might be related to the superior C_{5+} selectivity for (Pt)Co/Nb_2O_5 and (Pt)Co/γ-Al_2O_3 compared to (Pt)Co/α-Al_2O_3. No large influence of Pt on the CO and H_2 reaction orders for the supported Co catalysts studied was observed (Table 4.2). The pre-exponential factor (k') however was found to increase by a factor of 1.7 upon Pt-promotion of γ-Al_2O_3- and Nb_2O_5-supported catalysts, indicating an increased number of active sites. Furthermore, only slight influence of H_2 pressure on chain growth probability (α) was observed, whereas α was found to increase with increasing CO pressure for all catalysts (Appendix C, Figure C15).

A Steady-State Isotopic Transient Kinetic Analysis (SSITKA) study was performed during Fischer-Tropsch synthesis at 210 °C, H_2/CO = 10 v/v. Activity and selectivities at these conditions are shown in Appendix C, Table C4. ^{12}CO and $^{12}CH_4$ transients (Appendix C,

Table 4.2. Apparent turnover frequency (TOF_{app}) in Fischer-Tropsch synthesis at 20 bar, 220 °C, H_2/CO = 2.0 v/v, with the number of active sites based on H_2 chemisorption results. Reaction orders in H_2 and CO and pre-exponential factor (k') determined in a kinetic study at 1 bar, 220 °C. Surface coverage (θ) and TOF determined from a $^{12}CO/H_2/Ar$ to $^{13}CO/H_2/Kr$ switch during SSITKA at 210 °C, 1.85 bar, H_2/CO = 10 v/v, with the number of active sites based on CO chemisorption results.

	FT 20 bar	Kinetic study			SSITKA		
Catalyst	TOF_{app}	Reaction order		k'	θ_{CO}	θ_{CH_x}	TOF
	(s^{-1})	H_2	CO	($mol_{CO}\ g_{Co}^{-1}\ s^{-1}$)			(s^{-1})
Co/Nb_2O_5	0.083	0.73	0.13	$3.5 * 10^{-5}$	0.67	0.07	0.021
$PtCo/Nb_2O_5$	0.15	0.62	0.15	$6.0 * 10^{-5}$	0.60	0.07	0.034
$Co/\gamma\text{-}Al_2O_3$	0.071	0.71	0.05	$2.6 * 10^{-5}$	0.61	0.09	0.024
$PtCo/\gamma\text{-}Al_2O_3$	0.053	0.81	0.07	$4.4 * 10^{-5}$	0.53	0.11	0.023
$Co/\alpha\text{-}Al_2O_3$	0.034	0.91	-0.24	$1.5 * 10^{-5}$	0.66	0.07	0.013
$PtCo/\alpha\text{-}Al_2O_3$	0.037	0.91	-0.26	$1.9 * 10^{-5}$	0.62	0.06	0.013

Figure C16 - C17) were investigated from a $^{12}CO/Ar/H_2$ to $^{13}CO/Kr/H_2$ switch after reaching steady-state as described before.[32] CH_4 transient curves were fitted to a single pool and double parallel pool model[40] (Appendix C, Figure C18 and Table C6).

Surface residence times were determined by integration of the normalized transient curve: $\tau_i = \int Fi(t)\ dt$ and corrected for gas phase hold-up using the Ar signal. Residence times for CH_4, representing surface species which would eventually produce hydrocarbons (CH_x), were corrected for the chromatographic effect of CO[41] using: $\tau_{CH_x} = \tau_{CH_x measured} - 0.5 * \tau_{CO}$. Adsorbed amounts ($N_i$) were calculated from the exit flow ($Q_{i,\ exit}$): $N_i = \tau_i * Q_{i,\ exit}$ (Appendix C, Table C5). Surface coverages (θ_i) and turnover frequencies (TOF) were calculated based the number of active sites determined from CO chemisorption ($N_{CO,\ total}$, Table 4.1) using $\theta_i = N_i / (2 * N_{CO,\ total})$ and $TOF = \tau_{CH_4}^{-1} * \theta_{CH_x}$ and are presented in Table 4.2.

From fitting of the CH_4 transient curves (Appendix C, Figure C18 and Table C6), single pool behavior was concluded for all catalysts. This result is in line with previous reports on cobalt Fischer-Tropsch catalysts.[40] CH_x residence times (Appendix C, Table C5) were found to be shorter for Nb_2O_5-supported catalysts (4 - 5 s) than for $\gamma\text{-}Al_2O_3$- and $\alpha\text{-}Al_2O_3$-supported catalysts (7 - 8 s), indicating faster hydrogenation and desorption of hydrocarbons. For $\gamma\text{-}Al_2O_3$-supported catalysts higher CH_x coverage and lower CO coverage were calculated than for Nb_2O_5- and $\alpha\text{-}Al_2O_3$-supported catalysts (Table 4.2).

Upon Pt-promotion of $Co/\gamma\text{-}Al_2O_3$, CH_x residence times and coverages were found to increase. No large influence of Pt-promotion of Co/Nb_2O_5 or $Co/\alpha\text{-}Al_2O_3$ on CH_x coverage was observed (Table 4.2), whereas CO surface coverages were found to decrease. This indicates higher H- or OH_x- coverage and consequent higher hydrogenation probability, which is in line with the increasing paraffin-to-olefin ratio observed (Appendix C, Table C4).

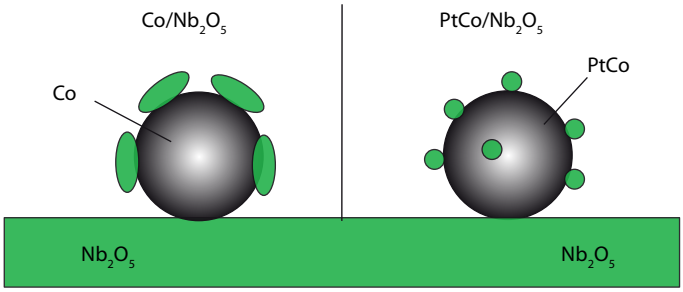

Figure 4.5. Envisaged structural model on the role of Pt in Co/Nb_2O_5 catalysts.

TOF were calculated assuming pseudo-first order kinetics and based on the number of active sites determined using CO chemisorption (vide supra). For $Co/\gamma\text{-}Al_2O_3$, $PtCo/\gamma\text{-}Al_2O_3$ and Co/Nb_2O_5 catalysts similar turnover frequencies were calculated (~ 0.02 s^{-1}, Table 4.2). For $Co/\alpha\text{-}Al_2O_3$ and $PtCo/\alpha\text{-}Al_2O_3$ lower TOF were calculated (~ 0.01 s^{-1}, Table 4.2). For $PtCo/Nb_2O_5$, the TOF based on SSITKA was found to be a factor of 1.6 higher than for Co/Nb_2O_5. Also based on the number of active sites determined using H_2 chemisorption increased TOF was calculated for $PtCo/Nb_2O_5$ (Appendix C, Table C5).

Based on the current study the origin of the factor of 2.4 increase of the cobalt-weight normalized activity upon Pt-promotion of Co/Nb_2O_5 was concluded to be a combination of an increased number of active sites by a factor of 1.7 and an increased turnover frequency by a factor of 1.6.

The current hypothesis on the origin of the increased TOF for $PtCo/Nb_2O_5$ is related to the mechanism how niobia promotes cobalt. As has been proposed before in the literature[11,42–44] for NbO_x ($x < 2.5$) as well as MnO_x, metal oxide species migrate onto cobalt during reduction and affect the nature of the cobalt active sites.[2,6] Assuming the impact of NbO_x on cobalt is short range, the interface between Co and NbO_x will be most relevant for promotion. Clearly, the extent of coverage of Co by NbO_x will be important as well as the size of the clusters of NbO_x. If the NbO_x clusters are large then interfacial sites will be limited and blocking of cobalt metal significant. The effect of Pt is tentatively assumed to be more efficient promotion of Co by NbO_x for example by formation of smaller clusters of the oxide as schematically shown in Figure 4.5. Future work will involve more detailed in situ TEM and spectroscopy investigations to prove or disprove this hypothesis.

Conclusions

Co/Nb_2O_5 and $PtCo/Nb_2O_5$ catalysts were prepared and investigated and compared to $\gamma\text{-}Al_2O_3$- and $\alpha\text{-}Al_2O_3$-supported catalysts. Using environmental XRD poor cobalt crystallinity was observed for Co/Nb_2O_5 and $PtCo/Nb_2O_5$ after reduction. Based on environmental TEM experiments no large cobalt particle size difference was observed upon Pt-promotion of Co/Nb_2O_5. Using CO chemisorption the number of adsorption sites was found to be a factor of 1.7 higher for $PtCo/Nb_2O_5$ than for Co/Nb_2O_5.

In Fischer-Tropsch synthesis at 1 bar and compared to α-Al_2O_3-supported catalysts, superior C_{5+} selectivities were observed for γ-Al_2O_3- and Nb_2O_5-supported catalysts, attributed to the presence of Co^{2+} due to incomplete cobalt oxide reduction and NbO_x species at the cobalt surface, respectively. At 20 bar, Nb_2O_5- and α-Al_2O_3-supported catalysts were found to exhibit superior C_{5+} selectivities of ~ 85 wt%, which were attributed to the larger pore sizes compared to Co/γ-Al_2O_3 and PtCo/γ-Al_2O_3 catalysts.

Upon Pt-promotion of Co/Nb_2O_5 the cobalt-weight normalized activity in Fischer-Tropsch catalysis at 20 bar was found to increase by a factor of 2.4, while the high C_{5+} selectivity was maintained. A kinetic study indicated that the number of active sites had increased by a factor of 1.7, in line with data from CO chemisorption experiments although a cobalt particle size difference was not observed using environmental TEM experiments. Steady-State Isotopic Transient Kinetic Analysis showed that a combination of an increased number of active sites and an increased turnover frequency is the origin of the activity increase in Co/Nb_2O_5 catalysts upon Pt-promotion. Pt was tentatively proposed to bring about more efficient promotion of Co by NbO_x being present as smaller clusters.

Acknowledgements

Dr. Robson Monteiro and Mr. Rogério Ribas (CBMM) are acknowledged for useful discussions and for supplying niobia samples. Dr. Hideto Yoshida (ISIR, Osaka, Japan) is acknowledged for execution of E-TEM experiments. Prof. De Chen, Dr. Cristian Ledesma Rodriguez and Ms. Yanying Qi (NTNU, Trondheim, Norway) are acknowledged for facilitation and assistance during SSITKA experiments. Mr. Hans Meeldijk (ultramicrotomy, TEM), Dr. Peter Munnik (ultramicrotomy, TEM), Mrs. Marjan Versluijs-Helder (XRD), Mr. Gang Wang (TPR) and Mr. Carlos Hernández Mejía (TPR) are acknowledged for assistance and execution of indicated analyses.

References

[1] Ali, S.; Chen, B.; Goodwin, J. G. *J. Catal.* **1995**, *157*, 35 – 41.
[2] Dinse, A.; Aigner, M.; Ulbrich, M.; Johnson, G. R.; Bell, A. T. *J. Catal.* **2012**, *288*, 104–114.
[3] den Breejen, J. P.; Frey, A. M.; Yang, J.; Holmen, A.; Schooneveld, M. M.; Groot, F. M. F.; Stephan, O.; Bitter, J. H.; de Jong, K. P. *Top. Catal.* **2011**, *54*, 768–777.
[4] Morales, F.; de Smit, E.; de Groot, F. M. F.; Visser, T.; Weckhuysen, B. M. *J. Catal.* **2007**, *246*, 91–99.
[5] Morales, F.; de Groot, F. M. F.; Gijzeman, O.; Mens, A. J. M.; Stephan, O.; Weckhuysen, B. M. *J. Catal.* **2005**, *230*, 301–308.
[6] Johnson, G. R.; Werner, S.; Bell, A. T. *ACS Catal.* **2015**, *5*, 5888–5903.
[7] Eschemann, T. O.; Bitter, J. H.; de Jong, K. P. *Catal. Today* **2014**, *228*, 89–95.
[8] Eschemann, T. O.; de Jong, K. P. *ACS Catal.* **2015**, *5*, 3181–3188.
[9] den Otter, J. H.; de Jong, K. P. *Top. Catal.* **2014**, *57*, 445–450.
[10] Soares, R. R.; Frydman, A.; Schmal, M. *Catal. Today* **1993**, *16*, 361–370.
[11] Silva, R. R. C. M.; Schmal, M.; Frety, R.; Dalmon, J. A. *J. Chem. Soc. - Faraday Trans.* **1993**, *89*, 3975–3980.
[12] de Souza, C. D.; Cesar, D. V.; Marchetti, S. G.; Schmal, M. *Stud. Surf. Sci. Catal.* **2007**, *167*, 147–152.

[13] Frydman, A.; Soares, R. R.; Schmal, M. *Stud. Surf. Sci. Catal.* **1993**, *75*, 2797–2800.

[14] de Oliveira, A. K.; dos Santos, B. C. A.; Monteiro, R. de S.; Moraes, L. J.; Pereira, T. A.; Schmal, M.; Sousa-Aguiar, F. E.; Sugaya, M. de F.; Vicentini, V. P. World patent WO 2005/085390 A1 **2005**.

[15] Ahón, V. R.; Lage, P. L. C.; de Souza, C. D.; Mendes, F. M. T.; Schmal, M. *J. Nat. Gas Chem.* **2006**, *15*, 307–312.

[16] Mendes, F. M. T.; Perez, C. A. C.; Noronha, F. B.; Schmal, M. *Catal. Today* **2005**, *101*, 45–50.

[17] Mendes, F. M. T.; Perez, C. A. C.; Noronha, F. B.; Souza, D. D.; Cesar, D. V.; Freund, H.-J.; Schmal, M. *J. Phys. Chem. B* **2006**, *110*, 9155–9163.

[18] Mendes, F. M. T.; Uhl, A.; Starr, D. E.; Guimond, S.; Schmal, M.; Kuhlenbeck, H.; Shaikhutdinov, S. K.; Freund, H.-J. *Catal. Letters* **2006**, *111*, 35–41.

[19] Noronha, F. B.; Perez, C. A.; Frety, R. *Phys. Chem. Chem. Phys.* **1999**, *1*, 2861–2867.

[20] Diehl, F.; Khodakov, A. Y. *Oil Gas Sci. Technol. - Rev. l'IFP* **2009**, *64*, 11–24.

[21] Conner, W. C.; Falconer, J. L. *Chem. Rev.* **1995**, *95*, 759–788.

[22] Jacobs, G.; Das, T. K.; Zhang, Y.; Li, J.; Racoillet, G.; Davis, B. H. *Appl. Catal., A* **2002**, *233*, 263–281.

[23] Das, T. K.; Jacobs, G.; Patterson, P. M.; Conner, W. A.; Li, J.; Davis, B. H. *Fuel* **2003**, *82*, 805–815.

[24] Iglesia, E.; Soled, S. L.; Fiato, R. A.; Via, G. H. *J. Catal.* **1993**, *143*, 345–368.

[25] Iglesia, E. *Appl. Catal., A* **1997**, *161*, 59–78.

[26] Noronha, F. B.; Frydman, A.; Aranda, D. A. G.; Perez, C.; Soares, R. R.; Morawek, B.; Castner, D.; Campbell, C. T.; Frety, R.; Schmal, M. *Catal. Today* **1996**, *28*, 147–157.

[27] Eschemann, T. O.; Oenema, J.; de Jong, K. P. *Catal. Today* **2016**, *261*, 60–66.

[28] Takeda, S.; Yoshida, H. *Microscopy* **2013**, *62*, 193–203.

[29] Ledesma, C.; Yang, J.; Chen, D.; Holmen, A. *ACS Catal.* **2014**, *4*, 4527–4547.

[30] Munnik, P.; de Jongh, P. E.; de Jong, K. P. *Chem. Rev.* **2015**, *115*, 6687–6718.

[31] Reuel, R. C. *J. Catal.* **1984**, *85*, 63–77.

[32] Frøseth, V.; Storsæter, S.; Borg, Ø.; Blekkan, E. A.; Rønning, M.; Holmen, A. *Appl. Catal., A* **2005**, *289*, 10–15.

[33] Matveev, V. V.; Baranov, D. A.; Yurkov, G. Y.; Akatiev, N. G.; Dotsenko, I. P.; Gubin, S. P. *Chem. Phys. Lett.* **2006**, *422*, 402–405.

[34] Dehghan, R.; Hansen, T. W.; Wagner, J. B.; Holmen, A.; Rytter, E.; Borg, Ø.; Walmsley, J. C. *Catal. Letters* **2011**, *141*, 754–761.

[35] Sadasivan, S.; Bellabarba, R. M.; Tooze, R. P. *Nanoscale* **2013**, *5*, 11139–11146.

[36] Borg, Ø.; Eri, S.; Blekkan, E. A.; Storsater, S.; Wigum, H.; Rytter, E.; Holmen, A. *J. Catal.* **2007**, *248*, 89–100.

[37] Rane, S.; Borg, Ø.; Yang, J.; Rytter, E.; Holmen, A. *Appl. Catal., A* **2010**, *388*, 160–167.

[38] Borg, Ø.; Hammer, N.; Eri, S.; Lindvåg, O. A.; Myrstad, R.; Blekkan, E. A.; Rønning, M.; Rytter, E.; Holmen, A. *Catal. Today* **2009**, *142*, 70–77.

[39] Vervloet, D.; Kapteijn, F.; Nijenhuis, J.; van Ommen, J. R. *Catal. Sci. Technol.* **2012**, *2*, 1221–1233.

[40] den Breejen, J. P.; Radstake, P. B.; Bezemer, G. L.; Bitter, J. H.; Frøseth, V.; Holmen, A.; de Jong, K. P. *J. Am. Chem. Soc.* **2009**, *131*, 7197–7203.

[41] Biloen, P.; Helle, J. N.; van den Berg, F. G. A.; Sachtler, W. M. H. *J. Catal.* **1983**, *81*, 450–463.

[42] Tauster, S. J.; Fung, S. C. *J. Catal.* **1978**, *55*, 29–35.

[43] Tauster, S. J.; Fung, S. C.; Garten, R. L. *J. Am. Chem. Soc.* **1978**, *100*, 170–175.

[44] Haller, G. L.; Resasco, D. E. *Adv. Catal.* **1989**, *36*, 173–235.

Chapter 5

Synergistic Promotion of Co/SiO_2 Fischer-Tropsch Catalysts by Niobia and Platinum

Abstract

Transition-metal oxides and noble metals are well-known selectivity and activity promoters in cobalt-based Fischer-Tropsch catalysis. Niobia has been shown as an effective selectivity promoter as support material; however, the low porosity limits the cobalt loading. To combine the selectivity-promoting properties of niobia with a highly porous support, niobia-modified silica was prepared and applied as support for Co and PtCo catalysts with cobalt loadings up to 21 wt%. Niobia promotion was found to increase the C_{5+} selectivity at 1 bar; however, appeared to be not effective at 20 bar. Promotion of Co/SiO_2 by a combination of platinum and niobia yielded an increase of the cobalt-weight normalized activity by a factor of 2 - 3 in the case of amorphous niobia and a factor of 3 - 4 with niobia nanocrystals present, due to both an increased number of active sites and an increased cobalt-surface specific activity (turnover frequency).

Introduction

The selectivity of cobalt Fischer-Tropsch catalysts is affected by process conditions such as temperature[1,2], pressure[3–5] and CO conversion[6] and by catalyst properties like support acidity[7,8], pore diameter[7,9] and transition-metal oxide (TMO) promotion.[3,4,10–15] These TMO promoters can be present as small particles in close vicinity to or on the cobalt particles or as support material.[15] For cobalt catalysts supported by niobia, high selectivities towards heavy hydrocarbons have been reported.[1,16–20] However, due to the low specific surface area and porosity compared to SiO_2 and γ-Al_2O_3 the cobalt loading is limited (< 10 wt%). Consequently, low catalyst-weight normalized activities are obtained for niobia-supported catalysts compared to catalysts with high cobalt loadings of 20 - 25 wt%. In this chapter niobia-modified silica is proposed as support to combine the selectivity-promoting electronic properties of niobia and a high-surface-area matrix to arrive at high catalyst-weight based activities.

Preparation of niobia-modified SiO_2, Al_2O_3, TiO_2, MgO and ZrO_2 was reported before using impregnation, chemical vapor deposition and sol-gel routes and various niobium precursors like niobium ethoxide, niobium pentachloride, niobium oxalate and ammonium niobium oxalate. The support surface area remained intact upon niobium deposition and after high-temperature calcination, retardation of support surface area loss was observed.[21,22] At low loading niobium was found to be present in isolated NbO_4 sites, at higher loading polymerization occurred to NbO_6 sites and ultimately Nb_2O_5 nanocrystals were formed.[23,24]

Niobia-modified Al_2O_3 (5 - 30 wt%) as support for cobalt Fischer-Tropsch catalysts was reported by Mendes et al.[25–27] and was prepared using an ammonium niobium oxalate complex. Niobia was found to form a multi-layered structure and the degree of polymerization increased with loading. At low niobia-loading and catalysis at 1 bar, high methane and low C_{5+} selectivities were observed compared to an Al_2O_3-supported catalyst, attributed to the formation of Co^{2+}-Co^0 species, responsible for methanation. At high niobia-loading after reduction at 500 °C lower methane and higher C_{5+} selectivity but reduced activity were observed, attributed to the formation of Co^0-NbO_x species, responsible for methyl radical formation and promoting chain growth.

In this chapter the influence of niobia and platinum promotion on the structure, activity and selectivity of Co/SiO_2 Fischer-Tropsch catalysts[28,29] is investigated. Niobia-modified silica is prepared and investigated as support material for cobalt and platinum-cobalt Fischer-Tropsch catalysts with industrially relevant cobalt loadings up to ~ 21 wt%. Using TPR, XRD, TEM and chemisorption studies, the effect of Pt and niobia on the Co/SiO_2 structure and mainly the number of active sites is studied. Catalyst performance is investigated at 1 bar and low CO conversion and at industrially relevant conditions, 20 bar and 30 - 40 % CO conversion, and correlated to the catalyst structure, especially to the number of active sites, to reveal the origin of activity promotion by Pt and niobia.

Experimental methods

Preparation

Niobia-modified silica supports were prepared by incipient wetness impregnation[30] of a silica gel (Davisil 643, Sigma Aldrich, > 99 %, SA_{BET}: 260 m^2 g^{-1}; PV: 1.1 mL g^{-1}, PD: 17 nm) with an aqueous 70 - 200 g L^{-1} (0.22 - 0.66 M) ammonium niobium oxalate (ANO, Companhia Brasileira de Metalurgia e Mineração) solution. After drying overnight at 60 °C in stagnant air, the niobium precursor was calcined in a 0.5 L min^{-1} g_{sample}^{-1} air flow at 550 - 900 °C (2 h, 5 °C min^{-1}). Niobia-modified silica samples with niobia loading Nb/Si = 0 - 0.12 at./at. were prepared in multiple impregnation cycles and will be referred to as XNbSi-Y, where X is the atomic ratio Nb/Si and Y is the calcination temperature. An overview of the prepared supports can be found in Appendix D, Table D1.

Cobalt was deposited on niobia-modified silica by impregnation[30] with an aqueous 4.0 M $Co(NO_3)_2 \cdot 6\ H_2O$ solution or by co-impregnation with an aqueous 4.0 M $Co(NO_3)_2 \cdot 6\ H_2O$, 0.03 M $Pt(NH_3)_4(NO_3)_2$ (Co/Pt = 140) solution, aiming for a cobalt loading of 0.9 mg_{Co} m^{-2}, corresponding to 9 - 21 wt% Co. After drying overnight at 60 °C in stagnant air, the cobalt nitrate precursor was calcined at 350 °C (2 h, 3 °C min^{-1}) in a 1 L min^{-1} g_{sample}^{-1} N_2 flow. Cobalt loading is expressed as the mass of metallic cobalt per gram of reduced catalyst. An overview of the prepared catalysts can be found in Table 5.1.

Characterization

Powder X-ray diffraction (XRD) patterns were measured using a Bruker-AXS D2 Phaser X-ray diffractometer using Co-Kα radiation (λ = 1.789 Å). Nb_2O_5 crystallite size was calculated by applying the Scherrer equation (k = 0.9) to the (180) diffraction at 33 ° 2θ, Co_3O_4 crystallite size was calculated using the (311) diffraction at 43 ° 2θ.

N_2 physisorption measurements were performed at -196 °C, using a Micromeritics TriStar 3000 apparatus. Prior to analysis, ~ 100 mg sample was dried at 200 °C for 20 h in an N_2 flow. Surface area was calculated using the BET theory for p/p_0 = 0.06 - 0.25. Pore diameter distribution was determined using the BJH theory applied to the adsorption branch. The pore volume was calculated from single point adsorption at p/p_0 = 0.98.

Back-scattered electron Scanning Electron Microscopy (BSE-SEM) images were acquired with an FEI Phenom type 1 SEM operated at 5 kV.

TEM samples were reduced in a 1 L min^{-1} g_{sample}^{-1} 25 vol% H_2/N_2 flow at 350 °C (2 h, 3 °C min^{-1}), exposed to air at room temperature and subsequently embedded in a two-component epoxy resin (Epofix, EMS) and cured at 60 °C for at least 16 h. Using a Diatome Ultra 35° diamond knife mounted on a Reichert-Jung Ultracut E microtome, an embedded sample was cut in sections with a nominal thickness of 50 nm which were collected on a TEM grid. Bright field TEM and High Angle Annular Dark Field (HAADF) STEM imaging was performed on a Tecnai 20 microscope equipped with a field emission gun operated at 200 kV and EDX detector.

Temperature programmed reduction (TPR) experiments were performed using a Micromeritics Autochem 2920 instrument. Typically 100 mg sample was dried at 120 °C for 1 h in an Ar flow and reduced up to 1000 °C (10 °C min^{-1}) in a 5 vol% H_2/Ar flow.

H_2 chemisorption measurements were performed using a Micromeritics ASAP 2020 instrument. Prior to the measurements, ~ 200 mg sample was dried for 1 h in dynamic vacuum at 100 °C and reduced in an H_2 flow at 350 °C (1 °C min^{-1}, 2 h). H_2 adsorption isotherms were measured at 150 °C, as recommended by Reuel for supported cobalt particles.[31] Metallic cobalt-specific surface area and average particle size were calculated assuming a surface stoichiometry H/Co = 1 and an atomic cross-sectional area of 0.0662 nm^2.

Fischer-Tropsch synthesis

Catalytic testing at 1 bar was performed using a U-shaped, continuous flow, fixed bed reactor system. Typically 10 mg catalyst (38 - 75 μm) was diluted with 200 mg SiC (200 - 400 μm) and loaded in a stainless steel reactor, i.d. = 3 mm, to achieve a bed height of 2 cm. 500 mg SiC was loaded on top of the catalyst bed to ensure gas preheating. The catalysts were reduced in situ at atmospheric pressure in a 33 vol% H_2/Ar flow, GHSV 180 * 10^3 h^{-1}, at 350 °C (2 h, 5 °C min^{-1}). After cooling to 220 °C the gas stream was switched to synthesis gas, H_2/CO = 2.0 v/v, GHSV 18 - 54 * 10^3 h^{-1}, CO conversion 2 - 4 %. Products up to C_{18} were analyzed using an online Varian 430-GC equipped with FID. Activity and selectivity were calculated based on the hydrocarbons formed. The reported catalyst performance was determined after at least 15 h on stream. Catalytic testing at 20 bar was performed using an Avantium Flowrence 16 parallel, continuous flow, fixed bed reactor system. 30 mg catalyst (38 - 75 μm) was diluted with 200 mg SiC (200 μm) and loaded in a stainless steel reactor, i.d. = 2 mm, to achieve a bed height of 4 - 5 cm. The catalysts were reduced in situ at atmospheric pressure in a 25 vol% H_2/He flow, GHSV 6 - 14 * 10^3 h^{-1}, at 350 °C (8 h, 1 °C min^{-1}). After cooling to 180 °C the gas stream was switched to synthesis gas, H_2/CO = 2.0 v/v, GHSV 3 - 8 * 10^3 h^{-1}, and the reactors were pressurized to 20 bar and subsequently heated to 220 °C. The GHSV was adjusted to obtain 30 - 40 % CO conversion. Products up to C_9 were analyzed using an online Agilent Technologies 7890A gas chromatograph. The reported catalyst performance was determined after at least 100 h on stream. The GHSV was defined as the total gas flow divided by the catalyst volume.

Results and discussion

Support modification

Niobia-modified silica was prepared by (multiple) impregnations with an aqueous solution of ammonium niobium oxalate and subsequent drying and calcination at 550 - 900 °C. The Nb/Si atomic ratio was calculated to be 0 - 0.12. Assuming 5 Nb atoms per square nanometer, Nb/Si = 0.12 at./at. was calculated to correspond to a monolayer of niobia on silica.[22,32] An overview of all samples including their designations is shown in Table 5.1, niobia loadings (0 - 21 wt%) and porosity data are shown in Appendix D, Table D1.

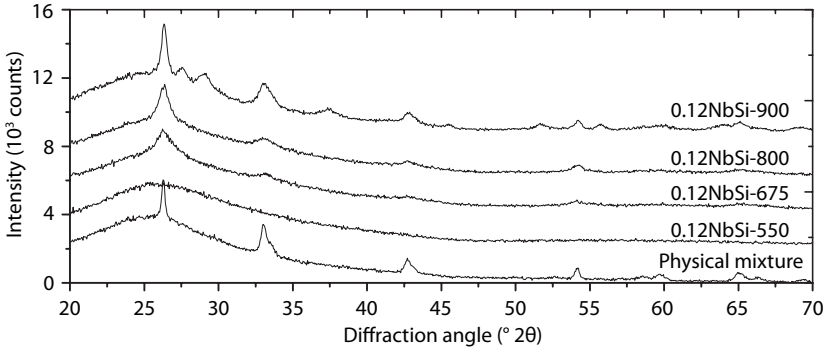

Figure 5.1. X-ray diffractograms (Co-Kα radiation) for a physical mixture of ANO and SiO_2 (Nb/Si =0.12 at./at.) after calcination at 550 °C and for 0.12NbSi-550, 0.12NbSi-675, 0.12NbSi-800 and 0.12NbSi-900. The dominant crystalline Nb_2O_5 phase was orthorhombic Nb_2O_5 (T-phase).

The silica porosity and pore diameter (~ 20 nm) was found to remain intact upon niobia-modification (Appendix D, Figure D1), as previously observed by Ko and Shiju.[33,34] The presence of niobia stabilized the SiO_2 structure during calcination at T > 550 °C resulting in a less pronounced decrease of surface area and porosity than for SiO_2 calcined without niobia-modification. After calcination at 550 °C, no niobia was observed using XRD, indicating strong interaction between niobia and silica. Calcination at higher temperatures led to niobia polymerization and formation of Nb_2O_5 crystallites (Figure 5.1). Niobia polymerization upon increased loading and calcination temperature was also inferred from Diffuse Reflectance Spectroscopy results (Appendix D, Figure D2).

Using TEM no niobia particles were observed after calcination at 550 °C (Figure 5.2A). After calcination at 900 °C, crystalline 15 - 20 nm niobia particles were observed (dark dots in Figure 5.2B). Using SEM, niobia was found to partially migrate to the exterior surface of the macroscopic grains (~ 50 μm) upon calcination at 900 °C (Appendix D, Figure D5).

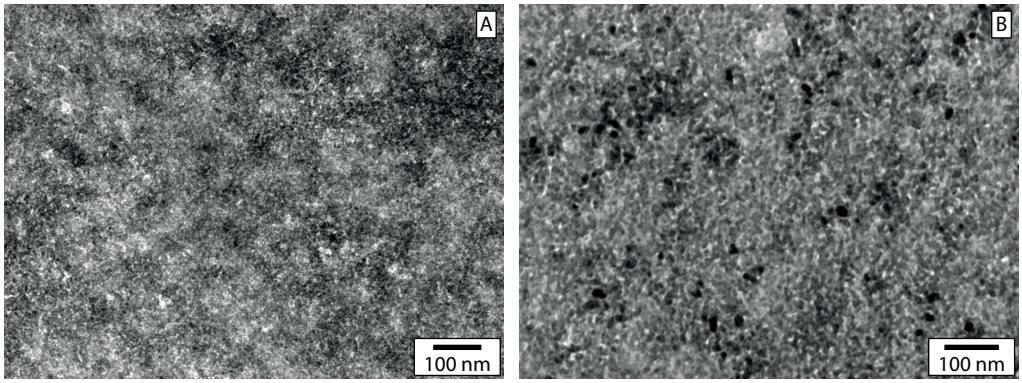

Figure 5.2. Bright field TEM images for 0.12NbSi-550 (A) and 0.12NbSi-900 (B), for more images see Appendix D, Figure D3.

Niobia-silica-supported cobalt catalysts

An overview of the cobalt and platinum-cobalt catalysts prepared using niobia-modified silica as support is shown in Table 5.1.

After impregnation of niobia-modified silica with a cobalt precursor or co-impregnation with cobalt and platinum precursor and subsequent decomposition, the catalysts were studied using X-ray diffraction (Figure 5.3). Cobalt was found to be present as Co_3O_4 and from the XRD line broadening, the Co_3O_4 crystallite size was found to be 8 - 9 nm for Co-(Nb)Si-550 and 7 - 8 nm for PtCo-(Nb)Si-550, Co-(Nb)Si-900 and PtCo-(Nb)Si-900 (Table 5.2).

Using TEM, the cobalt particle size was studied for reduced and passivated PtCo-NbSi catalysts after sample preparation using ultramicrotomy (Figure 5.4). The dark areas, which were well-distributed throughout the catalyst grain, were confirmed to be cobalt-rich; however,

Table 5.1. Nb/Si atomic ratio, (Nb-)Si calcination temperature (T_{calc}), (Nb-)Si-specific surface area (SA_{BET}) and Pt and Co loadings based on intake and assuming Nb to be present as Nb_2O_5 for (Pt)Co-(Nb)Si catalysts.

Catalyst	Support			Catalyst	
Designation	Nb/Si (at./at.)	T_{calc} (°C)	SA_{BET} ($m^2\ g^{-1}$)	Pt loading (wt%)	Co loading [a] (wt%)
Co-Si-550	-	550	269	-	21.0
Co-0.02NbSi-550	0.02	550	265	-	19.3
Co-0.04NbSi-550	0.04	550	262	-	18.8
Co-0.06NbSi-550	0.06	550	256	-	18.6
Co-0.09NbSi-550	0.09	550	250	-	19.8
Co-0.12NbSi-550	0.12	550	240	-	18.8
PtCo-Si-550	-	550	269	0.43	18.0
PtCo-0.02NbSi-550	0.02	550	265	0.46	19.1
PtCo-0.04NbSi-550	0.04	550	262	0.44	18.2
PtCo-0.06NbSi-550	0.06	550	256	0.43	17.8
PtCo-0.09NbSi-550	0.09	550	250	0.41	16.9
PtCo-0.12NbSi-550	0.12	550	240	0.40	16.6
Co-Si-900	-	900	115	-	9.2
Co-0.04NbSi-900	0.04	900	169	-	14.3
Co-0.12NbSi-900	0.12	900	155	-	11.6
PtCo-Si-900	-	900	115	0.21	8.6
PtCo-0.04NbSi-900	0.04	900	169	0.32	13.3
PtCo-0.12NbSi-900	0.12	900	155	0.28	11.8

[a] Corresponding to 0.8 - 1.0 $mg_{Co}\ m^{-2}$ for all catalysts, see Appedix D, Table D2

niobium oxide particles could not unambiguously be distinguished. Based on the analysis of 200 - 350 particles, the average cobalt particle sizes were calculated to be 5 - 9 nm, see Appendix D, Figure D6.

For PtCo-0.12NbSi-900 a significantly smaller apparent cobalt oxide particle size, ~ 5 nm, was determined in comparison to that for the other samples. In this support crystalline niobia particles were observed using TEM and XRD, which would also appear as bright spots and could be confused with cobalt oxide particles, limiting the reliability of these measurements. For the other samples, the crystallite size obtained using XRD was similar to the particle size obtained in this TEM study. In Table 5.2 an overview is given of the cobalt particle sizes estimated based on TEM.

The influence of niobia-modification and Pt-promotion on the cobalt oxide reduction behavior was studied using temperature programmed reduction (TPR). Multiple reduction peaks were observed for the reduction of Co-Si (Figure 5.5). The peak at 300 °C is thought to be the reduction of Co_3O_4 to CoO and usually occurs facile and quantitative.[35–37] Reduction peaks at higher temperatures were attributed to reduction of CoO to metallic Co. Due to strong interaction between CoO and silica and consequent formation of cobalt silicates, high reduction temperatures were required to obtain metallic cobalt.

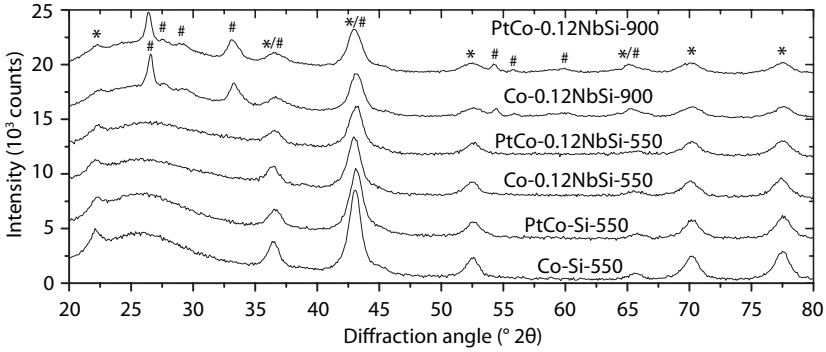

Figure 5.3. X-ray diffractograms (Co-Kα radiation) for calcined (Pt)Co-(Nb)Si catalysts. * indicate Co_3O_4 diffraction lines, # indicate Nb_2O_5 diffraction lines.

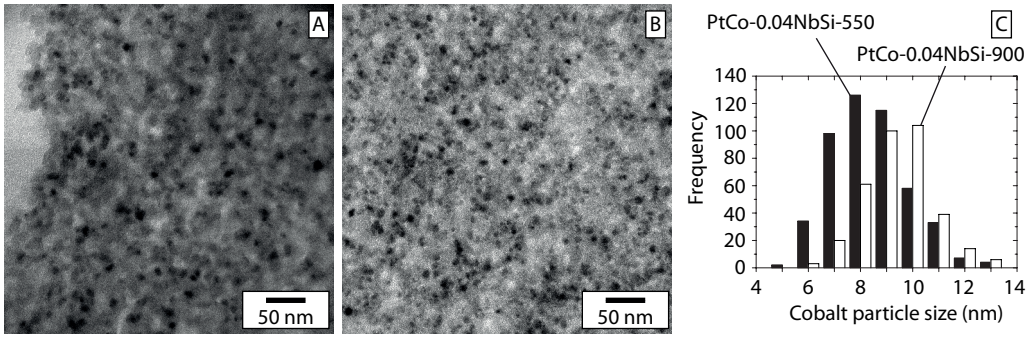

Figure 5.4. Bright field TEM images and cobalt particle size distributions for reduced and passivated PtCo-0.04NbSi-550 (A) and PtCo-0.04NbSi-900 (B).

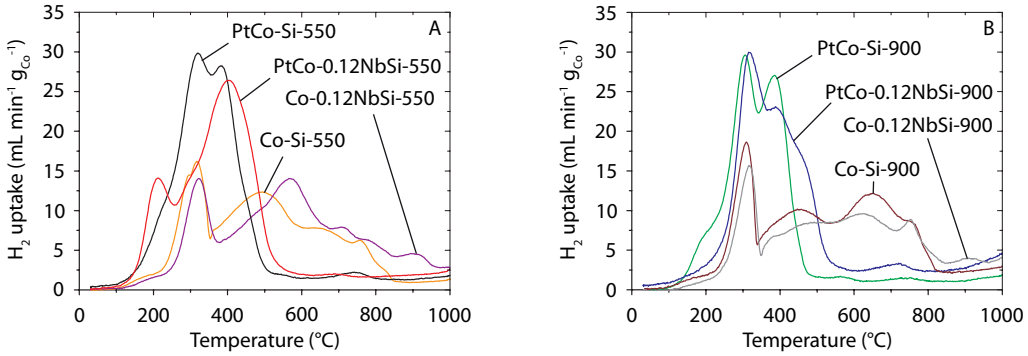

Figure 5.5. Temperature programmed reduction profiles for (Pt)Co-(0.12Nb)Si-550 (A) and (Pt)Co-(0.12Nb)Si-900 (B).

Niobia-modification did not have a large influence on the reducibility of Co-Si (Figure 5.5). The additional peak around 900 °C might be related to the formation of mixed Co-Nb oxides or Nb-Si oxides. Extensive overlap of reduction peaks of cobalt oxide, niobia and probably mixed Co-Nb oxides impeded accurate quantitative determination of the degree of cobalt oxide reduction. No large influence of niobia-modification (Figure 5.5) or support calcination temperature (Figure 5.5B) on the reduction behavior was observed and the consequential effect of niobia-modification on the degree of reduction was expected to be small based on TPR data.

Pt-promotion drastically reduced the temperature required for reduction of Co-Si (Figure 5.5), as observed before for noble metal-promoted cobalt catalysts.[38–40] This will lead to higher degree of cobalt oxide reduction for PtCo catalysts in comparison to Co catalysts after isothermal reduction at 350 °C. The small peak observed at 750 °C was attributed to reduction of cobalt silicates. For PtCo-0.12NbSi-550 (Figure 5.5A) this peak was not observed, indicating that niobia-modification of silica impeded the formation of cobalt silicates.

The metallic cobalt-specific surface area (MSA) after catalyst reduction at 350 °C was measured using H_2 chemisorption at 150 °C (Table 5.2). The MSA was found to increase by a factor of 2 upon Pt-promotion, most likely due to a higher degree of cobalt oxide reduction. Upon niobia-modification, the MSA decreased for both Pt-promoted catalysts and non-Pt-promoted catalysts. This decreasing MSA was also observed by Johnson et al. upon Mn promotion of Co/SiO_2[14] and is attributed to coverage of the cobalt surface by niobia due to SMSI. This suppressed H_2 chemisorption was found to be less severe for catalysts prepared after support calcination at 900 °C, indicating that niobia was less reactive after high-temperature calcination. A potential method to overcome suppressed H_2 chemisorption due to SMSI would be by reduction, subsequent mild oxidation to remove niobia from the cobalt surface, followed by a second reduction cycle at lower temperature as proposed for TiO_2-supported catalysts[41,42] and will be investigated in further studies on niobia-containing catalysts. Methods that could provide additional information on the number of sites participating in Fischer-Tropsch synthesis could be reversible CO chemisorption or sulfur poisoning; however, were not investigated within the scope of this study.

Table 5.2. Co_3O_4 crystallite size determined using XRD and calculated Co crystallite size, metallic cobalt-specific surface area (MSA) and apparent Co particle size (d_{app}) determined using H_2 chemisorption at 150 °C and Co particle size determined using TEM for Co-Si, PtCo-Si, Co-NbSi and PtCo-NbSi catalysts.

	XRD		H_2 chemisorption		TEM
Catalyst	Co_3O_4 (nm)	Co (nm)	MSA ($m^2\ g_{Co}^{-1}$)	Co d_{app} (nm)	Co (nm)
Co-Si-550	8.5	6.8	57	12	-
Co-0.04NbSi-550	8.6	6.8	39	17	-
Co-0.12NbSi-550	7.9	6.3	27	25	-
PtCo-Si-550	7.6	6.0	95	7	-
PtCo-0.04NbSi-550	7.1	5.7	76	9	8
PtCo-0.12NbSi-550	7.3	5.8	54	13	7[a]
Co-Si-900	6.8	5.4	50	14	-
Co-0.04NbSi-900	7.2	5.7	46	15	-
Co-0.12NbSi-900	7.6	6.0	-	-	6[a]
PtCo-Si-900	6.8	5.4	90	8	8[a]
PtCo-0.04NbSi-900	7.2	5.7	73	9	9
PtCo-0.12NbSi-900	7.0	5.6	73	9	5[a]

[a] Calculated from Co_3O_4 particle size using Co and Co_3O_4 densities, see Appendix D, Figure D6

Fischer-Tropsch synthesis

The performance of (Pt-)Co/(Nb)Si was investigated in Fischer-Tropsch catalysis at 1 and 20 bar, 220 °C, H_2/CO = 2.0. An overview of the C_{5+} selectivities is shown in Figure 5.6 and the cobalt-weight normalized activities are shown in Figure 5.7. Cobalt-weight normalized activity (CTY) at 20 bar during the first 150 h on stream is shown in Figure 5.8 for PtCo-Si and PtCo-NbSi catalysts. CH_4 and C_{5+} selectivities, CTY and turnover frequencies at 20 bar are shown in Table 5.3, for data at 1 bar see Appendix D, Table D3.

At 1 bar the C_{5+} selectivity of Co-Si and PtCo-Si was found to be around 30 wt% and increased to 45 - 50 wt% upon niobia-modification (Figure 5.6A). At 20 bar, the C_{5+} selectivity of Co-Si and PtCo-Si was 81 - 86 wt% and decreased slightly upon niobia-modification (Figure 5.6B). The influence of transition-metal oxide (TMO) promotion on the catalyst selectivity has been reported before to depend on the reactor pressure for MnO-promoted Co catalysts.[3–5] At elevated pressures no or only slight influence of TMO promotion on the catalyst selectivity was observed, which is thought to be related to the higher CO coverage at elevated pressure and consequent higher chain growth probability, even without the presence of a promoter, making TMO promotion for selectivity not mandatory.

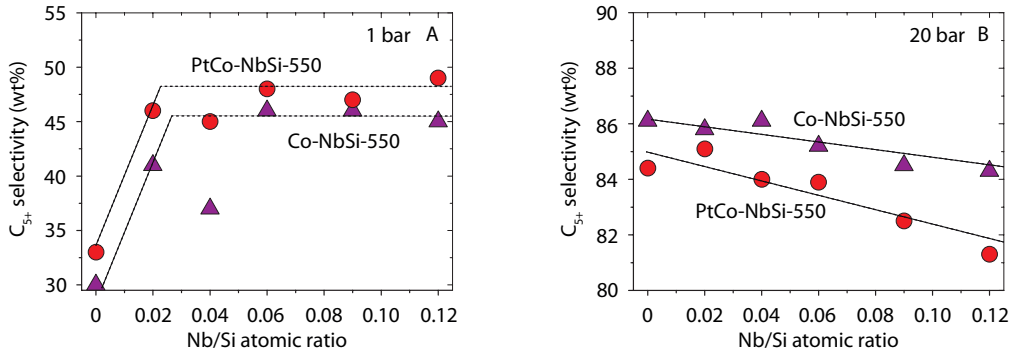

Figure 5.6. C_{5+} selectivity in Fischer-Tropsch synthesis at 220 °C, $H_2/CO = 2.0$ at 1 bar after 15 h on stream (A) and at 20 bar after 100 h on stream (B) for Co-NbSi-550 and PtCo-NbSi-550 catalysts.

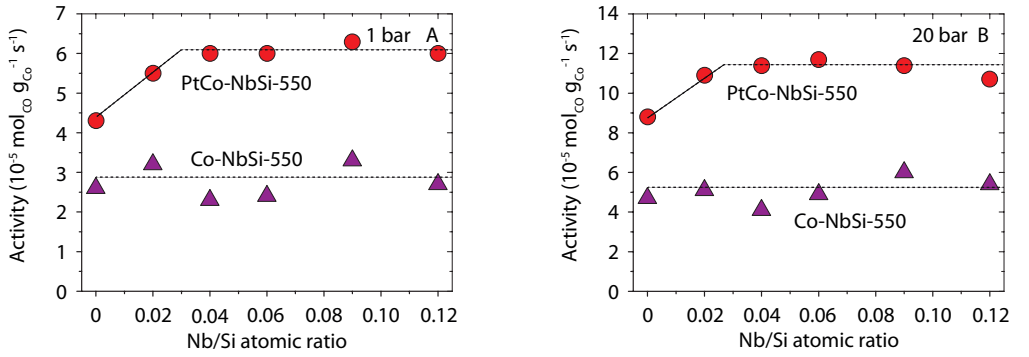

Figure 5.7. Cobalt-weight normalized Fischer-Tropsch activity at 220 °C, $H_2/CO = 2.0$ at 1 bar after 15 h on stream (A) and at 20 bar after 100 h on stream (B) for Co-NbSi-550 and PtCo-NbSi-550 catalysts. Lines were added to guide the eye.

5

Upon Pt-promotion of Co-Si, the CTY was found to increase by a factor of 2 (Figure 5.7). No large effect of niobia-modification on the CTY of Co-Si was observed. Promotion by a combination of platinum and niobia yielded a factor of 3 and 4 increase of the CTY compared to Co-Si for PtCo-NbSi-550 and PtCo-NbSi-900 respectively (Figure 5.8, Table 5.3). The CTY of Co-(Nb)Si and PtCo-(Nb)Si was found to be a factor of 2 higher at 20 bar than at 1 bar. The influence of Pt-promotion, niobia-modification and NbSi calcination temperature on the CTY was similar at 1 and at 20 bar.

Turnover frequencies (TOF) were calculated based on XRD, H_2 chemisorption and TEM results (Table 5.3). The TOF based on H_2 chemisorption results was calculated to be 0.033 s^{-1} and 0.037 s^{-1} for Co-Si-550 and PtCo-Si-550 respectively, which is similar to the TOF reported previously for Co/SiO_2 and $PtCo/SiO_2$ catalysts.[28] This indicates that the observed increase of the CTY upon Pt-promotion of Co-Si was largely caused by a higher number of active sites. This is in agreement with previous observations where noble-metal promotion of supported cobalt catalysts was reported to facilitate cobalt oxide reduction, leading to a higher degree of reduction, increased number of active sites and consequent higher CTY.[38–40]

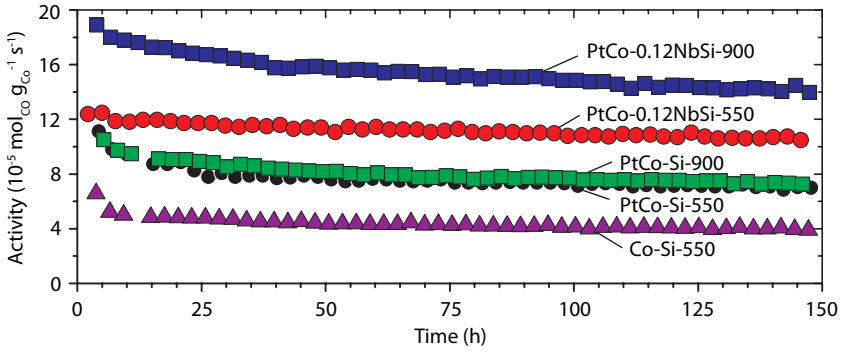

Figure 5.8. Cobalt-weight normalized Fischer-Tropsch activity at 20 bar, 220 °C, H_2/CO = 2.0 for (Pt)Co-(Nb)Si catalysts.

Table 5.3. Selectivity towards CH_4 and C_{5+}, CO conversion (X_{CO}), cobalt-weight normalized activity (CTY) and turnover frequency (TOF) in Fischer-Tropsch catalysis at 20 bar, 220 °C, H_2/CO = 2.0 after 125 h on stream for (Pt)Co-(Nb)Si catalysts.

	Selectivity				TOF		
Catalyst	CH_4 (wt%)	C_{5+} (wt%)	X_{CO} (%)	CTY (mol_{CO} g_{Co}^{-1} s^{-1})	H_2 (s^{-1})	XRD (s^{-1})	TEM (s^{-1})
Co-Si-550	7	86	35	$4.7 * 10^{-5}$	0.033	0.019	
Co-0.02NbSi-550	8	86	35	$5.1 * 10^{-5}$		0.020	
Co-0.04NbSi-550	7	86	28	$4.1 * 10^{-5}$	0.042	0.017	
Co-0.06NbSi-550	8	85	32	$4.9 * 10^{-5}$		0.018	
Co-0.09NbSi-550	9	85	29	$6.0 * 10^{-5}$		0.024	
Co-0.12NbSi-550	9	84	37	$5.4 * 10^{-5}$	0.080	0.020	
PtCo-Si-550	8	84	39	$8.8 * 10^{-5}$	0.037	0.031	
PtCo-0.02NbSi-550	8	85	39	$11 * 10^{-5}$		0.041	
PtCo-0.04NbSi-550	8	84	36	$11 * 10^{-5}$	0.060	0.038	0.057
PtCo-0.06NbSi-550	7	84	39	$12 * 10^{-5}$		0.039	
PtCo-0.09NbSi-550	8	83	36	$11 * 10^{-5}$		0.040	
PtCo-0.12NbSi-550	9	81	33	$11 * 10^{-5}$	0.079	0.037	0.035
Co-Si-900	10	83	11	$3.5 * 10^{-5}$	0.028	0.011	
Co-0.04NbSi-900	9	81	29	$5.6 * 10^{-5}$	0.049	0.019	
Co-0.12NbSi-900	9	84	24	$5.5 * 10^{-5}$		0.020	0.017
PtCo-Si-900	9	81	28	$8.8 * 10^{-5}$	0.039	0.028	0.031
PtCo-0.04NbSi-900	9	82	36	$15 * 10^{-5}$	0.080	0.050	0.082
PtCo-0.12NbSi-900	10	82	30	$14 * 10^{-5}$	0.078	0.047	0.033

The TOF calculated based on XRD results was significantly lower than the TOF calculated based on H_2 chemisorption results (Table 5.3). This was attributed to incomplete cobalt oxide reduction for Co-Si and Co-NbSi and suppressed H_2 chemisorption for Co-NbSi and PtCo-NbSi (vide supra). No large influence of niobia-modification of Co-Si on the TOF based on Co_3O_4 crystallite size from XRD was observed (Table 5.3). Based on H_2 chemisorption results, the TOF was calculated to increase upon niobia-modification; however, this is most likely related to an underestimated number of active sites due to SMSI as also observed by Johnson et al.[14]

With a combination of niobia- and platinum-promotion both an increased number of active sites (Table 5.2) and an increased TOF (Table 5.3) compared to Co-Si were calculated based on H_2 chemisorption, XRD and TEM data. The calculated increase of CTY and TOF was more pronounced for PtCo-NbSi-900 in which niobia was present as 15 - 20 nm nanocrystals than for PtCo-NbSi-550 where niobia was amorphous, indicating that the synergy between niobia nanocrystals and platinum more efficiently promoted the activity of Co-Si catalysts.

A turnover frequency increase was previously reported for noble metal-promoted Co/TiO_2[43–45] and Co/Nb_2O_5[46] catalysts, both being a combination of noble metal promotion and a partially reducible oxide support. In this study an increased TOF was also observed for catalysts promoted by niobia and for catalysts with high porosity and industrially relevant cobalt loadings.

A useful study that could provide additional insight in the role of Pt and niobia during reaction rather than ex situ, for example the influence of reactants and products including H_2O at reaction conditions, could be SSITKA; however, was not investigated within the scope of this study.

Conclusions

Niobia-modified silica (NbSi) with Nb/Si 0 - 0.12 at./at. was prepared by impregnation and subsequent calcination at 550 - 900 °C. At low loadings, Nb was present as small niobia particles or mixed Nb-Si species. Upon higher loadings and calcination temperatures a niobia layer was formed on SiO_2 and ultimately 15 - 20 nm nanocrystals were observed which partially migrated to the exterior surface of the silica grains. Co and PtCo catalysts with constant surface-specific loading of 0.8 - 1.0 $mg_{Co}\,m^{-2}$ (9 - 21 wt% Co) were prepared by impregnation of the NbSi supports.

Based on XRD, H_2 chemisorption and TEM data no evidence was found that niobia-modification of silica had a large influence on the cobalt particle size of around 8 nm. Upon Pt-promotion of Co-Si and Co-NbSi, cobalt oxide reduction was facilitated and the number of active sites was found to increase by a factor of 2.

At 1 bar the C_{5+} selectivity in Fischer-Tropsch catalysis increased significantly upon niobia-modification, whereas at 20 bar it was found to only slightly decrease. This pressure dependence of niobia promotion is thought to be related to a higher intrinsic CO coverage at elevated pressures, making promotion with a transition-metal oxide for selectivity less effective at more elevated pressures.

The influences of Pt-promotion, niobia-modification and NbSi calcination temperature on the catalyst activity were found to be identical at 1 bar and at 20 bar. Upon Pt-promotion of Co/SiO_2, the cobalt-weight normalized activity was found to increase by a factor of 2 due to a

higher number of active sites. Promotion of Co-Si by a combination of platinum and niobia yielded an increase of the cobalt-weight normalized activity by a factor of 2 - 3 in the case of amorphous niobia and a factor of 3 - 4 for niobia nanocrystals. This increase was partially attributed to an increased number of active sites and partially to an increased turnover frequency. The activity increase was highest for catalysts after NbSi calcination at 900 °C, indicating that synergistic promotion was more efficient between platinum and niobia nanocrystals than between platinum and amorphous or atomically dispersed niobia.

An increased turnover frequency was previously reported for noble metal-promoted Co/Nb_2O_5 and Co/TiO_2, which both display quite low specific surface areas. In this study an increased TOF was obtained for supported Co catalysts promoted by niobia plus noble metal with high surface area and industrially relevant cobalt loadings.

Acknowledgements

Dr. Robson Monteiro and Mr. Rogério Ribas (CBMM) are acknowledged for useful discussions and for supplying ANO samples. Mrs. Marjan Versluijs-Helder (XRD), Mr. Hans Meeldijk (ultramicrotomy and TEM), Ms. Nazila Masoud (ultramicrotomy), Dr. Korneel Cats (TPR), Mr. Gang Wang (TPR) and Ms. Ilse van Ravenhorst (DRS) are acknowledged for assistance and execution of indicated analyses.

This chapter was based on the work of Sebastiaan Nijveld, a brilliant M.Sc. student who contributed greatly to this research. He passed away during the period of this study.

References

[1] den Otter, J. H.; de Jong, K. P. *Top. Catal.* **2014**, *57*, 445–450.
[2] van der Laan, G. P.; Beenackers, A. A. C. M. *Catal. Rev.* **1999**, *41*, 255–318.
[3] Bezemer, G. L.; Radstake, P. B.; Falke, U.; Oosterbeek, H.; Kuipers, H. P. C. E.; Dillen, A. J. van; de Jong, K. P. *J. Catal.* **2006**, *237*, 152–161.
[4] Dinse, A.; Aigner, M.; Ulbrich, M.; Johnson, G. R.; Bell, A. T. *J. Catal.* **2012**, *288*, 104–114.
[5] Thiessen, J.; Rose, A.; Meyer, J.; Jess, A.; Curulla-Ferré, D. *Microporous Mesoporous Mater.* **2012**, *164*, 199–206.
[6] Bukur, D. B.; Pan, Z.; Ma, W.; Jacobs, G.; Davis, B. H. *Catal. Letters* **2012**, *142*, 1382–1387.
[7] Rane, S.; Borg, Ø.; Yang, J.; Rytter, E.; Holmen, A. *Appl. Catal., A* **2010**, *388*, 160–167.
[8] Rane, S.; Borg, Ø.; Rytter, E.; Holmen, A. *Appl. Catal., A* **2012**, *437-438*, 10–17.
[9] Borg, Ø.; Eri, S.; Blekkan, E. A.; Storsater, S.; Wigum, H.; Rytter, E.; Holmen, A. *J. Catal.* **2007**, *248*, 89–100.
[10] Khodakov, A. Y.; Chu, W.; Fongarland, P. *Chem. Rev.* **2007**, *107*, 1692–1744.
[11] Morales Cano, F.; de Smit, E.; de Groot, F. M. F.; Visser, T.; Weckhuysen, B. M. *J. Catal.* **2007**, *246*, 91–99.
[12] Morales Cano, F.; de Groot, F. M. F.; Gijzeman, O.; Mens, A. J. M.; Stephan, O.; Weckhuysen, B. M. *J. Catal.* **2005**, *230*, 301–308.
[13] Moradi, G. R.; Basir, M. M.; Taeb, A.; Kiennemann, A. *Catal. Commun.* **2003**, *4*, 27–32.
[14] Johnson, G. R.; Werner, S.; Bell, A. T. *ACS Catal.* **2015**, *5*, 5888–5903.
[15] Prieto, G.; De Mello, M. I. S.; Concepción, P.; Murciano, R.; Pergher, S. B. C.; Martínez, A. *ACS Catal.* **2015**, *5*, 3323–3335.
[16] Frydman, A.; Soares, R. R.; Schmal, M. *Stud. Surf. Sci. Catal.* **1993**, *75*, 2797–2800.
[17] Silva, R. R. C. M.; Schmal, M.; Frety, R.; Dalmon, J. A. *J. Chem. Soc. - Faraday Trans.* **1993**, *89*, 3975–3980.

[18] de Souza, C. D.; Cesar, D. V.; Marchetti, S. G.; Schmal, M. *Stud. Surf. Sci. Catal.* **2007**, *147*, 147–152.
[19] Soares, R. R.; Frydman, A.; Schmal, M. *Catal. Today* **1993**, *16*, 361–370.
[20] de Oliveira, A. K.; dos Santos, B. C. A.; Monteiro, R. de S.; Moraes, L. J.; Pereira, T. A.; Schmal, M.; Sousa-Aguiar, F. E.; Sugaya, M. de F.; Vicentini, V. P. World patent WO 2005/085390 A1 **2005**.
[21] Jehng, J.-M.; Wachs, I. E. *Catal. Today* **1993**, *16*, 417–426.
[22] Jehng, J.-M.; Wachs, I. E. *J. Mol. Catal.* **1991**, *67*, 369–387.
[23] Wachs, I. E. *Catal. Today* **1996**, *27*, 437–455.
[24] Wachs, I. E.; Briand, L. E.; Jehng, J.-M.; Burcham, L.; Gao, X. *Catal. Today* **2000**, *57*, 323–330.
[25] Mendes, F. M. T.; Perez, C. a. C.; Noronha, F. B.; Schmal, M. *Catal. Today* **2005**, *101*, 45–50.
[26] Mendes, F. M. T.; Perez, C. A. C.; Noronha, F. B.; Souza, D. D.; Cesar, D. V.; Freund, H.-J.; Schmal, M. *J. Phys. Chem. B* **2006**, *110*, 9155–9163.
[27] Mendes, F. M. T.; Perez, C. .; Soares, R. .; Noronha, F. .; Schmal, M. *Catal. Today* **2003**, *78*, 449–458.
[28] Munnik, P.; de Jongh, P. E.; de Jong, K. P. *J. Am. Chem. Soc.* **2014**, *136*, 7333–7340.
[29] Munnik, P.; Krans, N. A.; de Jongh, P. E.; de Jong, K. P. *ACS Catal.* **2014**, *4*, 3219–3226.
[30] Munnik, P.; de Jongh, P. E.; de Jong, K. P. *Chem. Rev.* **2015**, *115*, 6687–6718.
[31] Reuel, R. C. *J. Catal.* **1984**, *85*, 63–77.
[32] Prieto, G.; Concepción, P.; Martínez, A.; Mendoza, E. *J. Catal.* **2011**, *280*, 274–288.
[33] Ko, E. I.; Bafrali, R.; Nuhfer, N. T.; Wagner, N. J. *J. Catal.* **1985**, *95*, 260–270.
[34] Shiju, N. R.; Brown, D. R.; Wilson, K.; Rothenberg, G. *Top. Catal.* **2010**, *53*, 1217–1223.
[35] Jacobs, G.; Ji, Y.; Davis, B. H.; Cronauer, D.; Kropf, A. J.; Marshall, C. L. *Appl. Catal., A* **2007**, *333*, 177–191.
[36] Noronha, F. B.; Perez, C. A.; Fre, R. *Phys. Chem. Chem. Phys.* **1999**, *1*, 2861–2867.
[37] Sexton, B. *J. Catal.* **1986**, *97*, 390–406.
[38] Jacobs, G.; Das, T. K.; Zhang, Y.; Li, J.; Racoillet, G.; Davis, B. H. *Appl. Catal., A* **2002**, *233*, 263–281.
[39] Diehl, F.; Khodakov, A. Y. *Oil Gas Sci. Technol. - Rev. l'IFP* **2009**, *64*, 11–24.
[40] Das, T. K.; Jacobs, G.; Patterson, P. M.; Conner, W. A.; Li, J.; Davis, B. H. *Fuel* **2003**, *82*, 805–815.
[41] Soled, S. L.; Iglesia, E.; Fiato, R. A.; Baumgartner, J. E.; Vroman, H.; Miseo, S. *Top. Catal.* **2003**, *26*, 101–109.
[42] Tauster, S. J. *Acc. Chem. Res.* **1987**, *20*, 389–394.
[43] Iglesia, E. *Appl. Catal., A* **1997**, *161*, 59–78.
[44] Iglesia, E.; Soled, S. L.; Fiato, R. A.; Via, G. H. *J. Catal.* **1993**, *143*, 345–368.
[45] Eschemann, T. O.; Oenema, J.; de Jong, K. P. *Catal. Today* **2016**, *261*, 60–66.
[46] Noronha, F. B.; Frydman, A.; Aranda, D. A. G.; Perez, C.; Soares, R. R.; Morawek, B.; Castner, D.; Campbell, C. T.; Frety, R.; Schmal, M. *Catal. Today* **1996**, *28*, 147–157.

Chapter 6a

Summary and Concluding Remarks

Summary

The increasing demand for energy, the call for cleaner transportation fuels and the desire to be less dependent on crude oil, have stimulated the development of methods to synthesize liquid hydrocarbons from alternative feedstocks. Carbon-containing feedstocks such as natural gas, coal and biomass are alternatives and can be converted into synthesis gas, a mixture of CO and H_2. Via the Fischer-Tropsch reaction, typically catalyzed by iron or cobalt catalysts, hydrocarbons can be produced from synthesis gas and can be used as high-quality transportation fuels or chemicals.

Cobalt is the preferred Fischer-Tropsch catalyst for the production of transportation fuels, in particular kerosene and diesel, due its high selectivity towards heavy hydrocarbons. Reaction conditions, the addition of promoters and the morphology and chemical nature of the support are known to largely affect the catalyst performance. In industrial catalysts, typically cobalt nanoparticles of ~ 10 nm are supported on highly porous metal oxides like γ-Al_2O_3, SiO_2 or TiO_2, allowing for high metal loadings of 10 - 25 wt%. For niobia-supported catalysts very promising selectivities towards heavy hydrocarbons have previously been reported in Fischer-Tropsch synthesis. The goal of this thesis is to more extensively investigate the potential of niobia as support and promoter in cobalt based Fischer-Tropsch catalysts and to study the role of reaction conditions and noble metal promoters on the performance of niobia-containing catalysts.

In Co/niobia Fischer-Tropsch catalysts typically crystalline, low specific surface area supports are used with low cobalt loadings (~ 5 wt%) and dispersions. In **Chapter 2** the influence of temperature and atmosphere on the morphology, crystallinity and porosity of niobia was studied. Higher porosity crystalline niobia was prepared by carbon-templated crystallization of amorphous niobia and by niobia synthesis in a porous carbon template. 4 - 21 wt% cobalt was deposited on the prepared crystalline supports and on amorphous niobia by impregnation and deposition precipitation. Deposition precipitation of cobalt precursor led to precipitation in the solution separate from the crystalline niobia support due to insufficient interaction. After cobalt deposition on amorphous niobia, no easily reducible cobalt species were obtained and consequently only low activity in Fischer-Tropsch catalysis was observed. For 5 wt% Co/Nb_2O_5 prepared by impregnation of crystalline niobia both high cobalt-weight normalized activity and high C_{5+} selectivity were obtained, previously only observed for promoted Co catalysts. Application of higher cobalt loadings than 5 wt% led to increased catalyst-weight normalized activity; however, the cobalt-weight normalized activity decreased due to formation of larger cobalt particles and decreased interaction of cobalt with the support. Selectivity promotion by niobia was suppressed due to decreased cobalt-support interaction and consequently lower C_{5+} selectivities were observed.

In **Chapter 3**, the performance of 5 wt% Co/Nb_2O_5 was compared to that of 28 wt% Co/γ-Al_2O_3 for the Fischer-Tropsch synthesis at 20 bar and over the temperature range of 220 - 260 °C. The C_{5+} selectivity of Nb_2O_5-supported cobalt catalysts was found to be very high, up to 90 wt% C_{5+} at 220 °C. The cobalt-weight normalized activity was found to be similar for Nb_2O_5- and γ-Al_2O_3-supported catalysts at identical reaction temperature. However, due to the low cobalt loading, the catalyst-weight normalized activity of Co/Nb_2O_5 was lower than for Co/γ-Al_2O_3 catalysts with

higher cobalt loadings. This low activity could largely be compensated by increasing the reaction temperature, although the C_{5+} selectivity decreased upon increasing reaction temperature. Due to the high intrinsic C_{5+} selectivity, Nb_2O_5-supported catalysts could be operated up to ~ 250 °C at a target C_{5+} selectivity of 80 wt%, whereas γ-Al_2O_3-supported catalysts called for an operation temperature of ~ 210 °C. At this target C_{5+} selectivity, the catalyst-weight normalized activity was found to be identical for 5 wt% Co/Nb_2O_5 and 28 wt% Co/Al_2O_3, while the cobalt-weight normalized activity was a factor of four higher for the Nb_2O_5-supported catalyst.

Noble metal promotion is a common method to enhance the activity of cobalt Fischer-Tropsch catalysts, typically by increasing the number of active sites. In **Chapter 4,** Co/Nb_2O_5 catalysts and the effect of Pt-promotion thereon are investigated in comparison to γ-Al_2O_3- and α-Al_2O_3-supported catalysts. In Fischer-Tropsch catalysis at 1 bar and compared to α-Al_2O_3-supported catalysts, superior C_{5+} selectivities were observed for γ-Al_2O_3- and Nb_2O_5-supported catalysts, attributed to the presence of Co^{2+} due to incomplete cobalt oxide reduction and NbO_x species at the cobalt surface, respectively. At 20 bar, Nb_2O_5- and α-Al_2O_3-supported catalysts were found to exhibit superior C_{5+} selectivities of ~ 85 wt%, which were attributed to the larger pore sizes compared to γ-Al_2O_3-supported catalysts. Upon Pt-promotion of Co/Nb_2O_5 the cobalt-weight normalized activity was found to increase by a factor of 2.4, while the high C_{5+} selectivity of 85 wt% was maintained. Based on environmental TEM results no indications were found that Pt affected the cobalt particle size in Co/Nb_2O_5 catalysts. A kinetic study indicates an increased number of active sites upon Pt-promotion whereas Steady-State Isotopic Transient Kinetic Analysis experiments show that a combination of an increased number of active sites and an increased turnover frequency is at the origin of the enhanced activity in Co/Nb_2O_5 catalysts upon Pt-promotion. Pt was tentatively proposed to bring about more efficient promotion of Co by NbO_x being present as smaller clusters.

The influence of niobia independent of support morphology and the selectivity-promoting properties of niobia on a highly porous support were studied using niobia-modified silica as a support in **Chapter 5**. This support was prepared by impregnation of silica with a niobium precursor and after calcination the support structure was found to be largely preserved. Niobia-modified silica was applied as support for Co and PtCo catalysts with cobalt loadings up to 21 wt%. Niobia promotion was found to increase the C_{5+} selectivity at 1 bar; however, appeared to be not effective at 20 bar. Promotion of Co/SiO_2 by a combination of platinum and niobia yielded an increase of the cobalt-weight normalized activity by a factor of 2-3 in the case of amorphous niobia and by a factor of 3-4 with niobia nanocrystals present on the silica, due to both an increased number of active sites and an increased cobalt-surface specific activity (turnover frequency).

Concluding remarks

In this thesis niobia has been shown to be an attractive support for application in Fischer-Tropsch catalysis at industrially relevant conditions without apparent deactivation up to at least 200 hours of operation. This proves that the level of potentially poisoning contaminants is sufficiently low and niobia is stable up to 260 °C and CO conversion levels higher than 80 % with

concomitant high steam pressures. Niobia-supported cobalt catalysts were found to exhibit high selectivities towards liquid hydrocarbons at competitive cobalt-weight based activities. Due to the low porosity of crystalline niobia, only low cobalt loadings can be applied and consequently low catalyst-weight based activities could be obtained. However, using the reactor temperature or Pt-promotion, methods were found to compensate for the low cobalt loading and to obtain competing selectivities and catalyst-weight based activities while using a low amount of cobalt.

Transition-metal oxides are typical promoters added to cobalt Fischer-Tropsch catalysts to enhance the selectivity towards heavy hydrocarbons. In this thesis niobia was found to be a very efficient selectivity promoter particularly at 1 bar. At 20 bar, the influence of support pore size appeared to be important. This fundamentally different role of promoters at 1 and 20 bar is very relevant to understand the necessity and role of transition-metal oxide promoters in cobalt-based Fischer-Tropsch catalysts but also calls for characterization methods at conditions as close as possible to industrially applied conditions, for example SSITKA at elevated pressures.

Indications were found that the role of platinum in cobalt-based Fischer-Tropsch synthesis was not limited to facilitation of cobalt oxide reduction but also played a role during Fischer-Tropsch synthesis in $PtCo/Nb_2O_5$ catalysts. Due to the similar support nature, this observation is very relevant to Co/TiO_2, a catalyst relevant for industrial Fischer-Tropsch synthesis. Noble metal promoters are rarely applied in Co/TiO_2 since facile and complete reduction is typical without noble metals present. Following the observations presented in this thesis, the influence of noble metal promotion on the performance of Co/TiO_2 catalysts was investigated and the activity was found to be enhanced up to a factor of four upon noble metal promotion.

In future research, additional characterization techniques could give more insight into the structure of Co/Nb_2O_5 and $PtCo/Nb_2O_5$ catalysts. Environmental and high-resolution TEM studies could give information on the cobalt particle size and crystallinity, (in-situ) X-ray absorption spectroscopy (EXAFS/XANES) and Near Ambient Pressure X-ray excited Photoelectron Spectroscopy (NAP-XPS) could be useful to study the species present at the cobalt surface after reduction and during Fischer-Tropsch catalysis and additional kinetic studies, preferably SSITKA at elevated pressures, could provide additional insight into the origin of the increased apparent TOF, observed for niobia-promoted and -supported PtCo catalysts.

Niobia-based catalysts could also be attractive for the conversion of synthesis gas into products other than linear heavy paraffins. Copper, iron and nickel are well-known catalysts for the production of methanol, lower olefins and methane, respectively, and niobia could be explored as support. Furthermore, strong indications are present that acidic niobia surface groups can introduce hydrocracking and hydro-isomerization activity to Co/niobia catalysts. This might allow direct formation of liquid products rather than solid waxes and production of gasoline-like branched hydrocarbons instead of diesel or kerosene. Recent environmental concerns regarding emissions of diesel engines in passenger cars and the large demand in especially the United States make production of synthetic gasoline more attractive.

Chapter 6b

Nederlandse Samenvatting

Samenvatting

In de afgelopen decennia is de vraag naar energie drastisch toegenomen door een groeiende wereldbevolking en een toenemend welvaartsniveau. Vooral voor de productie van brandstoffen voor de transportsector is de afhankelijkheid van ruwe olie groot. De voorraden hiervan zijn groot maar het wordt steeds moeilijker en duurder deze te exploiteren door bijvoorbeeld hun locatie. Daarnaast is er een groeiende vraag naar schonere brandstoffen met minder aromaten en zwavel- en stikstofverbindingen om verbrandingsmotoren efficiënter en schoner te kunnen maken en te voldoen aan de steeds strenger wordende uitstooteisen.

Aardgas, steenkool en biomassa zijn alternatieven om op korte termijn te dienen als grondstof voor de productie van schone, synthetische brandstoffen zoals dieselolie en kerosine. Aardgas is hiervan de economisch meest aantrekkelijke optie door de grote beschikbare reserves. Omdat het moeilijk en duur is om gassen te transporteren worden deze momenteel vaak niet benut en aardgas dat vrijkomt tijdens oliewinning wordt soms zelfs afgefakkeld. Biomassa is, zeker als het geproduceerd is op een manier die niet in strijd is met de voedselvoorziening, het meest duurzame alternatief omdat hiervoor minder fossiele bronnen nodig zijn en er een meer CO_2-neutrale cyclus kan ontstaan.

Deze alternatieve energiebronnen kunnen echter niet op dezelfde manier als ruwe olie worden vervoerd en verwerkt tot dieselolie. Het is daarom wenselijk ze op de plaats waar ze beschikbaar komen om te zetten in vloeibare producten. Dit kan via een proces waarbij aardgas, steenkool of biomassa eerst wordt omgezet in synthesegas, een mengsel van koolmonoxide (CO) en waterstof (H_2). Via het Fischer-Tropschproces kan synthesegas daarna worden omgezet in koolwaterstoffen die de basis vormen van allerlei chemicaliën en brandstoffen.

Voor het splitsen en op de gewenste manier recombineren van CO en H_2 zijn katalysatoren nodig. Voor de synthese van Fischer-Tropschbrandstoffen zoals dieselolie en kerosine zijn dit bij voorkeur metallische kobaltdeeltjes van ongeveer 10 nanometer. Om te voorkomen dat de kobaltdeeltjes samenklonteren en daardoor hun actieve oppervlak verliezen worden deze afgezet op een poreuze drager zoals silica, alumina of titania. Naast het uit elkaar houden van de kobaltdeeltjes, kan de drager ook de selectiviteit en de activiteit van de katalysator beïnvloeden. Dit kan ook door de toevoeging van edelmetalen of overgangsmetaaloxiden, zogeheten promoters, aan het kobalt.

Van kobaltdeeltjes die afgezet zijn op niobiumoxide is bekend dat ze erg selectief zijn voor het maken van lange koolwaterstofketens. Het doel van dit proefschrift is om de toepassing van niobiumoxide als drager of promoter in kobaltkatalysatoren voor het Fischer-Tropschproces uitgebreider te onderzoeken. Belangrijke aspecten hierin zijn het ontwikkelen van een methode om katalysatoren te maken, het bestuderen van de structuur van de katalysatoren en het onderzoeken welke invloed de structuur van de drager, de toevoeging van edelmetalen en de reactiecondities hebben op de activiteit en selectiviteit in Fischer-Tropschsynthese.

In niobiumoxide-gedragen Fischer-Tropschkatalysatoren wordt doorgaans kristallijn niobiumoxide met een lage porositeit en specifiek oppervlak gebruikt. Het nadeel hiervan is dat slechts lage kobaltbeladingen van ongeveer 5 gewichtsprocent (gew%) mogelijk zijn,

terwijl voor katalysatoren die gebruikt worden in industriële toepassingen kobaltbeladingen tot 25 gew% gebruikelijk zijn. In **Hoofdstuk 2** is daarom onderzocht of het mogelijk is om amorf niobiumoxide met hogere porositeit te gebruiken als drager voor Fischer-Tropschkatalysatoren. Ook is onderzocht of het mogelijk is om kristallijn niobiumoxide met een hogere porositeit te maken door het variëren van de gasatmosfeer tijdens kristallisatie of de toepassing van een mal van koolstof. Door middel van impregnatie of depositieprecipitatie werd 4 - 21 gew% kobalt afgezet op zowel amorf als kristallijn niobium oxide. Na kobalt afzetting op amorf niobiumoxide werd tijdens reductie geen metallisch kobalt gevormd en daardoor waren deze katalysatoren niet actief in de Fischer-Tropschsynthese. Door onvoldoende interactie tussen de drager en het kobalt leidde depositieprecipitatie tot de groei van kobaltdeeltjes met groottes tot 1 μm in plaats van nanodeeltjes. Katalysatoren die gemaakt werden door impregnatie van kristallijn niobiumoxide (Nb_2O_5) bleken een hoge activiteit en selectiviteit naar vloeibare koolwaterstoffen (C_{5+}) te bezitten. De toepassing van hogere beladingen door middel van meerdere impregnaties leidde tot de vorming van grotere kobaltdeeltjes en daardoor afnemende activiteit per massa-eenheid kobalt. Ook de C_{5+}-selectiviteit nam af door de verminderde interactie tussen de drager en het kobalt.

In **Hoofdstuk 3** worden 5 gew% Co/Nb_2O_5 en 28 gew% $Co/\gamma\text{-}Al_2O_3$ vergeleken in Fischer-Tropschsynthese op 20 bar bij 220 - 260 °C. Voor Co/Nb_2O_5 werd een hoge C_{5+}-selectiviteit gemeten van 90 gew% bij 220 °C. De activiteit genormaliseerd naar de kobaltmassa was vergelijkbaar voor deze katalysatoren, maar door de lagere metaalbelading was de activiteit per massa-eenheid katalysator aanzienlijk lager voor Co/Nb_2O_5. Door het verhogen van de reactortemperatuur kan de lage activiteit grotendeels worden gecompenseerd, maar dit gaat wel deels ten koste van de selectiviteit. Bij een gewenste C_{5+}-selectiviteit van 80 gew% kan Co/Nb_2O_5, dankzij de hoge intrinsieke C_{5+}-selectiviteit, gebruikt worden bij ~ 250 °C, terwijl $Co/\gamma\text{-}Al_2O_3$ maar op ~ 210 °C kan worden gebruikt om deze selectiviteit te bereiken. Bij een gewenste C_{5+}-selectiviteit van 80 gew% was, hoewel bij een andere reactortemperatuur, de activiteit genormaliseerd naar de katalysatormassa gelijk voor Co/Nb_2O_5 en $Co/\gamma\text{-}Al_2O_3$. De activiteit per massa-eenheid kobalt was hierbij een factor vier hoger voor Co/Nb_2O_5.

Het toevoegen van een kleine hoeveelheid edelmetaal zoals platina is een gebruikelijke manier om de activiteit van Fischer-Tropschkatalysatoren te verhogen. Het veronderstelde mechanisme hiervoor is dat het edelmetaal de reductie van kobaltoxide tot metallisch kobalt katalyseert en hierdoor het aantal actieve centra toeneemt. In **Hoofdstuk 4** worden Co/Nb_2O_5-katalysatoren en de invloed van platinapromotie hierop bestudeerd in vergelijking met $\alpha\text{-}Al_2O_3$- en $\gamma\text{-}Al_2O_3$-gedragen katalysatoren. In Fischer-Tropschsynthese op 1 bar bleek de C_{5+}-selectiviteit van Nb_2O_5- en $\gamma\text{-}Al_2O_3$-gedragen katalysatoren hoger te zijn dan van $\alpha\text{-}Al_2O_3$-gedragen katalysatoren. Dit werd toegeschreven aan de aanwezigheid van Co^{2+} door onvolledige reductie van kobaltoxide in het geval van $\gamma\text{-}Al_2O_3$-gedragen katalysatoren en aan de aanwezigheid van gedeeltelijk gereduceerd niobia (NbO_x) op het kobaltoppervlak in Nb_2O_5-gedragen katalysatoren. Op 20 bar werd juist een hogere C_{5+}-selectiviteit gevonden voor Nb_2O_5- en $\alpha\text{-}Al_2O_3$-gedragen katalysatoren dan voor $\gamma\text{-}Al_2O_3$-gedragen katalysatoren, wat werd toegeschreven aan de grotere poriediameter van

deze dragers. In de aanwezigheid van platina bleek de activiteit van Co/Nb_2O_5, genormaliseerd naar de kobaltmassa, met een factor 2,4 toegenomen. Met een aantal analysetechnieken werd onderzocht of dit werd veroorzaakt door een toegenomen aantal actieve centra of door een hogere omzettingsfrequentie. Door Co/Nb_2O_5 en $PtCo/Nb_2O_5$ in een elektronenmicroscoop te reduceren werd de invloed van Pt op de grootte van de kobaltdeeltjes onderzocht; er bleek geen waarneembare invloed te zijn. Uit een studie naar de invloed van Pt op de reactiekinetiek van Co/Nb_2O_5 bleek dat de toegenomen activiteit veroorzaakt wordt door een combinatie van een toegenomen aantal actieve centra en een verhoogde omzettingsfrequentie. Als verklaring voor de rol van platina werd voorgesteld dat de aanwezigheid van platina ervoor zorgt dat kobalt efficiënter gepromoteerd werd door de aanwezigheid van kleinere NbO_x deeltjes op het kobaltoppervlak.

Om de invloed van niobia onafhankelijk van de morfologie van de drager te kunnen onderzoeken, werd silica gepromoteerd met niobiumoxide als drager bestudeerd in **Hoofdstuk 5**. Poreus silica met een hoog specifiek oppervlak werd geïmpregneerd met een oplossing van een niobiumzout. Na calcinatie bleek de structuur van het silica intact waardoor tot 21 gew% Co en PtCo afgezet konden worden op deze drager. In Fischer-Tropschsynthese op 1 bar bleek dat niobia-promotie van de drager een positieve invloed had op de C_{5+}-selectiviteit, echter op 20 bar werd deze invloed niet waargenomen. Na toevoeging van zowel niobia als platina werd een factor twee tot vier toename van de naar de kobaltmassa genormaliseerde activiteit waargenomen ten opzichte van Co/SiO_2. De toename werd verklaard door zowel een toename van het aantal actieve centra als een verhoogde omzettingsfrequentie.

Afsluitende opmerkingen

In dit proefschrift wordt getoond dat Nb_2O_5 een interessante drager is voor toepassing in Fischer-Tropschkatalysatoren. Uit het uitblijven van waarneembare deactivatie bij industrieel relevante condities (20 bar, 260 °C, 80 % CO conversie) bleek dat in de drager geen verontreinigingen aanwezig waren die de katalysator vergiftigden en dat de drager voldoende stabiel was tegen stoomdruk. Nb_2O_5-gedragen katalysatoren bleken daarnaast een hoge selectiviteit naar zware koolwaterstoffen te bezitten. Door de lage porositeit van kristallijn Nb_2O_5 konden slechts lage kobaltbeladingen worden toegepast waardoor de voor toepassing op industriële schaal belangrijke activiteit per massa-eenheid katalysator aanzienlijk lager was dan voor bijvoorbeeld SiO_2- of γ-Al_2O_3-gedragen katalysatoren. Echter, door gebruik te maken van de reactortemperatuur en platinapromotie werden methodes ontdekt om de lage kobaltbelading te compenseren waardoor minder kobalt benodigd was voor het behalen van vergelijkbare selectiviteit en activiteit per massa-eenheid katalysator.

Om de selectiviteit naar zware koolwaterstoffen te verhogen worden vaak overgangsmetaaloxiden als promoter toegevoegd aan Fischer-Tropschkatalysatoren. In dit proefschrift wordt getoond dat niobiumoxide kan dienen als een effectieve promoter van de selectiviteit, echter vooral in Fischer-Tropschkatalyse op 1 bar. Op 20 bar bleek de invloed van de poriegrootte belangrijker. Deze fundamenteel verschillende rol van overgangsmetaaloxiden is ook van belang om de noodzaak en rol van deze promoters te bepalen voor Fischer-Tropschkatalysatoren met andere

dragers, maar maakt ook de noodzaak duidelijk om karakterisering uit te voeren bij condities die zo dicht mogelijk liggen bij industrieel gebruikte condities, bijvoorbeeld door het bestuderen van kinetiek bij verhoogde druk.

In dit proefschrift worden aanwijzingen getoond dat platina in Fischer-Tropschkatalysatoren niet alleen de reductie van kobaltoxide katalyseert maar in het geval van $PtCo/Nb_2O_5$ ook een belangrijke rol speelt tijdens de Fischer-Tropschreactie zelf. Door de grote chemische overeenkomsten tussen Nb_2O_5 en TiO_2 kunnen deze resultaten van groot belang zijn voor Co/TiO_2-katalysatoren die worden toegepast in Fischer-Tropschproductie. Voor zover bekend werden tot op heden zelden edelmetalen toegepast in Co/TiO_2-katalysatoren omdat zij voor hun traditionele rol als reductiepromotor niet vereist waren. Naar aanleiding van de resultaten die beschreven zijn in dit proefschrift is de invloed van edelmetalen op Co/TiO_2-katalysatoren onderzocht en ook hierbij bleek de activiteit door toevoeging van platina met een factor vier toe te nemen.

Vervolgonderzoek met aanvullende karakterisatietechnieken zou meer inzicht kunnen geven in de structuur van Co/Nb_2O_5- en $PtCo/Nb_2O_5$-katalysatoren. Met elektronenmicroscopie zouden in een uitgebreidere studie de deeltjesgrootte en kristalliniteit van kobalt na reductie beter kunnen worden bepaald. Röntgenspectroscopie (EXAFS/XANES, NAP-XPS) zou extra informatie kunnen geven over de deeltjes die aanwezig zijn op het kobaltoppervlak na reductie en tijdens de Fischer-Tropschreactie. Studies naar de reactiekinetiek, bij voorkeur SSITKA bij industrieel relevante condities, zou inzicht kunnen geven wat de verhoogde omzettingsfrequentie veroorzaakt die werd waargenomen bij PtCo-katalysatoren die gedragen of gepromoteerd zijn door niobiumoxide.

Niobiumoxide-gebaseerde katalysatoren zouden ook interessant kunnen zijn voor de omzetting van synthesegas in andere producten dan lineaire paraffinen. Koper, ijzer en nikkel zijn belangrijke katalysatoren voor de productie van respectievelijk methanol, lichte olefinen en methaan en onderzocht zou kunnen worden wat de toepassing van niobiumoxide als drager voor invloed heeft op deze katalysatoren. Verder zijn er sterke aanwijzingen dat de aanwezigheid van zure groepen op het niobiumoxide extra functionaliteit zou kunnen introduceren, namelijk het hydrokraken of -isomeriseren van de gevormde producten. Dit zou kunnen leiden tot de directe vorming van vloeibare producten in plaats van vaste wassen en zou de vervolgstap waarin de was gekraakt wordt overbodig kunnen maken. Ook zouden vertakte koolwaterstoffen gevormd kunnen worden die typisch voorkomen in benzine. Gezien de recente zorgen rondom de uitstoot van dieselmotoren in personenauto's en de grote vraag naar benzine in vooral de Verenigde Staten zou de productie van synthetische benzine zeer interessant zijn.

Appendix A

Supporting Information Chapter 2

Exploratory Studies for Synthesis of Niobia-supported Cobalt Fischer-Tropsch Catalysts

Purity data Niobium oxide hydrate

Niobium oxide hydrate (HY-340, AD/4465), 72.6 wt% Nb_2O_5, LOI 26.7 wt%, 179 ppm Cl Free, 60 ppm Fe, 57 ppm Na, 66 ppm K, 629 ppm Ta, 54 ppm Si, 2229 ppm Ti, < 50 ppm P, < 20 ppm S, < 30 ppm C.

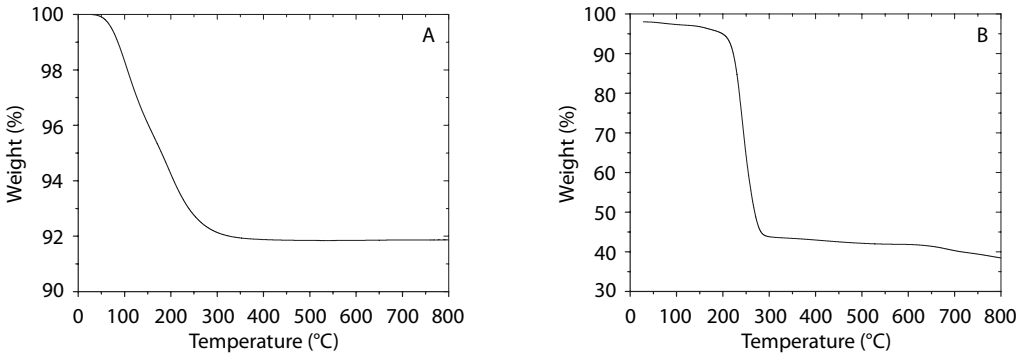

Figure A1. Weight loss upon thermal treatment in 10 mL min^{-1} N_2 for niobium oxide hydrate (10 °C min^{-1}, A) and ammonium niobium oxalate (3 °C min^{-1}, B), determined using TGA after drying at 120 °C.

Porosity niobium oxide

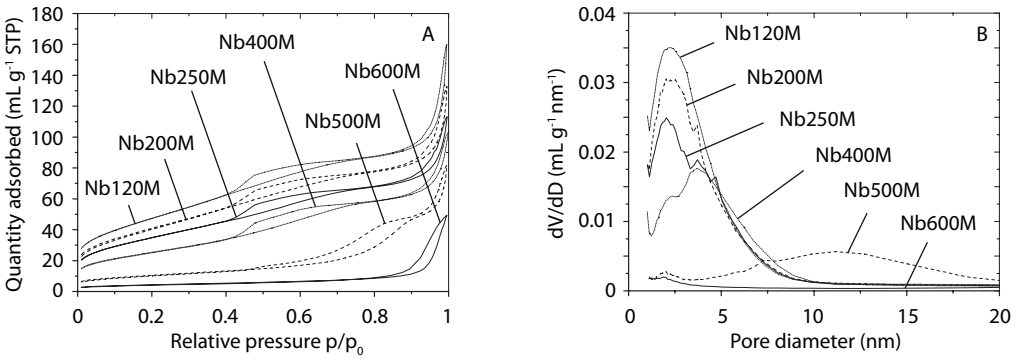

Figure A2. N_2 physisorption isotherms (A) and pore size distributions (B) for Nb120-600M.

Table A1. Specific surface area and pore volume obtained for Nb120-900M.

Sample	SA_{BET} ($m^2\ g^{-1}$)	Pore volume ($mL\ g^{-1}$)
Nb120M	173	0.19
Nb400M	95	0.13
Nb600M	16	0.06
Nb900M	< 1	< 0.01

Influence of gas atmosphere during niobia calcination

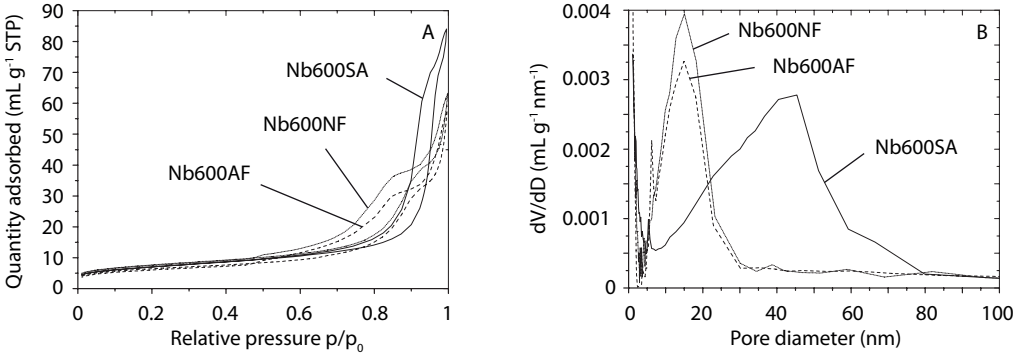

Figure A3. N_2 physisorption isotherms (A) and pore size distributions (B) for Nb600SA, Nb600AF and Nb600NF.

A

Carbon-templated niobia crystallization

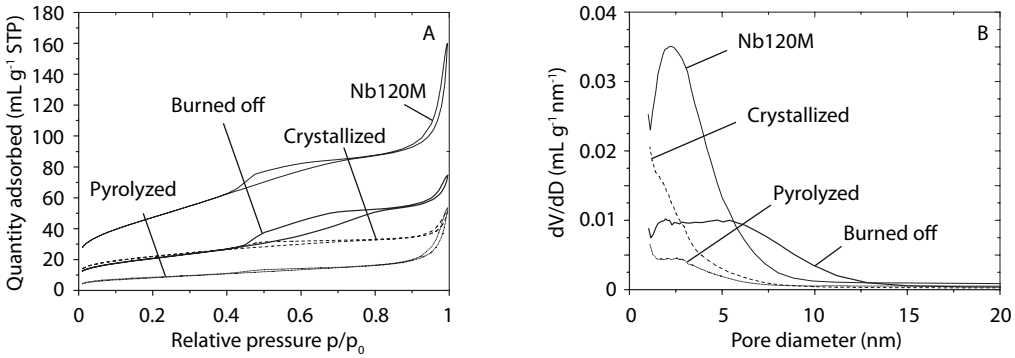

Figure A4. N_2 physisorption isotherms (A) and pore size distributions (B) for niobium oxide hydrate (Nb120M), after impregnation with sucrose solution and pyrolysis, after crystallization in N_2 and after carbon burn-off in air (Nb-CTC-S).

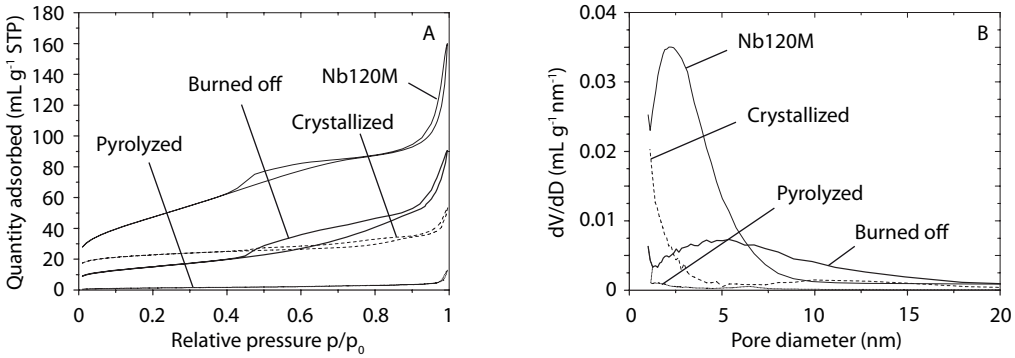

Figure A5. N_2 physisorption isotherms (A) and pore size distributions (B) for niobium oxide hydrate (Nb120M), after impregnation with furfuryl alcohol and pyrolysis, after crystallization in N_2 and after carbon burn-off in air (Nb-CTC-F).

After niobium oxide hydrate impregnation with furfuryl alcohol or a sucrose solution and subsequent pyrolysis, the niobium oxide pores were filled and not accessible for N_2 physisorption (Figure A4 - A5). Since the nature of the carbon template was unknown, the weight fraction of niobia in the pyrolyzed sample could not be determined without further quantitative elemental analysis and the degree of pore filling could not be calculated. After niobia crystallization small pores (< 3 nm) were accessible and after carbon burn-off larger pores up to 10 nm diameter were accessible.

Carbon-templated niobia synthesis

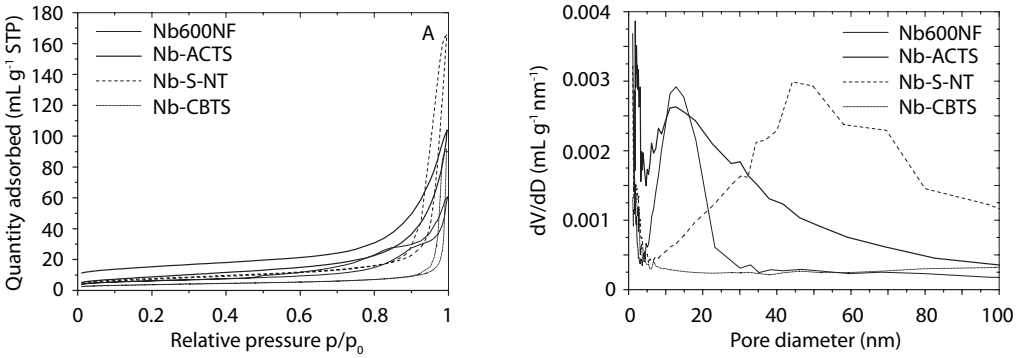

Figure A6. N_2 physisorption isotherms (A) and pore size distributions (B) for Nb600SA, Nb-S-NT, Nb-ACTS and Nb-CBTS.

Porosity Co/niobia

The surface area and porosity loss during cobalt nitrate decomposition at 350 °C after cobalt deposition Nb120M was less pronounced than upon thermal treatment of niobium oxide hydrate at 350 °C (Nb350M), indicating that the presence of cobalt stabilized the niobia structure (Table A2). Also the 2 - 5 nm mesopores, which largely disappeared upon thermal treatment of niobia at 350 °C, were preserved in the presence of cobalt, see Figure A7.

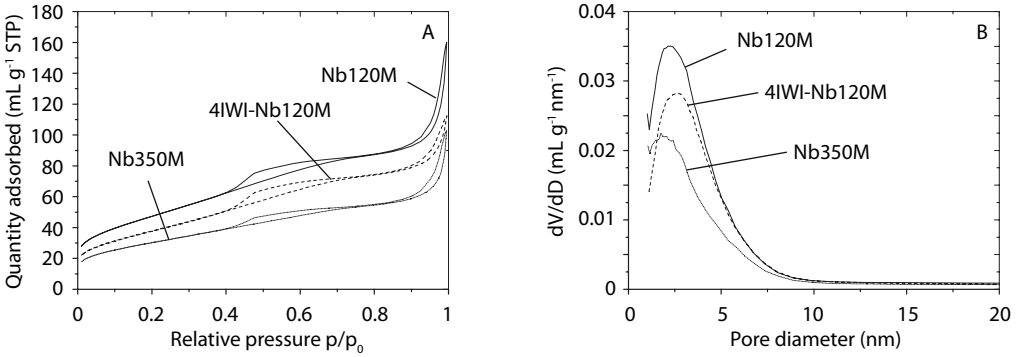

Figure A7. N_2 physisorption isotherms (A) and pore size distributions (B) for Nb120M, Nb350M and 4IWI-Nb120M.

Table A2. Specific surface area (SA_{BET}) and pore volume for Nb120M, Nb350M and 4IWI-Nb120M.

Sample	SA_{BET} ($m^2\ g^{-1}$)	Pore volume (mL g^{-1})
Nb120M	173	0.19
Nb350M	110	0.12
4IWI-Nb120M	139	0.15

X-ray diffraction Co/niobia

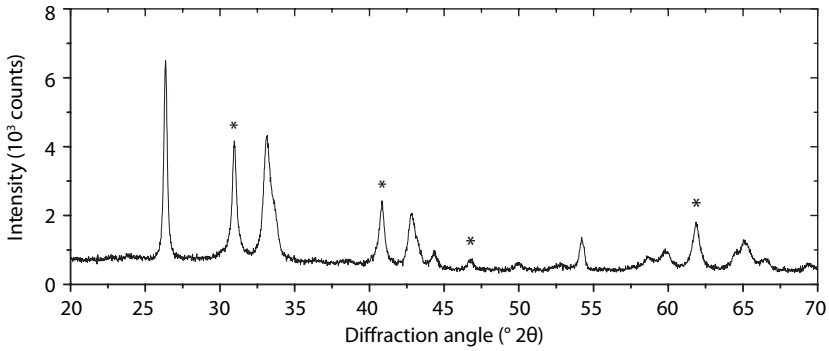

Figure A8. X-ray diffractogram (Co-Kα radiation) for amorphous niobia after impregnation with cobalt nitrate and subsequent heat treatment at 600 °C in stagnant air. * indicate $CoNb_2O_6$ lines, other lines represent Nb_2O_5 (pseudohexagonal TT-phase and orthorhombic T-phase).

Thermal treatment at 600 °C of 5IWI-Nb120M in order to crystallize niobia after cobalt deposition led to the formation of $CoNb_2O_6$ (Figure A8), which could not be reduced up to 600 °C. Formation of $CoNb_2O_6$ was not observed upon thermal treatment at 600 °C after cobalt deposition on crystalline Nb_2O_5.

Fischer-Tropsch synthesis

Table A3. H_2 uptake and apparent Co particle size (d_{app}) determined using H_2 chemisorption and activity and selectivity in Fischer-Tropsch synthesis at 1 bar, 220 °C, $H_2/CO = 2.0$ for 5-21IWI-Nb600M after at least 20 h on stream.

	H_2 uptake	d_{app}	Activity		Selectivity	
Catalyst	($\mu mol_{H2}\ g_{cat}^{-1}$)	(nm)	($mol_{CO}\ g_{cat}^{-1}\ s^{-1}$)	($mol_{CO}\ g_{Co}^{-1}\ s^{-1}$)	CH_4 (wt%)	C_{5+} (wt%)
5IWI-Nb600M	23	18	$1.7 * 10^{-6}$	$3.0 * 10^{-5}$	14	70
10IWI-Nb600M	29	29	$2.5 * 10^{-6}$	$2.5 * 10^{-5}$	15	64
15IWI-Nb600M	63	19	$3.1 * 10^{-6}$	$2.2 * 10^{-5}$	17	60
17IWI-Nb600M	72	23	$3.0 * 10^{-6}$	$1.5 * 10^{-5}$	19	55
21IWI-Nb600M	51	35	$4.0 * 10^{-6}$	$2.1 * 10^{-5}$	25	42

Appendix B

Supporting Information Chapter 3

Highly Selective and Active Niobia-supported Cobalt Catalysts for Fischer-Tropsch Synthesis

Support and catalyst porosity

Table B1. Specific surface area (SA_{BET}) and pore volume (p/p_0 = 0.98, pores < 100 nm) determined using N_2 physisorption at -196 °C for Nb_2O_5 after calcination at 600 °C, 5 wt% Co/ Nb_2O_5, γ-Al_2O_3 and 28 wt% Co/γ-Al_2O_3.

Sample	SA_{BET} ($m^2\ g^{-1}$)	Pore volume ($mL\ g^{-1}$)
Nb_2O_5	16	0.07
5 wt% Co/Nb_2O_5	14	0.05
γ-Al_2O_3	185	0.5
28 wt% Co/γ-Al_2O_3	130	0.3

Temperature programmed reduction

To determine the degree of reduction during isothermal reduction, the H_2 uptake during TPR at 350 °C (5 wt% Co/Nb_2O_5) or 500 °C (28 wt% $Co/\gamma\text{-}Al_2O_3$) for 3 h was measured (Figure B1). For Co/Nb_2O_5 reduced at 350 °C, the degree of reduction was calculated to be ~ 90 %, for $Co/\gamma\text{-}Al_2O_3$ reduced at 500 °C ~ 60 % reduction was calculated, assuming $H_2/Co = 1.33$ for full reduction from Co_3O_4 to Co.

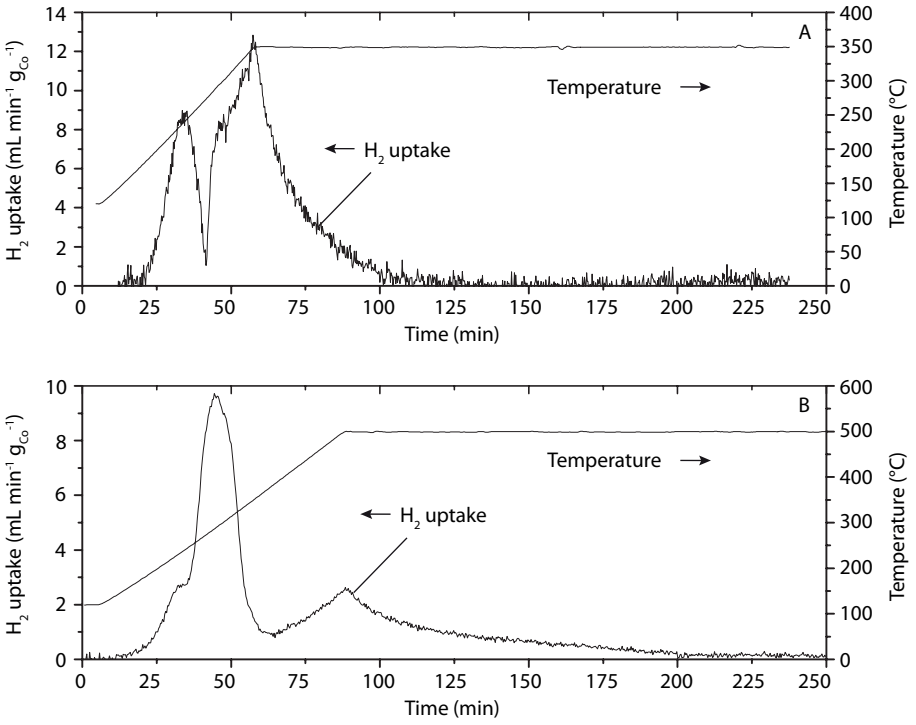

Figure B1. H_2 uptake during isothermal reduction in 5 vol% H_2/Ar for 5 wt% Co/Nb_2O_5 at 350 °C (A) and for 28 wt% $Co/\gamma\text{-}Al_2O_3$ at 500 °C (B).

Appendix C

Supporting Information Chapter 4

On the Superior Activity and Selectivity of $PtCo/Nb_2O_5$ Fischer-Tropsch Catalysts

Porosity data supports

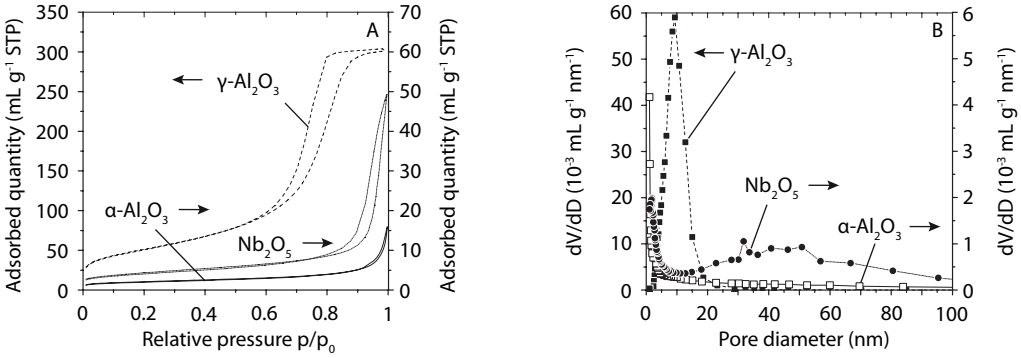

Figure C1. N_2 physisorption isotherms at -196 °C (A) and pore size distributions (B) for N_2O_5 after calcination at 600 °C and for γ-Al_2O_3 and α-Al_2O_3.

Environmental XRD

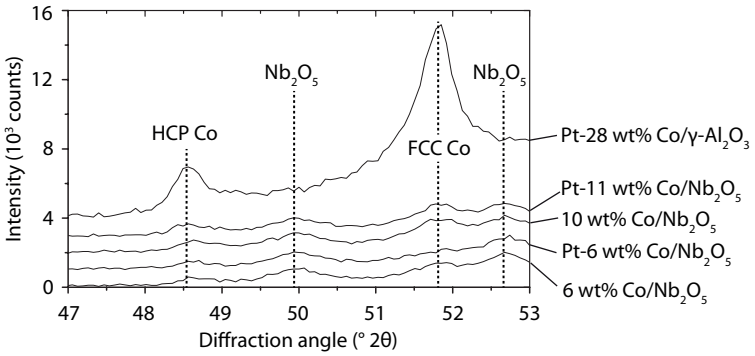

Figure C2. Environmental X-ray diffractograms (Co-Kα radiation) at 350 °C in 25 vol% H_2/He for Co/Nb_2O_5, PtCo/Nb_2O_5 and PtCo/γ-Al_2O_3.

Transmission electron microscopy

Co/Nb_2O_5 and PtCo/Nb_2O_5 catalysts were analyzed using TEM after cobalt nitrate decomposition (calcined), after reduction at 350 °C, 3 °C min^{-1}, 2 h in 25 vol% H_2/N_2 (GHSV 60 * 10^3 h^{-1}) and subsequent exposure to air at room temperature (passivated) and after at least 100 h on stream in Fischer-Tropsch synthesis at 20 bar (spent).

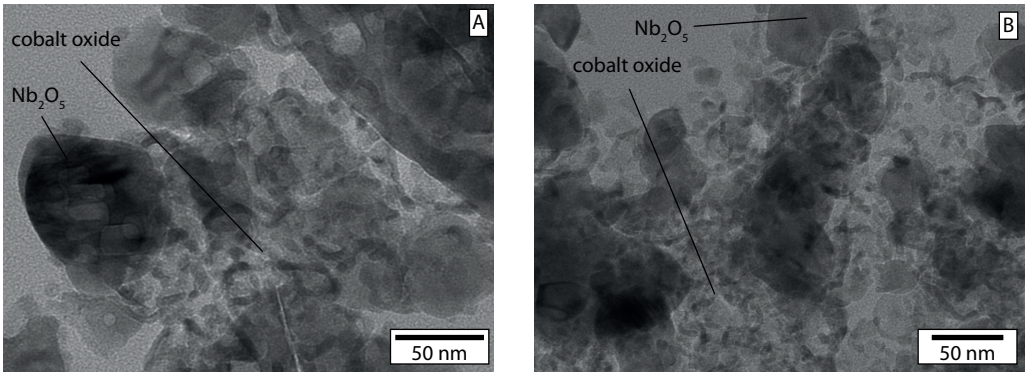

Figure C3. TEM images of calcined 9 wt% Co/Nb_2O_5 (A) and Pt-9 wt% Co/Nb_2O_5 (B). TEM imaging using an FEI Tecnai 20 microscope, sample preparation using ultramicrotomy.

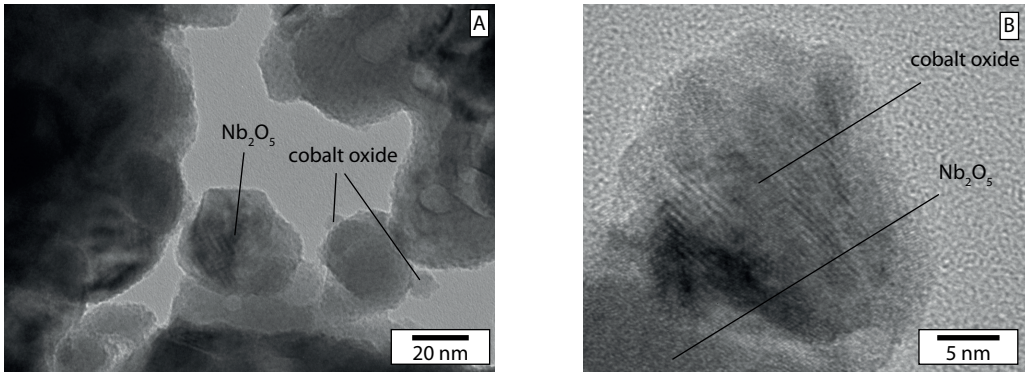

Figure C4. TEM images of passivated 6 wt% Co/Nb_2O_5 catalysts. TEM imaging using an FEI Tecnai 20 microscope, sample preparation using ultramicrotomy.

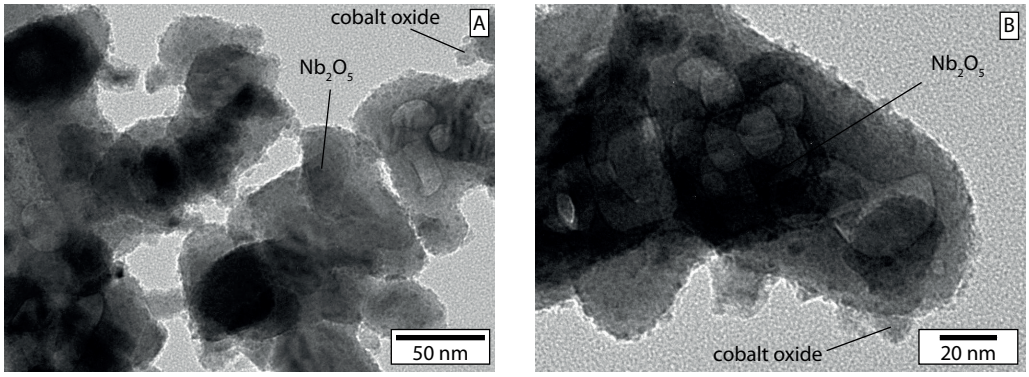

Figure C5. TEM images of spent 6 wt% Co/Nb_2O_5 catalysts. TEM imaging using an FEI Tecnai 12 microscope.

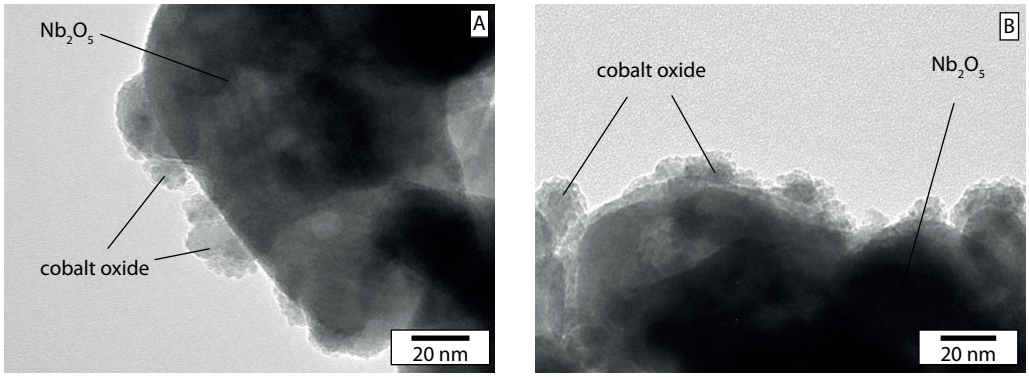

Figure C6. TEM images of spent Pt-6 wt% Co/Nb_2O_5 catalysts. TEM imaging using an FEI Tecnai 12 microscope.

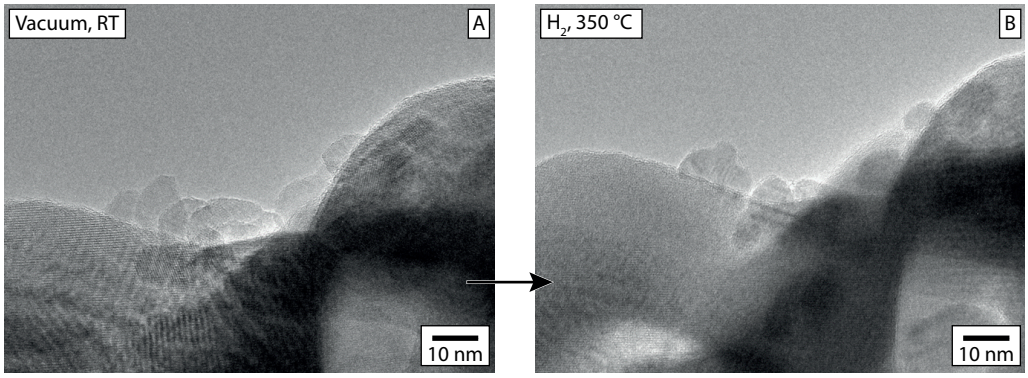

Figure C7. Bright field TEM images in vacuum at room temperature (A) and in 100 Pa H_2 at 350 °C (B) for passivated Pt-6 wt% Co/Nb_2O_5. TEM imaging using an FEI Titan ETEM G2 microscope.

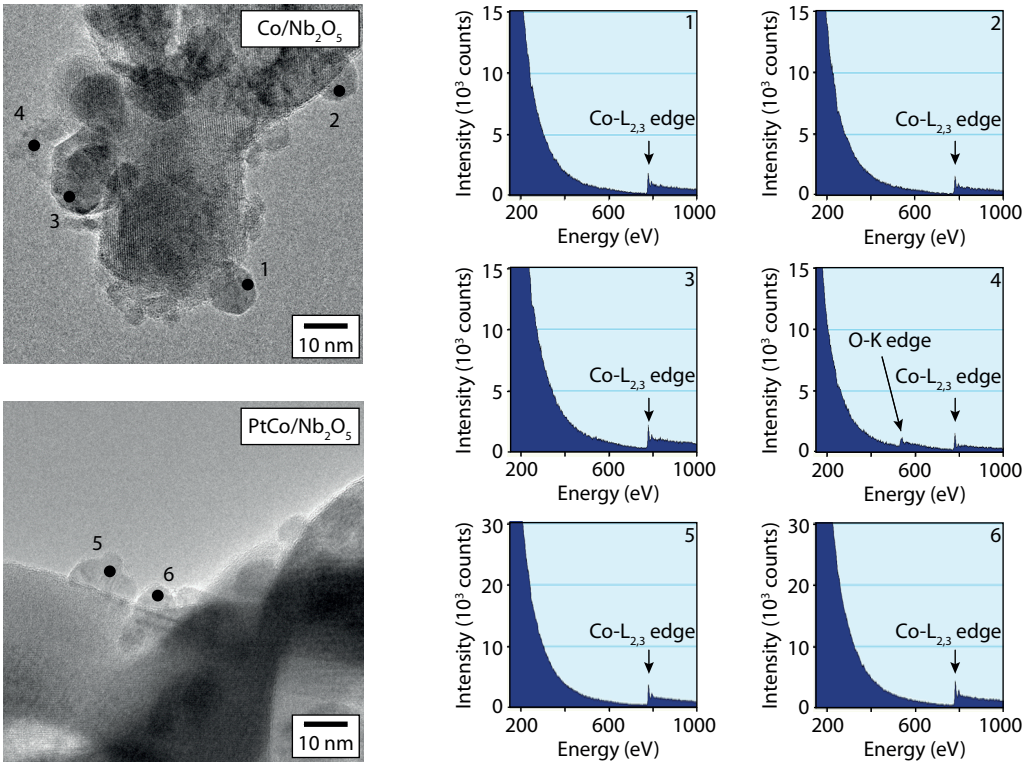

Figure C8. STEM-EELS data obtained in 100 Pa H_2 at 350 °C for 6 wt% Co/Nb_2O_5 and Pt-6 wt% Co/Nb_2O_5 using an FEI Titan ETEM G2 microscope.

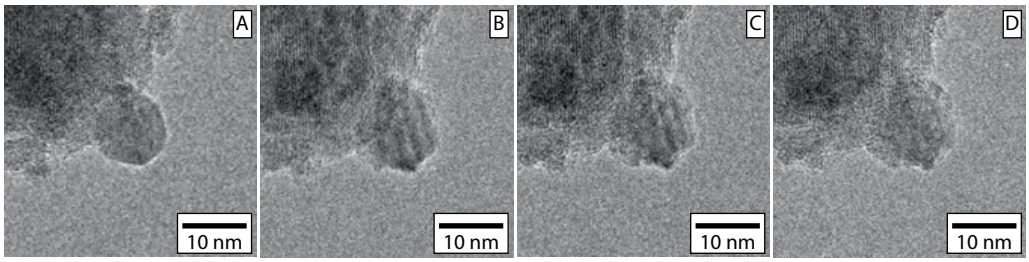

Figure C9. Bright field TEM images for passivated Co/Nb_2O_5 in 100 Pa H_2 at 350 °C (A) and in 100 Pa H_2 at room temperature after 0 s (B), 87 s (C) and 168 s (D) exposure to the electron beam. TEM imaging using an FEI Titan ETEM G2 microscope.

Temperature programmed reduction

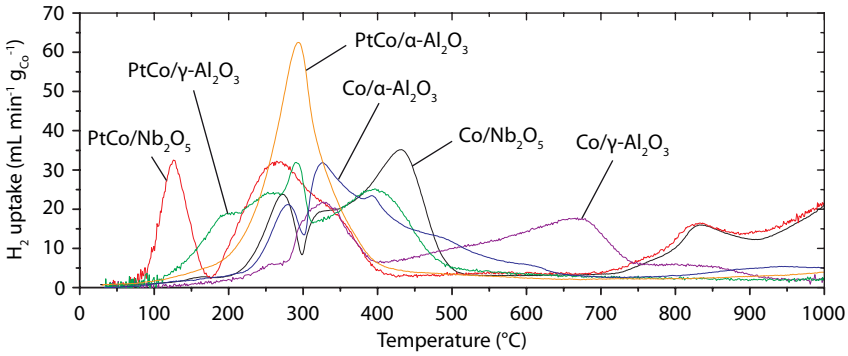

Figure C10. Temperature programmed reduction profiles (10 °C min^{-1} in 5 vol% H_2/Ar) for calcined (Pt)Co/Nb_2O_5, (Pt)Co/γ-Al_2O_3 and (Pt)Co/α-Al_2O_3 catalysts.

CO chemisorption

Table C1. Surface residence time (τ_{CO}) and amount of reversibly adsorbed CO ($N_{CO,\ total}$) determined using CO chemisorption at 100 °C from a ^{12}CO/Ar to ^{13}CO/Kr switch and adsorbed amount of H_2 (N_{H_2}) determined using H_2 chemisorption at 150 °C.

Catalyst	τ_{CO} (s^{-1})	$N_{CO,\ total}$ ($\mu mol_{CO}\ g_{cat}^{-1}$)	$N_{CO,\ total}$ ($mmol_{CO}\ g_{Co}^{-1}$)	N_{H_2} ($\mu mol_{H_2}\ g_{cat}^{-1}$)	N_{H_2} ($mmol_{H_2}\ g_{Co}^{-1}$)
Co/Nb_2O_5	1.4	16	0.28	21	0.36
$PtCo/Nb_2O_5$	2.5	28	0.48	25	0.45
Co/γ-Al_2O_3	1.8	50	0.20	124	0.45
$PtCo/\gamma$-Al_2O_3	2.9	109	0.43	180	0.65
Co/α-Al_2O_3	2.1	24	0.38	34	0.53
$PtCo/\alpha$-Al_2O_3	2.9	32	0.55	37	0.62

Fischer-Tropsch synthesis

Table C2. CO conversion (X_{CO}), activity and selectivity in Fischer-Tropsch synthesis at 1 bar, 220 °C, H_2/CO = 2.0 v/v after 15 h on stream for (Pt)Co/Nb_2O_5, (Pt)Co/γ-Al_2O_3 and (Pt)Co/α-Al_2O_3 catalysts.

		Activity		Selectivity			Paraffin-to-olefin ratio			
Catalyst	X_{CO} (%)	CTY (mol_{CO} g_{Co}^{-1} s^{-1})	TOF_{app} (s^{-1})	CH_4 (wt%)	C_{5+} (wt%)	α	C_5	C_6	C_7	C_8
Co/Nb_2O_5	0.8	2.4 * 10^{-5}	0.034	21	47	0.84	0.3	1.0	2.4	3.7
PtCo/Nb_2O_5	3.6	6.7 * 10^{-5}	0.074	23	44	0.83	0.8	2.1	4.8	6.0
Co/γ-Al_2O_3	5.2	4.2 * 10^{-5}	0.046	21	51	0.86	0.3	0.7	1.4	2.3
PtCo/γ-Al_2O_3	4.7	7.1 * 10^{-5}	0.054	29	38	0.83	0.5	1.0	2.0	2.9
Co/α-Al_2O_3	1.0	1.8 * 10^{-5}	0.017	39	24	0.78	0.4	0.8	1.6	2.3
PtCo/α-Al_2O_3	1.2	2.2 * 10^{-5}	0.018	42	21	0.76	0.6	1.1	2.0	2.5

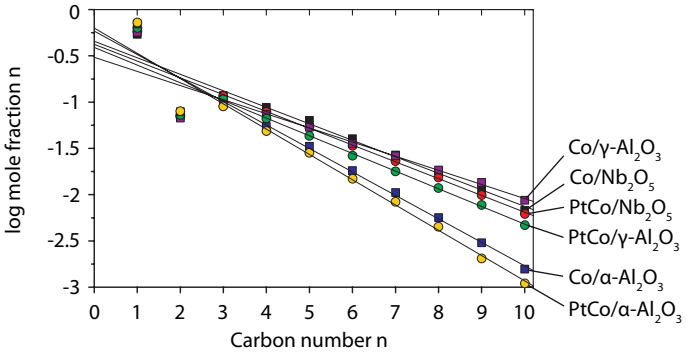

Figure C11. ASF distribution in Fischer-Tropsch synthesis at 1 bar, 220 °C, H_2/CO = 2.0 v/v after at least 15 h on stream for (Pt)Co/Nb_2O_5, (Pt)Co/γ-Al_2O_3 and (Pt)Co/α-Al_2O_3 catalysts.

$Co/\gamma\text{-}Al_2O_3$ was reduced at 500 °C since using TPR high reduction temperatures were observed and low activity and in situ activation during the first 40 h on stream was observed after reduction at 350 °C (Figure C12). Apparent activation energies were calculated to be 96 - 107 kJ mol^{-1} for all catalysts, indicating no diffusion limitation occurred (Table C3 and Figure C13).

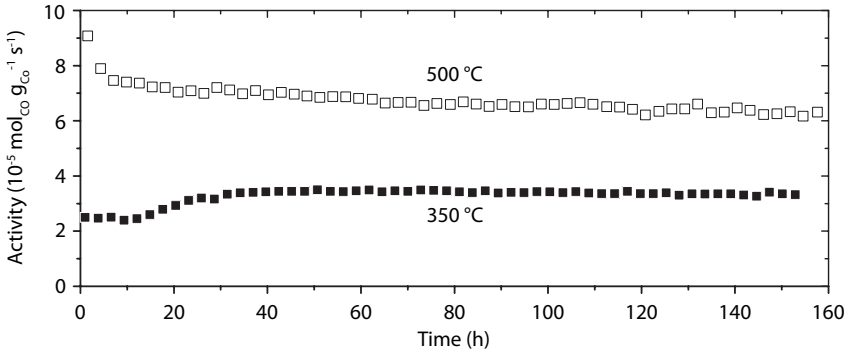

Figure C12. Cobalt-weight normalized activity in Fischer-Tropsch synthesis as a function of time on stream at 220 °C, 20 bar, H_2/CO = 2.0 v/v for $Co/\gamma\text{-}Al_2O_3$ after reduction at 350 °C and 500 °C.

Table C3. CO conversion (X_{CO}), activity and selectivity in Fischer-Tropsch synthesis at 20 bar, 220 °C, H_2/CO = 2.0 v/v after 100 h on stream for $(Pt)Co/Nb_2O_5$, $(Pt)Co/\gamma\text{-}Al_2O_3$ and $(Pt)Co/\alpha\text{-}Al_2O_3$ catalysts. Apparent TOF based on H_2 chemisorption data. Apparent activation energy determined at 200 - 220 °C, data in Figure C13.

Catalyst	X_{CO} (%)	Activity		$E_{act, app}$ (kJ mol^{-1})	Selectivity	
		CTY (mol_{CO} g_{Co}^{-1} s^{-1})	TOF_{app} (s^{-1})		CH_4 (wt%)	C_{5+} (wt%)
Co/Nb_2O_5	29	$5.9 * 10^{-5}$	0.083	107	8	87
$PtCo/Nb_2O_5$	25	$14 * 10^{-5}$	0.15	96	8	86
$Co/\gamma\text{-}Al_2O_3$	21	$6.4 * 10^{-5}$	0.071	102	15	74
$PtCo/\gamma\text{-}Al_2O_3$	34	$6.8 * 10^{-5}$	0.053	103	15	74
$Co/\alpha\text{-}Al_2O_3$	26	$3.6 * 10^{-5}$	0.034	104	7	88
$PtCo/\alpha\text{-}Al_2O_3$	30	$4.6 * 10^{-5}$	0.037	103	7	89

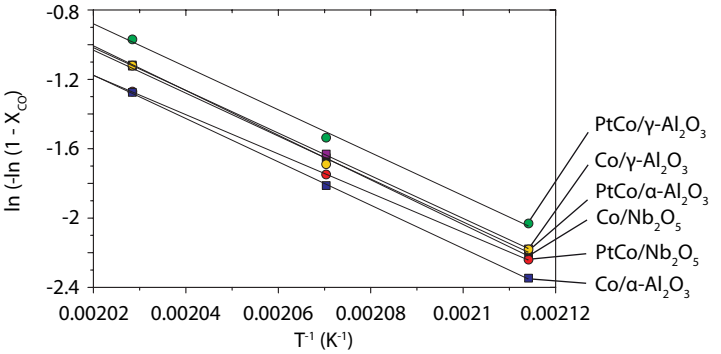

Figure C13. Activity in Fischer-Tropsch synthesis at 20 bar, 200 - 220 °C, H_2/CO = 2.0 v/v, 9 - 32 % CO conversion after at least 100 h on stream for (Pt)Co/Nb_2O_5, (Pt)Co/γ-Al_2O_3 and (Pt)Co/α-Al_2O_3 catalysts.

Kinetic study 1 bar

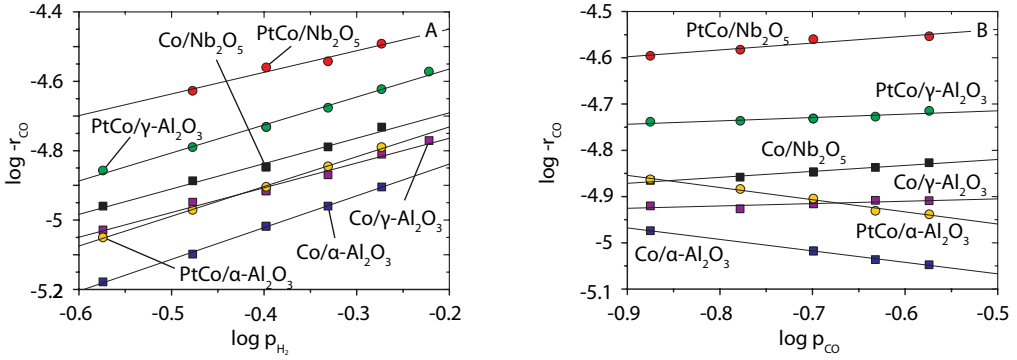

Figure C14. Influence of partial pressures of H_2 (p_{CO} = 0.2 bar, A) and CO (p_{H_2} = 0.4 bar, B) on the cobalt-weight normalized activity in Fischer-Tropsch catalysis at 220 °C, 1 bar after at least 40 h on stream for (Pt)Co/Nb_2O_5, (Pt)Co/γ-Al_2O_3 and (Pt)Co/α-Al_2O_3 catalysts.

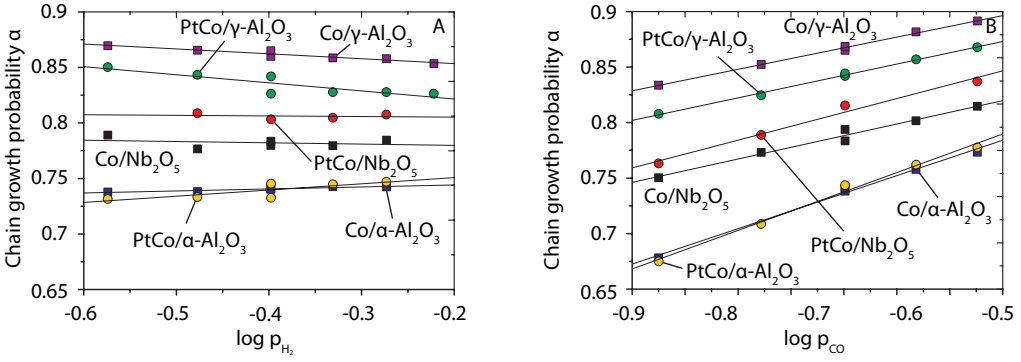

Figure C15. Influence of partial pressures of H_2 (p_{CO} = 0.2 bar, A) and CO (p_{H_2} = 0.4 bar, B) on the chain growth probability α in Fischer-Tropsch catalysis at 220 °C, 1 bar after at least 40 h on stream for (Pt)Co/Nb_2O_5, (Pt)Co/γ-Al_2O_3 and (Pt)Co/α-Al_2O_3 catalysts.

Steady-state isotopic transient kinetic analysis

Table C4. CO conversion (X_{CO}), activity, selectivity towards CH_4 and C_{5+} and paraffin-to-olefin ratio during Fischer-Tropsch catalysis at 210 °C, 1.85 bar, H_2/CO = 10 v/v after at least 15 h on stream.

	X_{CO}	Activity	Selectivity		Paraffin-to-olefin ratio		
Catalyst	(%)	($mol_{CO}\ g_{Co}^{-1}\ s^{-1}$)	CH_4 (wt%)	C_{5+} (wt%)	C_2	C_3	C_4
Co/Nb_2O_5	6.0	$1.1 * 10^{-5}$	64	7	7.7	0.7	0.4
$PtCo/Nb_2O_5$	17	$3.3 * 10^{-5}$	53	13	25	2.9	1.0
$Co/\gamma\text{-}Al_2O_3$	8.8	$1.0 * 10^{-5}$	51	12	6.9	0.7	0.4
$PtCo/\gamma\text{-}Al_2O_3$	14	$2.0 * 10^{-5}$	56	12	19	1.8	0.8
$Co/\alpha\text{-}Al_2O_3$	5.6	$1.0 * 10^{-5}$	63	5	8.4	0.5	0.3
$PtCo/\alpha\text{-}Al_2O_3$	7.5	$1.4 * 10^{-5}$	68	4	22	1.7	0.5

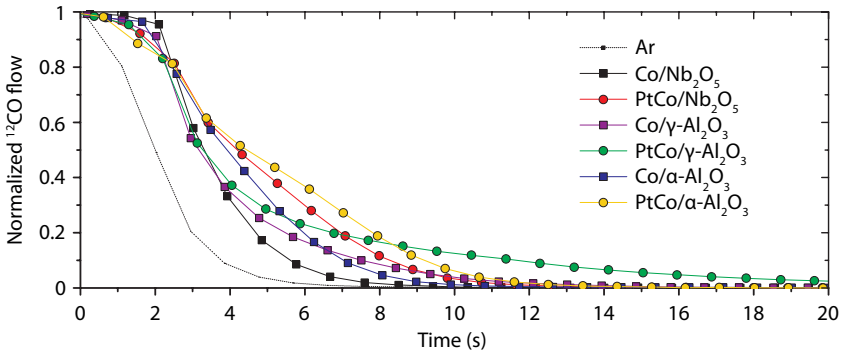

Figure C16. Normalized ^{12}CO transient curves from a ^{12}CO/Ar to ^{13}CO/Kr switch at 100 °C during CO chemisorption for (Pt)Co/Nb_2O_5, (Pt)$Co/\gamma\text{-}Al_2O_3$ and (Pt)$Co/\alpha\text{-}Al_2O_3$ catalysts.

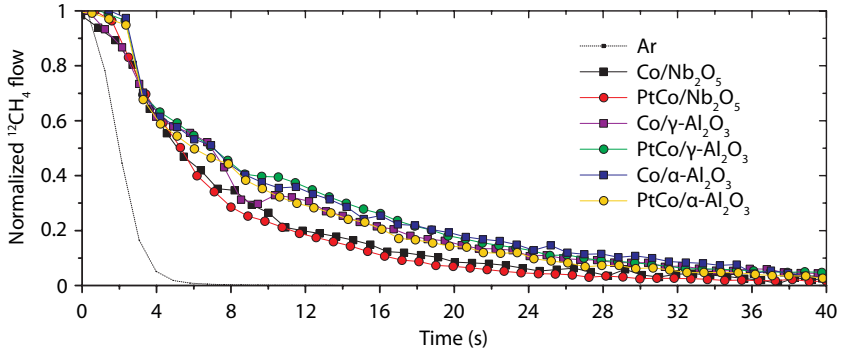

Figure C17. Normalized $^{12}CH_4$ transient curves from a $^{12}CO/H_2$/Ar to $^{13}CO/H_2$/Kr switch at 210 °C, 1.85 bar, H_2/CO = 10 v/v after at least 15 h on stream for (Pt)Co/Nb_2O_5, (Pt)$Co/\gamma\text{-}Al_2O_3$ and (Pt)$Co/\alpha\text{-}Al_2O_3$ catalysts.

Table C5. Residence time (τ_i), adsorbed amounts (N_i), surface coverage (θ_i) and TOF determined from a $^{12}CO/H_2/Ar$ to $^{13}CO/H_2/Kr$ switch during Fischer-Tropsch catalysis at 210 °C, 1.85 bar, H_2/CO = 10 v/v after at least 15 h on stream. Total number of active sites based on H_2 chemisorption data (Table C1) using $\theta_i = N_i / (2 * N_{H_2})$ and $TOF = \tau_{CH_x}^{-1} * \theta_{CH_x}$.

Catalyst	τ_{CO} (s)	τ_{CH_x} (s)	N_{CO} (μmol g_{cat}^{-1})	N_{CH_x} (μmol g_{cat}^{-1})	θ_{CO}	θ_{CH_x}	TOF (s^{-1})
Co/Nb_2O_5	2.1	5.2	21	2.2	0.51	0.05	0.016
$PtCo/Nb_2O_5$	3.6	4.2	33	4.2	0.66	0.08	0.038
$Co/\gamma\text{-}Al_2O_3$	2.4	7.6	61	9.2	0.24	0.04	0.010
$PtCo/\gamma\text{-}Al_2O_3$	3.6	8.3	114	23	0.32	0.07	0.014
$Co/\alpha\text{-}Al_2O_3$	3.0	8.1	31	3.1	0.47	0.05	0.009
$PtCo/\alpha\text{-}Al_2O_3$	3.8	6.6	40	3.7	0.53	0.05	0.011

CH_x transient curves were fitted to a single pool and double pool model:

- Single pool: $F(t) = e^{-t/\tau}$
- Double parallel pools: $F(t) = N_1 e^{-t/\tau_1} + N_2 e^{-t/\tau_2}$; $\tau_{fit} = N_1\tau_1 + N_2\tau_2$

Table C6. ^{12}CO and $^{12}CH_4$ Residence time (τ) from three consecutive $^{12}CO/H_2$/Ar to $^{13}CO/H_2$/Kr switches during Fischer-Tropsch catalysis at 210 °C, 1.85 bar, H_2/CO = 10 v/v after at least 15 h on stream, determined by integration and by fitting of the CH_4 transient curves.

Catalyst	$\tau_{CH_4,\ integrated}$ (s^{-1})	$\tau_{CH_4,\ corrected}$ (s^{-1})	Fit single pool $\tau_{CH_4,\ fit}$ (s)	Fit single pool R^2	Fit double pool $\tau_{CH_4,\ fit}$ (s)	Fit double pool R^2
	6.2	5.1	7.6 ± 0.3	0.9924	7.7	0.9927
Co/Nb_2O_5	6.0	5.0	6.9 ± 0.3	0.9939	7.0	0.9943
	6.3	5.3	7.2 ± 0.3	0.9946	7.3	0.9949
	6.0	4.1	6.1 ± 0.2	0.9937	6.2	0.9942
$PtCo/Nb_2O_5$	6.1	4.3	6.0 ± 0.2	0.9936	6.0	0.9943
	5.9	4.1	6.1 ± 0.3	0.9914	6.2	0.9923
	9.9	8.6	10.1 ± 0.2	0.9975	10.1	0.9975
$Co/\gamma\text{-}Al_2O_3$	8.8	7.6	10.2 ± 0.2	0.9972	10.2	0.9972
	7.8	6.5	10.2 ± 0.2	0.9978	10.2	0.9978
	10.3	8.5	12.7 ± 0.2	0.9985	12.7	0.9985
$PtCo/\gamma\text{-}Al_2O_3$	9.9	8.1	12.5 ± 0.2	0.9984	12.5	0.9984
	8.1	6.3	12.0 ± 0.2	0.9986	12.0	0.9986
	9.8	8.4	11.8 ± 0.3	0.9967	11.8	0.9967
$Co/\alpha\text{-}Al_2O_3$	9.9	8.4	12.1 ± 0.3	0.9950	12.1	0.9951
	9.2	7.7	11.8 ± 0.3	0.9957	11.8	0.9957
	8.8	6.9	10.9 ± 0.1	0.9992	10.9	0.9992
$PtCo/\alpha\text{-}Al_2O_3$	8.6	6.7	10.9 ± 0.1	0.9991	10.9	0.9991
	8.3	6.3	10.5 ± 0.2	0.9984	10.5	0.9984

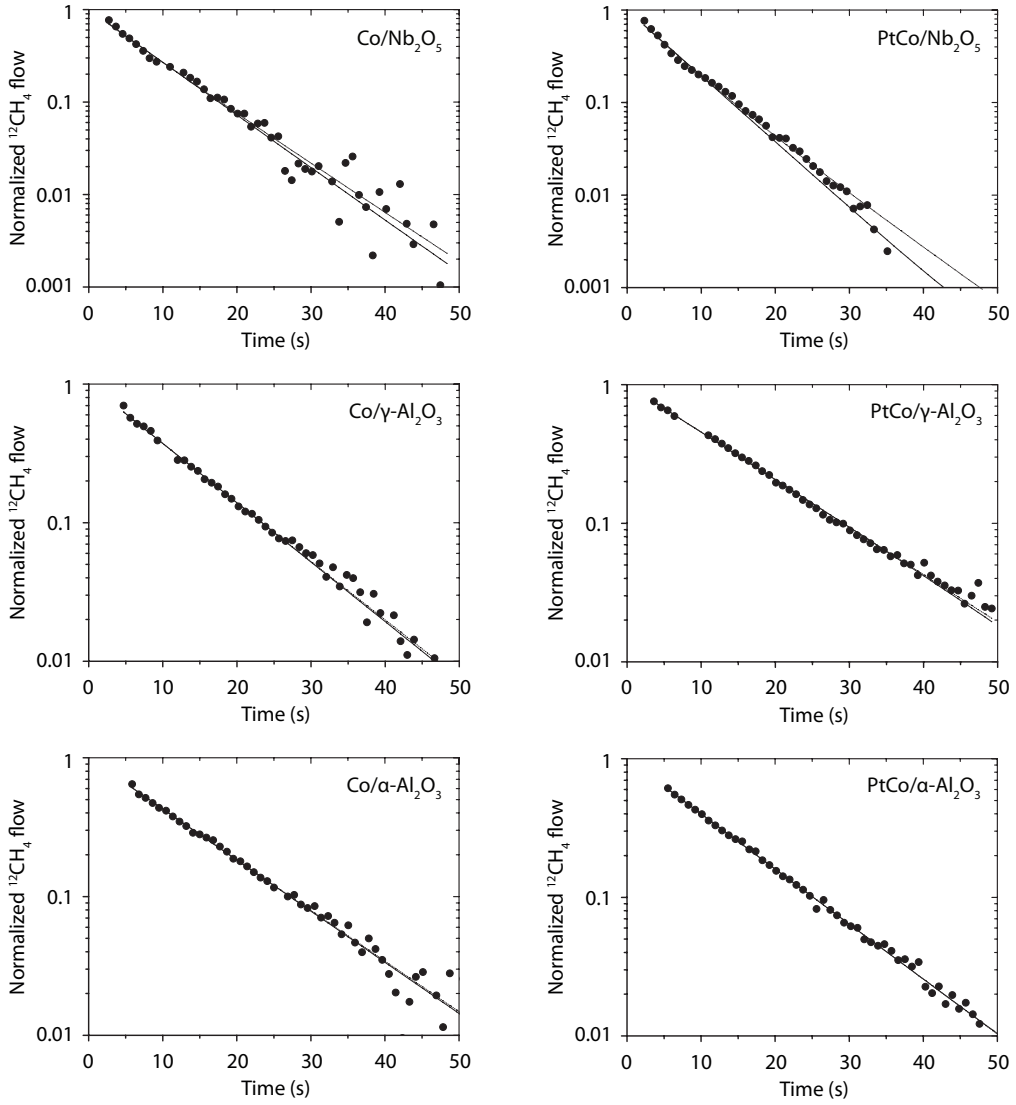

Figure C18. Normalized $^{12}CH_4$ transient curves from a $^{12}CO/H_2/Ar$ to $^{13}CO/H_2/Kr$ switch at 210 °C, 1.85 bar, $H_2/CO = 10$ v/v after at least 15 h on stream. Dots indicate measured data, solid line indicates fit to single pool model, dotted line indicates fit to double parallel pool model.

Appendix D

Supporting Information Chapter 5

Synergistic Promotion of Co/SiO_2 Fischer-Tropsch Catalysts by Niobia and Platinum

Overview supports

Table D1. Niobia-loading based on intake and assuming Nb to be present as Nb_2O_5, (Nb-)Si calcination temperature (T_{calc}) and sample-weight normalized and silica-weight normalized surface area (SA_{BET}) and pore volume (PV) for Si and NbSi supports.

Support designation	Nb/Si	Niobia loading	T_{calc}	SA_{BET}	PV	SA_{BET}	PV
	(at./at.)	(wt%)	(°C)	($m^2\ g_{sample}^{-1}$)	(mL g_{sample}^{-1})	($m^2\ g_{silica}^{-1}$)	(mL g_{silica}^{-1})
Si-550	-	-	550	269	1.11	269	1.1
0.02NbSi-550	0.02	4.6	550	265	1.07	277	1.1
0.04NbSi-550	0.04	8.4	550	262	1.02	286	1.1
0.06NbSi-550	0.06	12.3	550	256	0.99	292	1.1
0.09NbSi-550	0.09	15.9	550	250	0.95	297	1.1
0.12NbSi-550	0.12	21.4	550	240	0.88	305	1.1
Si-675	-	-	675	265	1.04	265	1.0
0.04NbSi-675	0.04	8.7	675	252	0.99	276	1.1
0.12NbSi-675	0.12	21.5	675	223	0.82	284	1.0
Si-800	-	-	800	226	0.93	226	0.9
0.04NbSi-800	0.04	8.7	800	232	0.95	253	1.0
0.12NbSi-800	0.12	21.5	800	209	0.80	266	1.0
Si-900	-	-	900	115	0.36	115	0.4
0.04NbSi-900	0.04	8.7	900	169	0.70	185	0.8
0.12NbSi-900	0.12	21.5	900	155	0.64	197	0.8

N_2 physisorption

Using N_2 physisorption, the influence of niobia-modification on the surface area and porosity of SiO_2 were studied (Table D1). After niobia-modification and calcination at 550 °C, the SiO_2 normalized surface area and pore volume were found to be conserved or slightly enhanced, indicating that the SiO_2 structure was largely preserved upon niobia modification. Previously Ko and Shiju also reported a preserved surface upon niobia-modification of silica and calcination at 500 °C.[1,2] After calcination at higher temperatures, the surface area and pore volume decreased; however, the presence of niobia appeared to stabilize the SiO_2 structure since the observed surface area and porosity (Figure D1) decrease was less pronounced than for SiO_2 without niobia modification.

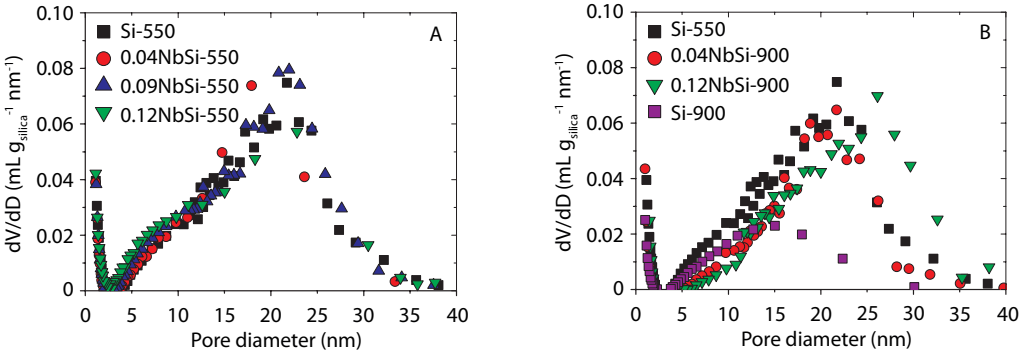

Figure D1. Silica-weight normalized pore size distributions for Si-550, NbSi-550, Si-900 and NbSi-900.

X-ray diffraction

Using X-ray diffraction, no crystalline niobia species were observed in niobia-modified silica up to Nb/Si = 0.12 at./at. after calcination at 550 °C (Figure 5.1). For a physical mixture of ANO and SiO_2, orthorhombic Nb_2O_5 was observed after calcination at 550 °C. This indicates that no large crystalline niobia particles were present and that strong interaction between niobia and SiO_2 exists in the niobia-modified silica as also observed and suggested by Shiju and He.[2,3] This also indicates that impregnation with a niobium precursor solution is required to obtain niobia-modified silica, in contrast to reports published on MoO_3-loaded silica-alumina where thermal treatment of a physical mixture of MoO_3 and silica-alumina was sufficient to obtain MoO_3-loaded silica-alumina.[4] After calcination at 675 °C or higher, the formation of crystalline niobia (orthorhombic T-phase Nb_2O_5) was observed. Similar observations were made by Shiju et al. who reported sintering of Nb_2O_5 crystallites, based on shifting XPS binding energies.[2] Higher niobia loadings were suggested to exceed the critical layer thickness, leading to instability and consequent growth of niobia crystallites. For 0.12NbSi, the Nb_2O_5 crystallite size was determined to be 13 and 23 nm after calcination at 675 and 900 °C respectively. Also for 0.04NbSi crystallization of Nb_2O_5 was observed at T > 675 °C, however less intense and broader diffraction peaks were observed indicating lower crystallinity and smaller crystallites.

Diffuse reflectance Spectroscopy

UV-Vis Diffuse Reflectance Spectroscopy (UV-Vis DRS) absorbance spectra were obtained in the range of 200 - 800 nm using a Varian Cary 500 UV-Vis-NIR spectrophotometer equipped with accessory for performance of DRS measurements. Samples were placed in a sample holder with quartz window, baseline spectra were acquired by measurement of white Spectralon DR standard (99 % transmittance).

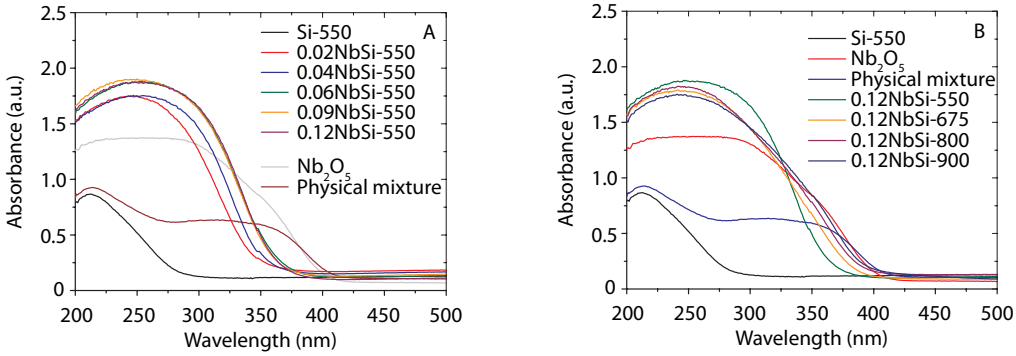

Figure D2. UV-Vis diffuse reflectance spectroscopy (DRS) spectra for niobia-modified silica. Spectra for SiO_2, crystalline Nb_2O_5 (TT-phase) and a physical mixture of ANO and SiO_2 (Nb/Si = 0.12 at./at.) calcined at 550 °C were added for comparison.

UV-Vis diffuse reflectance spectroscopy (DRS) measurements were performed to study the nature of niobia and the degree of niobia polymerization in niobia-modified silica. For crystalline Nb_2O_5 and for a physical mixture of ANO and SiO_2 calcined at 550 °C, an absorption band around 350 nm was observed, attributed to charge transfer from O^{2-} to Nb^{5+}.[2] For niobia-modified silica with Nb/Si = 0.12 at./at., this band was found to arise and shift to higher wavelengths with increasing calcination temperature, indicating a decreasing bandgap (Figure D2). At lower niobia loading the rise of the band around 350 nm and shift towards higher wavelength were also observed but less pronounced. This indicates that with increasing calcination temperature and at higher niobia loading its degree of polymerization increased in agreement with XRD results. Strong dependence of the band gap energy on niobia loading was previously observed by He et al.[3]

Transmission electron microscopy

The nanoscale distribution of niobia and the influence of the calcination temperature thereon were studied using TEM. After calcination at 550 °C no dark dots were observed, indicating that niobium was not present as niobia particles larger than 2 nm (Figure 5.2A). This is in agreement with observations from XRD measurements where no crystalline niobia was observed after calcination at 550 °C and DRS measurements where niobium was found to be present in strong interaction with silica rather than as particles. This might indicate that a niobia layer was formed, strongly interacting with SiO_2.

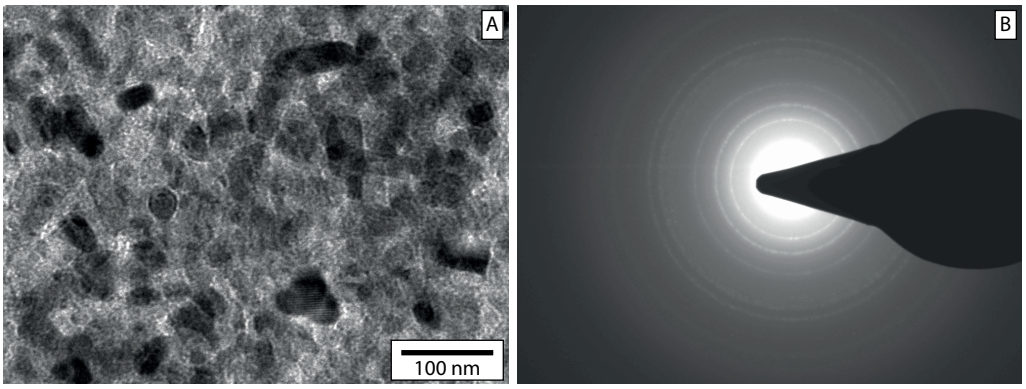

Figure D3. Bright field TEM image and diffraction pattern of 0.12NbSi-900.

After calcination at 900 °C, dark dots with a diameter of 15 - 20 nm were observed, well-distributed throughout the SiO_2 grains (Figure D3A). These particles were confirmed to be niobia particles using EDX and were found to be crystalline (Figure D3B). These observations support the conclusions from XRD and DRS measurements that niobium was mobile during high-temperature calcination and formed crystalline 15 - 25 nm Nb_2O_5 particles after calcination at 900 °C distributed both inside and outside the SiO_2 grains. Also the primary SiO_2 particles appeared to have grown due to sintering at 900°C, which is in agreement with the decreased surface area determined using N_2 physisorption.

Scanning electron microscopy

The morphology of the SiO_2 grains before and after modification with niobia was studied using scanning electron microscopy using a back-scattered electron detector. Heavy elements, in this case Nb, are imaged as bright areas compared to SiO_2 and a clear contrast between Nb_2O_5 and SiO_2 was observed for a physical mixture of SiO_2 and crystalline Nb_2O_5 (Figure 5.4). For 0.12NbSi-550 and 0.04NbSi-900 no or only few bright spots were observed on the exterior surface of the SiO_2 grains (Figure D5A, B). For 0.12NbSi-900, more niobia was observed on the exterior surface of the SiO_2 grains (Figure D5C), indicating that niobia was mobile during calcination at 900 °C and formed crystallites on the exterior surface of the grains.

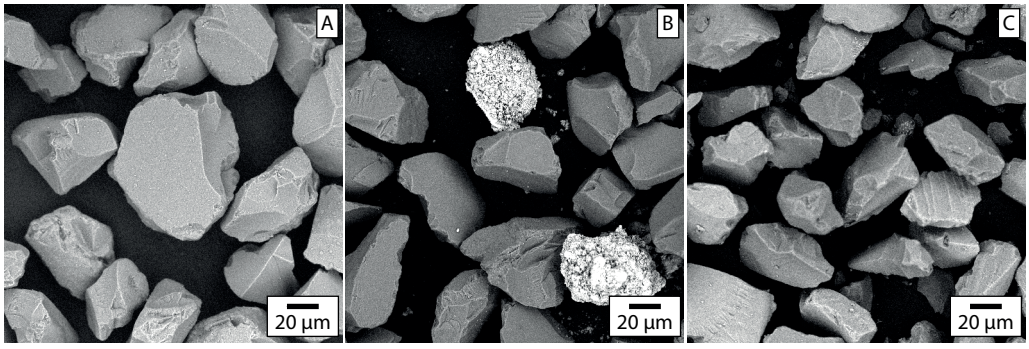

Figure D4. Back-scattered electron-SEM images of SiO_2 (A), a physical mixture of crystalline Nb_2O_5 and SiO_2 (B) and niobia-modified silica (0.12NbSi-550, C).

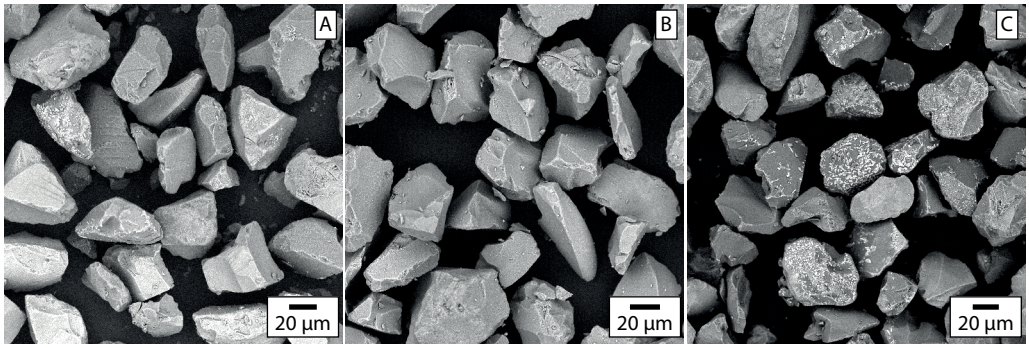

Figure D5. BSE-SEM images of niobia-modified silica 0.12NbSi-550 (A), 0.04NbSi-900 (B) and 0.12NbSi-900 (C). Bright spots indicate heavy elements.

Overview catalysts

Table D2. Nb/Si atomic ratio, (Nb-)Si calcination temperature (T_{calc}), niobia, Pt and Co loadings based on intake and assuming Nb to be present as Nb_2O_5 for (Pt)Co-(Nb)Si catalysts.

Catalyst designation	Nb/Si	T_{calc}	Niobia loading	Pt loading	Co loading	
	(at./at.)	(°C)	(wt%)	(wt%)	(wt%)	(mg_{Co} m^{-2})
Co-Si-550	-	550	-	-	21.0	0.99
Co-0.02NbSi-550	0.02	550	3.4	-	19.3	0.90
Co-0.04NbSi-550	0.04	550	6.4	-	18.8	0.88
Co-0.06NbSi-550	0.06	550	9.4	-	18.6	0.99
Co-0.09NbSi-550	0.09	550	11.9	-	19.8	0.98
Co-0.12NbSi-550	0.12	550	16.1	-	18.8	0.86
PtCo-Si-550	-	550	-	0.43	18.0	0.84
PtCo-0.02NbSi-550	0.02	550	3.4	0.46	19.1	0.91
PtCo-0.04NbSi-550	0.04	550	6.4	0.44	18.2	0.88
PtCo-0.06NbSi-550	0.06	550	9.4	0.43	17.8	0.86
PtCo-0.09NbSi-550	0.09	550	12.4	0.41	16.9	0.82
PtCo-0.12NbSi-550	0.12	550	16.6	0.40	16.6	0.84
Co-Si-900	-	900	-	-	9.2	0.88
Co-0.04NbSi-900	0.04	900	7.1	-	14.3	0.99
Co-0.12NbSi-900	0.12	900	18.3	-	11.6	0.85
PtCo-Si-900	-	900	-	0.21	8.6	0.83
PtCo-0.04NbSi-900	0.04	900	7.2	0.32	13.3	0.92
PtCo-0.12NbSi-900	0.12	900	18.1	0.28	11.8	0.87

TEM analysis catalysts

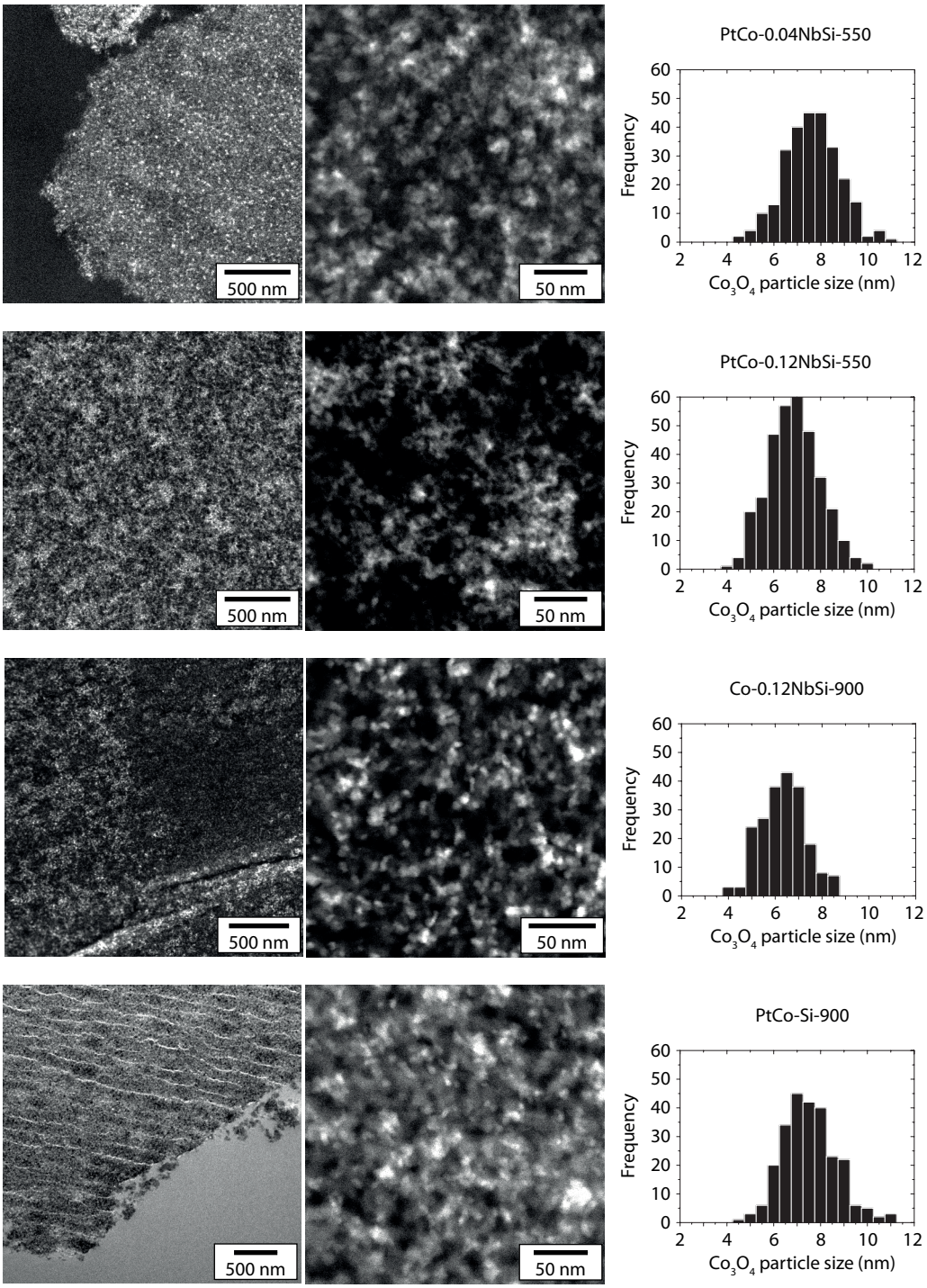

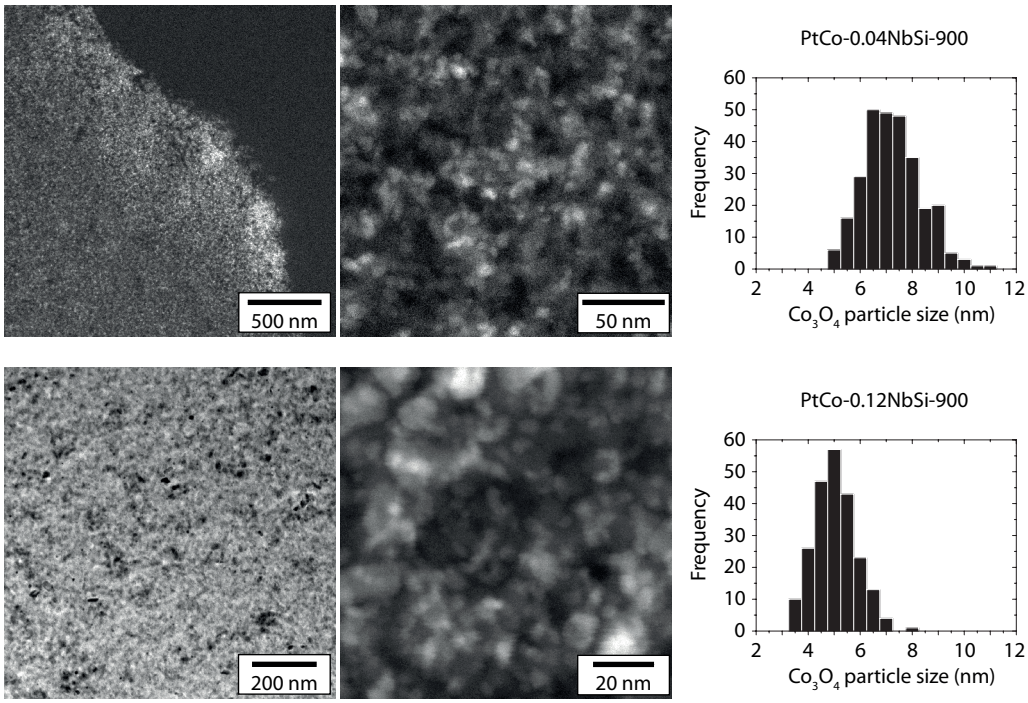

Figure D6. TEM images and Co_3O_4 particle size distributions of calcined catalysts.

Catalyst activity and selectivity in Fischer-Tropsch synthesis

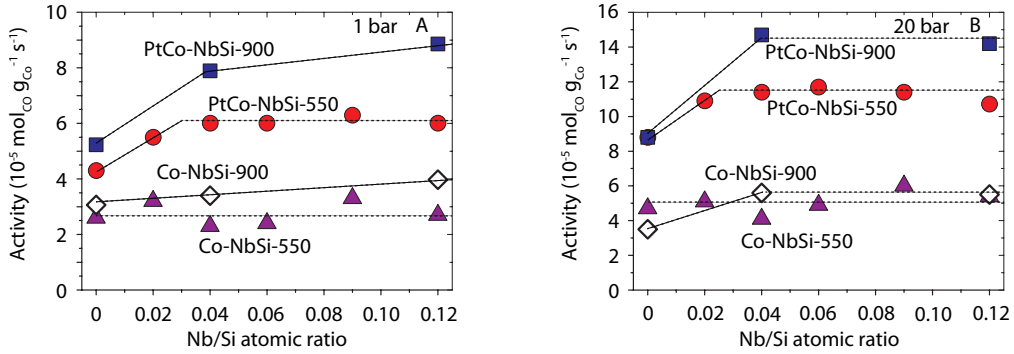

Figure D7. Cobalt-weight normalized Fischer-Tropsch activity at 220 °C, H_2/CO = 2.0 at 1 bar after 15 h on stream (A) and at 20 bar after 100 h on stream (B) for (Pt)Co-(Nb)Si catalysts. Lines were added to guide the eye.

.

Table D3. Selectivity towards CH_4 and C_{5+}, CO conversion (X_{CO}) , cobalt-weight normalized activity (CTY) and turnover frequency (TOF) in Fischer-Tropsch catalysis at 1 bar, 220 °C, H_2/CO = 2.0 after 15 h on stream for (Pt)Co-(Nb)Si catalysts

Catalyst designation	Selectivity				TOF		
	CH_4 (wt%)	C_{5+} (wt%)	X_{CO} (%)	CTY ($mol_{CO}\ g_{Co}^{-1}\ s^{-1}$)	H_2 (s^{-1})	XRD (s^{-1})	TEM (s^{-1})
Co-Si-550	34	30	1.9	$2.6 * 10^{-5}$	0.018	0.010	
Co-0.02NbSi-550	27	41	3.1	$3.2 * 10^{-5}$		0.012	
Co-0.04NbSi-550	30	37	3.6	$2.3 * 10^{-5}$	0.024	0.009	
Co-0.06NbSi-550	24	46	4.0	$2.4 * 10^{-5}$		0.009	
Co-0.09NbSi-550	24	46	3.3	$3.3 * 10^{-5}$		0.013	
Co-0.12NbSi-550	24	45	4.4	$2.7 * 10^{-5}$	0.040	0.010	
PtCo-Si-550	32	33	3.3	$4.3 * 10^{-5}$	0.018	0.015	
PtCo-0.02NbSi-550	25	46	2.7	$5.5 * 10^{-5}$		0.020	
PtCo-0.04NbSi-550	25	45	3.1	$6.0 * 10^{-5}$	0.031	0.020	0.021
PtCo-0.06NbSi-550	23	48	2.2	$6.0 * 10^{-5}$		0.020	
PtCo-0.09NbSi-550	23	47	3.1	$6.3 * 10^{-5}$		0.022	
PtCo-0.12NbSi-550	21	49	2.2	$6.0 * 10^{-5}$	0.044	0.021	0.019
Co-Si-900	32	32	1.3	$3.1 * 10^{-5}$	0.024	0.010	
Co-0.04NbSi-900	23	46	2.3	$3.4 * 10^{-5}$	0.029	0.012	
Co-0.12NbSi-900	25	42	2.2	$4.0 * 10^{-5}$		0.014	0.012
PtCo-Si-900	31	34	2.2	$5.2 * 10^{-5}$	0.023	0.017	0.019
PtCo-0.04NbSi-900	27	38	2.7	$7.9 * 10^{-5}$	0.043	0.027	0.027
PtCo-0.12NbSi-900	24	44	2.8	$8.9 * 10^{-5}$	0.048	0.029	0.021

References

[1] Ko, E. I.; Bafrali, R.; Nuhfer, N. T.; Wagner, N. J. *J. Catal.* **1985**, *95*, 260–270.

[2] Shiju, N. R.; Brown, D. R.; Wilson, K.; Rothenberg, G. *Top. Catal.* **2010**, *53*, 1217–1223.

[3] He, J.; Li, Q.-J.; Fan, Y.-N. *J. Solid State Chem.* **2013**, *202*, 121–127.

[4] Debecker, D. P.; Stoyanova, M.; Rodemerck, U.; Eloy, P.; Léonard, A.; Su, B.-L.; Gaigneaux, E. M. *J. Phys. Chem. C* **2010**, *114*, 18664–18673.

List of publications

This thesis was based on the following publications

Journal articles:

J.H. den Otter, H. Yoshida, C. Ledesma, D. Chen and K.P. de Jong, "On the Superior Activity and Selectivity of PtCo/Nb_2O_5 Fischer Tropsch Catalysts" *submitted for publication*

J.H. den Otter, S.R. Nijveld and K.P. de Jong, "Synergistic Promotion of Co/SiO2 Fischer–Tropsch Catalysts by Niobia and Platinum" *ACS Catal.* 2016, 6 (3) 1616-1623

J.H. den Otter and K.P. de Jong, "Highly Selective and Active Niobia-Supported Cobalt Catalysts for Fischer-Tropsch Synthesis", *Top. Catal.* 2014, 57 (6) 445-450

Oral presentations:

J.H. den Otter, H. Yoshida and K.P. de Jong, Highly Active and Selective Pt-promoted Co/Nb_2O_5 Catalysts for Fischer Tropsch Synthesis, 24th North American Catalysis Society Meeting (NAM24), Pittsburgh, PA, USA, June 14-19th, 2015

J.H. den Otter and K.P. de Jong, Highly Active and Selective Pt-promoted Co/Nb_2O_5 Catalysts for Fischer Tropsch Synthesis, XVIth Netherlands' Catalysis and Chemistry Conference (NCCC XVI), Noordwijkerhout, the Netherlands, March 2-4th, 2015

J.H. den Otter and K.P. de Jong, "Highly Selective and Active Niobia Supported Catalysts for Fischer Tropsch Synthesis", 7th Tokyo Conference on Advanced Catalytic Science and Technology (TOCAT7), Kyoto, Japan, June, 1-6th, 2014

J.H. den Otter, J.H. Bitter and K.P. de Jong, Highly Selective Niobia Supported Cobalt Catalysts for Fischer Tropsch Synthesis, 23rd North American Catalysis Society Meeting (NAM23), Louisville, KY, USA, June 2-7th, 2013

J.H. den Otter, J.H. Bitter and K.P. de Jong, Highly Selectivity Niobia Supported Cobalt Catalysts for Fischer Tropsch Synthesis, XIVth Netherlands' Catalysis and Chemistry Conference (NCCC XIV), Noordwijkerhout, the Netherlands, March 11-13th, 2013

Poster presentation:

J.H. den Otter, K.P. de Jong "Highly Active Pt-Co/Nb_2O_5 Catalysts for Fischer Tropsch Synthesis", XVth Netherlands' Catalysis and Chemistry Conference (NCCC XV), Noordwijkerhout, the Netherlands, March 10-12th, 2014

Dankwoord

Krijn, als eerste wil ik jou bedanken voor de kans die je me hebt gegeven om een promotieonderzoek te doen en de begeleiding daarbij. Doordat niobiumoxide in Fischer-Tropschkatalyse binnen onze groep een nieuw onderwerp was, had ik alle ruimte om mijn project zelf vorm te geven, bedankt voor de vrijheid daarin die me ook de kans gaf mijn vrijdagmiddagexperimenten uit te werken. Je betrokkenheid bij mij en ons project en je enorme ervaring met onder andere Fischer-Tropschkatalyse, onderzoek doen, presenteren, begeleiden en projectmanagement zorgden er voor dat we de rode draad niet kwijtraakten en ik leerde prioriteiten te stellen. Je motivatie om me bij elk gesprek iets te leren of op zijn minst ergens kritisch over na te laten denken en dat ook nog in correct Nederlands te verwoorden maakte elk overleg waardevol, of het nu twee minuten bij de koffieautomaat of anderhalve dag naast elkaar zittend onderweg naar Araxá was. Ook Harry, mijn ex-copromotor, wil ik bedanken voor de open deur tijdens eerste twee jaar van mijn onderzoek. Je vormde een perfect team met Krijn.

I would like to thank CBMM for funding this research and for the confidence and freedom we got during this project. I would especially like to thank Robson Monteiro and Rogério Ribas for their enthusiasm about the project, the many visits to the Netherlands (and even to Schiermonnikoog), for useful discussions about our research and for their hospitality during our visit to Brazil.

This research and especially Chapter 4 would not have been possible without researchers and facilities abroad. I would like to Hideto Yoshida from ISIR in Osaka for his hospitality during my stay in Osaka, for the excellent environmental TEM work and his many useful suggestions. I would also like to thank De Chen, Cristian Ledesma and Yanying Qi from NTNU in Trondheim for their hospitality and the opportunity to perform SSITKA experiments in their lab and the assistance during the experiments.

All (former) ICC colleagues, thank you for collaborating, chatting, drinking coffee, beer and sangria, having BBQs, borrels, Tricolore and LIITs. I really enjoyed my time in the ICC group, maybe that's why it took me so long to leave.

Peter^{M}, thank you for everything you and Gonzalo taught me about catalyst preparation and FT experiments , for being my sparring partner on all aspects of doing research and for supporting me during my defense. Together with Thomas and Rien we managed to get (and keep) the Flowrence working, I really feel we were a great team. The assistance of Avantium, and especially Gosia, Graham, Alex and Gerard was essential to get and keep the Flowrence running. Thank you for sharing your expertise and your willingness to help whenever we broke something or wanted to try something new. Also the rest of the expanding Flowrence team, in order of appearance JX, Tom, Lennart, Martin and Carlos, I enjoyed working with you and transferring our Flowrence (knowledge) to you. Take good care of her! Carlos, thanks for taking over my project so enthusiastically and good luck during your PhD.

De vaste staf van onze vakgroep blijft onmisbaar voor het uitvoeren van onderzoek en voor de continuïteit in de groep. Hans, bedankt voor de vele uren die we achter de microscoop hebben doorgebracht met die steeds terugkerende vraag of we nu naar niobiumoxide of kobaltoxide

keken. Ad^{M}, bedankt voor alle hulp in het lab, bij het persen van rubbers in reactiestangen maar zeker ook voor je adviezen om mijn eigen onderzoek voorrang te geven op dat van anderen. Ad^{E}, bedankt voor alles wat ik van je heb mogen leren over gasdetectie, veiligheid en ontruimingen. Marjan, bedankt voor alle pogingen om kobalt op niobiumoxide met XRD zichtbaar te krijgen, helaas is het ons zelfs bij 350 °C in H_2 niet gelukt. Fouad, bedankt voor het bestellen van alle gasflessen en broodjes Italiano met parma maar vooral ook, als je niet weer eens op vakantie was, voor je onmisbare rol als sociaal spinnenweb van de vakgroep. Pascal, Oscar, Herrick en Jan Willem, bedankt voor jullie hulp als ik een inbussleutel in een onmogelijke maat of een nieuwe heat tracing nodig had, alle ferrules weer op mysterieuze wijze waren verdwenen of de stoppen er weer uit lagen. Iris, Monique en vooral Dymph, bedankt voor alle praktische dingen, het in de gaten houden van de planning en al die andere dingetjes waar ik voor binnen kon vallen, zeker ook in de laatste maanden.

Ook de studenten die ik heb mogen begeleiden hebben mooie bijdragen geleverd aan mijn onderzoek. Tom, het werk dat je tijdens je masteronderzoek hebt gedaan heeft helaas (nog?) niet tot een publicatie geleid maar het was wel erg nuttig om de resultaten die in hoofdstuk 4 en 5 staan te begrijpen. Ik heb met alle vertrouwen onze Flowrence aan je durven toevertrouwen. Melanie, Ludo, Petra, Rob en Sven, bedankt voor jullie inzet tijdens jullie onderzoeksprojecten. Het vele werk dat Sebastiaan tijdens zijn masteronderzoek heeft gedaan heeft geleid tot hoofdstuk 5 en een mooie publicatie; helaas heeft hij dit zelf niet meer mee kunnen maken.

Timo, bedankt voor alles in de afgelopen 11 jaar, van de sausjes en sapjes tijdens het esterproject tot je hulp bij de opmaak van dit boekje en het willen zijn van mijn paranimf. Anke, Bieneke, Christine, Els, Fanny, Frank, Janne-Mieke, Jeroen, Joost vd L, Joost W, Nikki, Paul, Peter, Remi, Robin, Suuz, Tiemen, Tim, Tom en Winnie, bedankt voor wintersport, Primus, Reiger, feestjes, BBQ, oud & nieuw, bestuurseten, bestuursweekend en alle andere dingen die nodig zijn om een promotieonderzoek draaglijk te maken.

Ook mijn familie en schoonfamilie wil ik bedanken voor de steun de afgelopen vier jaar en lang daarvoor. Ik heb jullie interesse in mijn onderzoek altijd erg gewaardeerd, ook al vond ik het soms lastig uit te leggen wat ik nu precies deed.

Lieve Anoeska, bedankt voor de schoppen onder mijn kont, dat je me achter mijn bureau vandaan haalde voor ik kromgroeide en vooral dat je me geleerd hebt dat er nog veel meer te doen is dan alleen onderzoek.

Arjan

Curriculum Vitae

Arjan den Otter was born on January 30th, 1986 in 's-Hertogenbosch, the Netherlands. After graduating from Koningin Wilhelmina College in Culemborg in 2004, he started his bachelor studies in Chemistry at Utrecht University. In 2006-2007 he served as treasurer on the board of the Utrecht chemistry student association "U.S.S. Proton". He completed his bachelor studies in 2008 with a research project on the electrochemical etching of SiC under supervision of dr. Dennis van Dorp and prof. John Kelly. In the same year he started his master studies Nanomaterials: Chemistry & Physics at Utrecht University. The main research project was on the synthesis of silver nanoparticles with controlled size and shape and their application as substrates for Surface-Enhanced Raman Spectroscopy under supervision of dr. Clare Harvey and prof. Bert Weckhuysen. In 2010-2011, he worked on the application of a robotic platform for the synthesis of catalyst supports during an internship at Albemarle Catalysts Company in Amsterdam under supervision of dr. Peter Heines. In 2011, he started his PhD research project on the development and application of niobia-supported catalysts for Fischer-Tropsch synthesis at the group of Inorganic Chemistry and Catalysis under supervision of prof. Krijn de Jong. The results of this work are described in this thesis.